REPORT 1103

CONTENTS

REPORT 1103

GENERALIZED THEORY FOR SEAPLANE IMPACT [1]

By Benjamin Milwitzky

SUMMARY

The motions, hydrodynamic loads, and pitching moments experienced by V-bottom seaplanes during step-landing impacts are analyzed and the theoretical results are compared with experimental data. In the analysis, the primary flow about the immersed portion of a keeled hull or float is considered to occur in transverse flow planes and the concept of virtual mass is applied to determine the reaction of the water to the motions of the seaplane. The entire immersion process is analyzed from the instant of initial contact until the seaplane rebounds from the water surface. The analysis is applicable to the complete range of initial contact conditions between the case of impacts where the resultant velocity is normal to the keel and the limiting condition of planing.

In order to reduce the number of independent constants which have to be considered, the equations relating the displacement, velocity, acceleration, pitching moment, and time during the impact are generalized by introduction of suitable dimensionless variables which take into account the effects of such factors as the weight of the seaplane, the dead-rise angle, the trim angle, the flight-path angle, and the initial velocity, in accordance with the laws governing the behavior of the seaplane. As a result of this generalization, the number of solutions required to cover the entire range of seaplane and impact parameters is greatly reduced, the presentation of both theoretical and experimental results is simplified, and a basis is provided for convenient correlation of test data obtained under diverse conditions.

It is shown that all generalized variables can be related during the impact through a single parameter, called the approach parameter κ, which is determined by the trim angle and the flight-path angle at initial contact. Thus, the relationship between any two of the generalized variables during impact can be represented by a single curve for each value of κ. Furthermore, a single variation with κ exists for each of the generalized variables corresponding to any particular stage of the impact.

In order to permit convenient use of the derived results in the design of seaplanes and in further research, charts are presented which show the relationships among the various generalized variables during impact for a wide range of values of κ; charts are also presented which show the variations with κ of the generalized variables corresponding to the instant of maximum acceleration, the instant of maximum pitching moment about the step, the instant of maximum penetration, and the instant of exit during rebound. In addition, charts are presented showing the results of a simplified analysis of the effects on the maximum load produced by chine immersion due to increased beam loading or unusually high flight-path angles.

Extensive experimental data obtained with hull models having 22½°, 30°, and 40° angles of dead rise are presented to permit evaluation of the theoretical results.

INTRODUCTION

In order to provide a more rational foundation upon which to base water-loading requirements for the design of seaplanes, an extensive program of theoretical and experimental investigations dealing with hydrodynamic impact loads has been conducted during the last 10 years by the National Advisory Committee for Aeronautics. In reference 1 a survey of the literature revealed that existing seaplane-impact theories were valid only for impacts where the resultant velocity is normal to the keel since these theories neglected the effects of the component of velocity parallel to the keel. By taking into consideration the velocity parallel to the keel, reference 1 extended the theory of seaplane impact to include oblique impacts and presented an equation for the hydrodynamic force which is valid for the entire range of oblique-impact conditions.

References 2 and 3 made use of this force equation in an analysis of the motions, hydrodynamic loads, and pitching moments experienced by the seaplane throughout the course of an impact. These studies also showed that all the characteristics of an impact can be expressed in terms of generalized variables, the variations of which during an impact are governed by a single parameter, called the approach parameter κ. The basic theoretical concepts were also extended to provide a simplified analysis of the effects on the maximum load produced by chine immersion resulting from increased beam loading or unusually high flight-path angles.

The present report, which is based largely on references 2 and 3, has been prepared in order to present a unified development of the generalized theory, to make available in one source extensive experimental data obtained over a period of years in the Langley impact basin, and to provide various types of generalized charts which may be useful in seaplane design and in further research.

[1] Based on NACA TN 1516, "A Generalized Theoretical and Experimental Investigation of the Motions and Hydrodynamic Loads Experienced by V-Bottom Seaplanes During Step-Landing Impacts" by Benjamin Milwitzky, 1948, and NACA TN 1630, "A Generalized Theoretical Investigation of the Hydrodynamic Pitching Moments Experienced by V-Bottom Seaplanes During Step-Landing Impacts and Comparisons With Experiment" by Benjamin Milwitzky, 1948.

272483—54——61

SYMBOLS

(Any consistent set of units may be employed)

A hydrodynamic aspect ratio

a distance between center of moments and step, parallel to keel (see fig. 38)

b beam of seaplane (see fig. 1 (a))

c distance between center of moments and center of gravity, normal to keel (see fig. 38)

d distance between center of moments and center of gravity, parallel to keel (see fig. 38)

f two-dimensional hydrodynamic force

F total hydrodynamic force, positive upward

g gravitational constant

l_{cp} distance of center of pressure forward of step, parallel to keel

l_k wetted keel length

m_w two-dimensional virtual mass

M pitching moment, positive nose up

n_{t_w} impact load factor, normal to water surface, $-\frac{\ddot{z}_w}{g}$

n_{t_k} impact load factor, normal to keel, $-\frac{\ddot{z}_k}{g}$

t time after initial contact with water surface

V velocity of seaplane

W weight

x_s displacement of step-keel point relative to point of initial contact with water surface, parallel to water surface, positive forward (see fig. 1 (b))

z_w displacement of step-keel point relative to point of initial contact with water surface (draft), normal to water surface, positive downward (see fig. 1 (b))

x_k displacement of step-keel point relative to point of initial contact with water surface, parallel to keel, positive forward (see fig. 1 (b))

z_k displacement of step-keel point relative to point of initial contact with water surface, normal to keel, positive downward (see fig. 1 (b))

ξ distance between step and any fixed flow plane, parallel to keel, positive forward (see fig. 1 (b))

ζ distance from keel to undisturbed water surface in any given flow plane, normal to keel, positive upward (see fig. 1 (b))

ζ_s distance from keel to undisturbed water surface at step, normal to keel, positive upward (see fig. 1 (b))

β angle of dead rise, radians except where otherwise noted

τ trim angle

γ flight-path angle

ρ mass density of water

Δ load on water

$\epsilon(\beta), f(\beta)$ dead-rise-angle functions, relate two-dimensional virtual mass and penetration normal to keel

$\psi(\beta)$ dead-rise-angle function; ratio of normal penetration to wetted width, two-dimensional

$\phi(A)$ aspect-ratio correction to total virtual mass and total hydrodynamic force calculated on two-dimensional basis

$\phi_1(A)$ aspect-ratio correction to hydrodynamic pitching moment calculated on two-dimensional basis

C_Δ load coefficient, $\frac{\Delta}{\rho g b^3}$

C_{Δ_0} gross-load coefficient, $\frac{W}{\rho g b^3}$

C_V speed coefficient, $\frac{\dot{x}_w}{\sqrt{g b}}$

Subscripts:

a about any point a

c at instant of chine immersion

e effective

h hull model

H horizontal

max maximum

N normal to keel

0 at instant of initial contact with water surface

R resultant

s at or about step

T total

V vertical

Generalized variables:

κ approach parameter, $\frac{\sin \tau}{\sin \gamma_0} \cos(\tau+\gamma_0)$

u generalized displacement, $\zeta_s\Gamma$ or $z_w\Lambda$

u' generalized velocity, $\frac{\dot{\zeta}_s}{\dot{\zeta}_{s_0}}$ or $\frac{\dot{z}_w}{\dot{z}_{w_0}}$

u'' generalized acceleration, $\frac{\ddot{z}_k}{\dot{\zeta}_{s_0}^2\Gamma}$ or $\frac{\ddot{z}_w}{\dot{z}_{w_0}^2\Lambda}$

σ generalized time, $t\dot{\zeta}_{s_0}\Gamma$ or $t\dot{z}_{w_0}\Lambda$

m generalized pitching moment, $\frac{M}{\dot{\zeta}_{s_0}^2}\frac{\phi(A)}{\phi_1(A)}\frac{\tan\tau}{W/g}$ or $\frac{M}{\dot{z}_{w_0}^2}\frac{\phi(A)}{\phi_1(A)}\frac{\sin\tau\cos\tau}{W/g}$

p generalized center-of-pressure distance, $l_{cp}\tan\tau\frac{\phi(A)}{\phi_1(A)}\Gamma$ or $l_{cp}\sin\tau\frac{\phi(A)}{\phi_1(A)}\Lambda$

r generalized ratio of center-of-pressure distance to wetted keel length, $\frac{l_{cp}}{l_k}\frac{\phi(A)}{\phi_1(A)}$

u_c chine-immersion parameter, equal to generalized displacement at instant of chine immersion, $\frac{\Pi}{C_{\Delta_0}^{1/3}}$

In the foregoing definitions for the generalized variables,

$$\Gamma=\left[\frac{\epsilon(\beta)\,\phi(A)\,\rho}{3\frac{W}{g}\tan\tau}\right]^{1/3}$$

$$\Lambda=\left[\frac{\epsilon(\beta)\ \phi(A)\ \rho}{3\ \frac{W}{g}\sin\ \tau\ \cos^2\ \tau}\right]^{1/3}$$

and

$$\Pi=\left\{\frac{[\psi(\beta)]^3\epsilon(\beta)\ \phi(A)}{3\ \tan\ \tau}\right\}^{1/3}$$

Axes:

x_k,z_k respectively parallel and perpendicular to keel line, positive forward and downward; origin at point of initial contact with water surface

x_w,z_w respectively parallel and perpendicular to water surface, positive forward and downward; origin at point of initial contact with water surface

ξ,ζ respectively parallel and perpendicular to keel line, positive forward and upward; origin at step-keel point

Derivatives:

The use of dots over a variable denotes differentiation with respect to time t; prime marks indicate differentiation with respect to generalized time σ.

THEORY

TWO-DIMENSIONAL CONSIDERATIONS

The classical impact theory of Von Kármán for vertical impact of a wedge at zero trim (ref. 4), upon which much subsequent work appears to be founded, was based on the concept that during the course of an impact the momentum lost by the impacting body can be considered to be transferred to some finite mass of water in contact with the body, which has a downward velocity equal to that of the body. This fictitious mass of water has been variously termed the "virtual mass," "associated mass," "equivalent mass," or "apparent mass" of the water. Since the entire initial momentum of the body is thus assumed to be distributed between the body and the virtual mass, the momentum of the body and the virtual mass is constant throughout the impact, and the motions of the body subsequent to the instant of initial contact can be determined from the basic relationship

$$\frac{W}{g}\dot{\zeta}_0=\left(\frac{W}{g}+m_w\right)\dot{\zeta}$$

if the variation of the virtual mass m_w is specified.

Von Kármán proposed that the virtual mass be taken equal to the mass of a semicylinder of water having a diameter equal to the instantaneous width of the body in the plane of the undisturbed water surface. This treatment assumes the virtual mass to be the same as that on one side (one-half the total mass) of a flat plate equal in width to the intersected width of the body and moving in an unbounded fluid. Wagner attempted to obtain improved values for the virtual mass by taking into account the rise of the water surface (see fig. 1 (a)) which is generated in the vicinity of the body during the impact and references 5 and 6 determined two different solutions for the virtual mass which were derived by separate methods.

The treatments by Von Kármán, Wagner, and Pabst (ref. 7), as well as most other investigations published prior to about 1940, although differing in some details, have one important hypothesis in common—namely, that the momentum of the seaplane and its "attached" virtual mass is constant throughout the impact. This concept is valid for the vertical impact of a hull at zero trim and is also applicable to the impact of a hull with a finite trim angle, provided the resultant velocity is normal to the keel, since, in both cases, the momentum lost by the hull is transmitted to the water which remains in contact with the hull throughout the impact. The concept is not valid, however, whenever a component of velocity parallel to the keel is present, as in impacts of conventional seaplanes, since the motion of the hull along its axis causes a loss of momentum to the downwash behind the step, thus violating the assumption of momentum conservation between the hull and its attached virtual mass.

THREE-DIMENSIONAL CASE

Basic assumptions.—The general three-dimensional problem is concerned with the case of an oblique impact of a wedge-shaped body at a finite trim angle. The resultant velocity may make any angle with the keel and with the water surface. In the present analysis the trim angle is considered to be constant throughout the impact. As in reference 1, it is assumed that the primary flow about an immersing slender shape, such as a keeled seaplane float or hull, occurs in transverse flow planes which may be considered fixed in space and oriented essentially perpendicular to the keel. (See fig. 1.) Because of the absence of a satisfactory three-dimensional theory, the motion of the fluid in each flow-plane element is treated as a two-dimensional phenomenon and is assumed to be independent of that in the other flow planes. In order to account for the effects of longitudinal components of flow and end losses that exist in the three-dimensional case, the total hydrodynamic forces and moments on the seaplane, which are obtained by integrating the reactions of the individual flow-plane elements in contact with the hull, are somewhat modified (reduced) by application of an aspect-ratio type of correction. The effects of gravitational and viscous forces, which in an impact are normally small in comparison with the inertia forces, are neglected.

Momentum considerations.—The flow process within a particular stationary flow-plane element begins when the keel penetrates the water surface and enters that flow-plane element. At all times thereafter, the momentum imparted to the water in the flow plane is determined solely by the growth of the hull cross-sectional shape intersected by the flow plane and may be expressed as the product of the virtual mass associated with the immersed cross section and the velocity of penetration into the flow plane (velocity normal to the keel), that is, Momentum$=m_w\dot{\zeta}$, as in the two-dimensional case. In the three-dimensional case, however, after the step has passed through a given flow plane due to the

component of motion along the axis of the hull, the intersected cross section ceases to exist and the plane and the momentum contained therein become part of the wake or downwash behind the step where they remain thereafter, independent of the subsequent progress of the impact.

In the case of a prismatic body, the component of velocity parallel to the keel has no effect on the amount of momentum contained in the fluid within each of the flow planes in contact with the hull but does determine the number of flow planes left behind and, therefore, the distribution of momentum between the water still in contact with the hull and the downwash behind the step. As a result, the time history of the motion of the seaplane during impact is greatly influenced by the magnitude of the velocity parallel to the keel since the motion is governed not solely by the amount of momentum transferred to the water directly in contact with the hull bottom (virtual mass) but by the total transfer of momentum. In other words, conservation of momentum exists not just between the body and its "attached" virtual mass, as in the two-dimensional case, but between the body, the virtual mass, and the downwash. Herein lies the essential difference between the classical two-dimensional approach to the seaplane-impact problem and the practical three-dimensional phenomenon.

Hydrodynamic reactions.—The previous section discussed the impact process from the momentum standpoint. The behavior of the seaplane can also be analyzed by consideration of the hydrodynamic reactions produced by the impact.

The instantaneous reaction of the fluid contained in a given flow-plane element is determined by the rate at which momentum is imparted to the fluid within the flow plane; therefore, on a two-dimensional basis, the hydrodynamic force in a flow plane is given by

$$f=\frac{d}{dt}(\text{Momentum in flow plane})$$

$$=\frac{d}{dt}(m_w\dot{\zeta})$$

$$=\frac{dm_w}{dt}\dot{\zeta}+m_w\ddot{\zeta} \tag{1}$$

In the case of a prismatic body, since viscous forces are considered negligible, the force contributed by a particular flow-plane element is normal to the keel and is independent of the velocity parallel to the keel. As shown by equation (1), the hydrodynamic reaction in the flow-plane element is governed solely by the rate of growth of the virtual mass associated with the intersected cross section, by the instantaneous magnitude of the virtual mass, and by the components of velocity and acceleration normal to the keel.

Although the force in any given flow plane is unaffected by the motion parallel to the keel, the total hydrodynamic force on the hull at any instant, on the other hand, does depend greatly on the component of velocity parallel to the keel since this component, in conjunction with the velocity normal to the keel, governs the degree of penetration relative to the water surface of the hull as a whole and, therefore, the wetted length and the number of flow-plane elements in contact with the hull bottom at any given instant. Since the only elements capable of producing reactions on the hull are those in contact with the hull, the importance of the velocity parallel to the keel, with regard to both the instantaneous force as well as the time-history behavior of the seaplane, is again established.

As previously indicated, considerations of the hydrodynamic reactions rather than of momentum conservation are employed to derive the basic equations upon which the mathematical development of the present report is based. The same results can be obtained, of course, by either approach.

Virtual mass.—The analysis of the impact process, whether by consideration of hydrodynamic reactions or conservation of momentum, requires the determination of the virtual mass of the immersed part of the hull. As previously indicated, this is accomplished in the present analysis by summing up the two-dimensional increments of virtual mass associated with the intersected hull cross sections and applying an overall aspect-ratio type of correction factor to take into account deviations from the idealized representation considered.

In potential flow, the two-dimensional virtual mass of any hull cross section is determined by the size and the shape of the intersected cross section immersed in the flow plane. In the case of straight-sided V-shaped cross sections, if the chines are not immersed, the flow patterns at all degrees of penetration are geometrically similar. Thus, any characteristic dimension which may be used to represent the geometric size of the virtual mass is directly proportional to the penetration, and the magnitude of the virtual mass is consequently proportional to the square of the penetration. The proportionality factor $\epsilon(\beta)$ is determined by the dead-rise angle β. The two-dimensional virtual mass of any V-shaped cross section may therefore be defined as

$$m_w=\epsilon(\beta)\ \rho\zeta^2 \tag{2}$$

where ρ is the mass density of the fluid and ζ is the penetration normal to the keel. If the virtual mass is interpreted in terms of an equivalent circular semicylinder of water, as has been done in many papers,

$$m_w=[f(\beta)]^2\frac{\rho\pi}{2}\zeta^2 \tag{2a}$$

where the quantity $f(\beta)\zeta$ represents the radius of the equivalent semicylinder. With this interpretation

$$\epsilon(\beta)=[f(\beta)]^2\frac{\pi}{2}$$

The correction factors representing the reductions in total force and pitching moment due to finite aspect ratio in the three-dimensional case may, for the present, be written as $\phi(A)$ and $\phi_1(A)$, respectively. Since the quantities $\epsilon(\beta)$, $f(\beta)$, $\phi(A)$, and $\phi_1(A)$ are constant during an impact of a prismatic V-shaped body at fixed trim, the mathematical derivations and the general solutions of the equations of motion are independent of the explicit forms of the functions. The first part of the analysis is therefore carried out in terms of the foregoing undefined functional notation in order to

keep the over-all treatment general and to permit use of improved functions as a better understanding of the flow phenomenon is obtained. In a subsequent section of the report, explicit expressions for the dead-rise-angle variation and the aspect-ratio correction factors, derived from previous work, are suggested and discussed in order to permit direct application of the basic theoretical results to the prediction of the motions, forces, and moments experienced by any given V-bottom seaplane during a step impact.

GENERAL RELATIONSHIPS DURING IMPACT

On the basis of the foregoing theoretical concepts, an analysis is made to determine the motions, hydrodynamic loads, and pitching moments encountered by a V-bottom seaplane during a step impact. The analysis applies equally to a first impact or to a subsequent impact occurring after the seaplane has rebounded from the water surface, provided the initial conditions are taken at the beginning of the impact under consideration. Since conventional seaplane floats and hulls are essentially prismatic for an appreciable distance forward of the step, the analysis is carried out under the assumption that the immersed part of the body has constant cross section. The trim angle is assumed to remain essentially constant during the relatively short duration of the impact.

Figure 1 (b) shows a schematic representation of a seaplane with a prismatic bottom in the process of immersion during an impact at a positive trim angle τ. The water beneath the keel is considered to be divided into flow-plane elements of thickness $d\xi$ which are fixed in space and oriented normal to the keel. Two sets of stationary axes and one set of moving axes are shown. The axes x_w and z_w are taken parallel and perpendicular to the water surface, respectively, with positive directions as shown and with the origin fixed at the point of initial contact between the step and the water surface. The axes x_k and z_k are taken parallel and perpendicular to the keel line, with origin fixed at the point of initial contact. The axes ξ and ζ move with the seaplane and are taken parallel and perpendicular to the keel, with origin at the step-keel point.

The coordinates x_w, z_w, x_k, and z_k denote displacements of the step-keel point relative to the point of initial contact. The coordinate ξ denotes the distance between the step and any given fixed flow plane. The penetration into any such flow plane is given by ζ, which represents the distance from the keel to the undisturbed water surface in the flow plane. The penetration at the step is designated by the dimension ζ_s which moves with the body. The wetted keel length is represented by l_k.

DYNAMICAL RELATIONSHIPS

Instantaneous force.—In accordance with the previous discussion, the reaction of the fluid in any given flow-plane element to the motion of the body is given by equation (1):

$$f=\frac{dm_w}{dt}\frac{d\zeta}{dt}+m_w\frac{d^2\zeta}{dt^2}$$

The total hydrodynamic force on the body, which acts normal to the keel, is the sum of the reactions of all the flow planes in contact with the body. Integrating along the wetted keel length and applying the aspect-ratio factor $\phi(A)$ as an over-all correction for end-flow losses gives

$$F_N=\phi(A)\int_0^{l_k} f\,d\xi=\phi(A)\left(\int_0^{l_k}\frac{dm_w}{dt}\frac{d\zeta}{dt}\,d\xi+\int_0^{l_k} m_w\frac{d^2\zeta}{dt^2}\,d\xi\right)$$

The two-dimensional virtual mass was previously expressed in terms of the penetration into the flow plane by

$$m_w=\epsilon(\beta)\,\rho\,\zeta^2$$

Therefore,

$$\frac{dm_w}{dt}=2\,\epsilon(\beta)\,\rho\,\zeta\frac{d\zeta}{dt}$$

Substituting for m_w and $\frac{dm_w}{dt}$ and bringing to the outside of the integrals the terms that are constant along the length permits the equation for the total force to be written as

$$F_N=2\,\epsilon(\beta)\,\phi(A)\,\rho\left(\frac{d\zeta}{dt}\right)^2\int_0^{l_k}\zeta\,d\xi+\epsilon(\beta)\,\phi(A)\,\rho\frac{d^2\zeta}{dt^2}\int_0^{l_k}\zeta^2\,d\xi$$

Since $\zeta=(l_k-\xi)\tan\tau$ and $l_k=\frac{\zeta_s}{\tan\tau}$ from geometric considerations, substituting and performing the indicated integrations gives

$$F_N=\frac{\epsilon(\beta)\,\phi(A)\,\rho}{3\tan\tau}\left[3\zeta_s^2\left(\frac{d\zeta}{dt}\right)^2+\zeta_s^3\frac{d^2\zeta}{dt^2}\right]$$

From figure 1(b) it can be seen that $\frac{\zeta}{\tan\tau}=\frac{z_k}{\tan\tau}-(x_k+\xi)$. Since each flow-plane element is considered fixed in space, the distance $(x_k+\xi)$ is constant with respect to time; therefore, differentiating with respect to time gives

$$\frac{d\zeta}{dt}=\frac{dz_k}{dt}=\dot{z}_k$$

and

$$\frac{d^2\zeta}{dt^2}=\frac{d^2z_k}{dt^2}=\ddot{z}_k$$

These simple kinematic relationships are, of course, evident by inspection since, for a straight-line keel, motion parallel to the keel has no effect on the value of ζ in any given flow plane in contact with the keel. Therefore, the equation for the total hydrodynamic force becomes

$$F_N=\frac{\epsilon(\beta)\,\phi(A)\,\rho}{3\tan\tau}\left(3\zeta_s^2\dot{z}_k^2+\zeta_s^3\ddot{z}_k\right)\qquad(3)$$

Equations of motion.—The motions of the seaplane during impact can be analyzed by treating the seaplane as a free body and applying Newton's second law. If the wing lift is assumed constant and equal to the weight of the seaplane, the hydrodynamic force must be equal to the inertia reaction and the equation of motion for the seaplane is given by

$$F_N=-\frac{W}{g}\ddot{z}_k=\frac{\epsilon(\beta)\,\phi(A)\,\rho}{3\tan\tau}\left(3\zeta_s^2\dot{z}_k^2+\zeta_s^3\ddot{z}_k\right)\qquad(4)$$

which expresses the instantaneous relationship among the motion variables at any time during the impact. In applying equation (4) it is important to bear in mind that, due to the effect of the component of velocity parallel to the keel, $\dot{z}_k$ is not equal to the first derivative of ζ_s in the general case of an impact where the resultant velocity is oblique to the keel. Only when the resultant velocity is normal to the keel is $\dot{z}_k$ equal to $\dot{\zeta}_s$.

The behavior of the seaplane can be analyzed either in terms of the coordinate system oriented with respect to the keel or in terms of the coordinates relative to the water surface. The first approach is valuable for correlation with flight-test data obtained with airborne instrumentation, whereas the second approach is useful when dealing with data obtained in laboratory testing where measurements are normally taken with respect to the water surface. For the purposes of this report, the basic equations of motion are derived in terms of both sets of coordinates.

(a) Coordinates oriented with respect to the keel:

Equation (4) can be written as

$$(1+\Gamma^3\zeta_s^3)\ddot{z}_k+3\Gamma^3\zeta_s^2\dot{z}_k^2=0 \tag{4a}$$

where

$$\Gamma=\left[\frac{\epsilon(\beta)\,\phi(A)\,\rho}{3\dfrac{W}{g}\tan\tau}\right]^{1/3}$$

From figure 1(b) it can be seen that

$$z_k=\zeta_s+x_k\tan\tau$$

Thus,

$$\dot{z}_k=\dot{\zeta}_s+\dot{x}_k\tan\tau$$

Since the resultant force is normal to the keel, the velocity parallel to the keel $\dot{x}_k$ is constant throughout the impact and is equal to the initial value $\dot{x}_{k_0}$; therefore,

$$\dot{z}_k=\dot{\zeta}_s+\dot{x}_{k_0}\tan\tau$$

and

$$\ddot{z}_k=\ddot{\zeta}_s$$

Substituting for $\dot{z}_k$ and $\ddot{z}_k$ in equation (4a) gives

$$(1+\Gamma^3\zeta_s^3)\ddot{\zeta}_s+3\Gamma^3\zeta_s^2\left(\dot{\zeta}_s+\dot{x}_{k_0}\tan\tau\right)^2=0 \tag{5}$$

Since $\ddot{\zeta}_s=\dot{\zeta}_s\dfrac{d\dot{\zeta}_s}{d\zeta_s}$, equation (5) can be readily integrated between limits by direct quadrature in the following form:

$$\int_{\dot{\zeta}_{s_0}}^{\dot{\zeta}_s}\frac{\dot{\zeta}_s\,d\dot{\zeta}_s}{\left(\dot{\zeta}_s+\dot{x}_{k_0}\tan\tau\right)^2}+\int_0^{\zeta_s}\frac{3\Gamma^3\zeta_s^2 d\zeta_s}{1+\Gamma^3\zeta_s^3}=0$$

This integration gives

$$\log_e\left[(1+\Gamma^3\zeta_s^3)\frac{\dot{\zeta}_s+\dot{x}_{k_0}\tan\tau}{\dot{\zeta}_{s_0}+\dot{x}_{k_0}\tan\tau}\right]+$$

$$\dot{x}_{k_0}\tan\tau\left(\frac{1}{\dot{\zeta}_s+\dot{x}_{k_0}\tan\tau}-\frac{1}{\dot{\zeta}_{s_0}+\dot{x}_{k_0}\tan\tau}\right)=0$$

or, in terms of $\dot{z}_k$,

$$(1+\Gamma^3\zeta_s^3)\frac{\dot{z}_k}{\dot{z}_{k_0}}e^{\dot{x}_{k_0}\tan\tau\left(\frac{1}{\dot{z}_k}-\frac{1}{\dot{z}_{k_0}}\right)}-1=0 \tag{6}$$

The foregoing equations permit the determination of the velocity, the displacement, and the acceleration (or hydrodynamic force) encountered by the seaplane throughout the course of an impact for any given initial conditions $\dot{x}_{k_0}$ and $\dot{z}_{k_0}$. By assuming successive values of the normal velocity $\dot{z}_k<\dot{z}_{k_0}$, the normal penetration of the step ζ_s and the normal acceleration $\ddot{z}_k$ during the impact can be calculated from equations (6) and (4a), respectively. Since integration of equation (6) in closed form does not appear feasible, the corresponding values of the time after contact can be determined by numerical or graphical integration as indicated by

$$t=\int_0^{\zeta_s}\frac{d\zeta_s}{\dot{\zeta}_s}$$

or

$$t=\int_{\dot{z}_{k_0}}^{\dot{z}_k}\frac{d\dot{z}_k}{\ddot{z}_k}$$

(b) Coordinates oriented with respect to the water surface:

Since the resultant force is normal to the keel

$$F_V=F_N\cos\tau \tag{7}$$

In order to write the equation for F_N in terms of the coordinates relative to the water surface, it is necessary to substitute the respective relationships between ζ_s, $\dot{z}_k$, $\ddot{z}_k$ and z_w, $\dot{z}_w$, $\ddot{z}_w$ into equation (4).

From figure 1 (b) it is evident from geometric considerations that

$$\zeta_s=\frac{z_w}{\cos\tau} \tag{8}$$

It can also be seen that

$$\dot{z}_k=\dot{z}_w\cos\tau+\dot{x}_w\sin\tau$$

and

$$\dot{x}_k=\dot{x}_w\cos\tau-\dot{z}_w\sin\tau$$

Combining the expressions for $\dot{z}_k$ and $\dot{x}_k$ to eliminate $\dot{x}_w$ gives

$$\dot{z}_k=\frac{\dot{z}_w}{\cos\tau}+\dot{x}_k\tan\tau$$

Since $\dot{x}_k=\dot{x}_{k_0}$ is a constant,

$$\dot{z}_k=\frac{\dot{z}_w}{\cos\tau}+\dot{x}_{k_0}\tan\tau \tag{8a}$$

and, differentiating equation (8a) gives

$$\ddot{z}_k=\frac{\ddot{z}_w}{\cos\tau} \tag{8b}$$

This result is, of course, immediately evident by inspection since the resultant acceleration, like the resultant force, is normal to the keel.

Substituting equations (8), (8a), and (8b) into equation (4) and applying equation (7) permits the vertical force to be expressed as

$$F_V=-\frac{W}{g}\ddot{z}_w=\frac{\epsilon(\beta)\,\phi(A)\,\rho}{3\sin\tau\cos^2\tau}\left[3z_w^2(\dot{z}_w+\dot{x}_{k_0}\sin\tau)^2+z_w^3\ddot{z}_w\right] \quad (9)$$

or

$$(1+\Lambda^3 z_w^3)\ddot{z}_w+3\Lambda^3 z_w^2(\dot{z}_w+\dot{x}_{k_0}\sin\tau)^2=0 \quad (9a)$$

where

$$\Lambda=\left[\frac{\epsilon(\beta)\,\phi(A)\,\rho}{3\frac{W}{g}\sin\tau\cos^2\tau}\right]^{1/3}=\frac{\Gamma}{\cos\tau}$$

and

$$\dot{x}_{k_0}=\dot{x}_{w_0}\cos\tau-\dot{z}_{w_0}\sin\tau=\text{Constant}$$

Integrating equation (9a) by quadrature or transforming coordinates in equation (6) gives

$$(1+\Lambda^3 z_w^3)\frac{\dot{z}_w+\dot{x}_{k_0}\sin\tau}{\dot{z}_{w_0}+\dot{x}_{k_0}\sin\tau}\,e^{\dot{x}_{k_0}\sin\tau\left(\frac{1}{\dot{z}_w+\dot{x}_{k_0}\sin\tau}-\frac{1}{\dot{z}_{w_0}+\dot{x}_{k_0}\sin\tau}\right)}-1=0 \quad (10)$$

The motions of the seaplane during impact can be determined by assuming arbitrary values of $\dot{z}_w<\dot{z}_{w_0}$ and calculating corresponding values of z_w and $\ddot{z}_w$ from equations (10) and (9a), respectively. The corresponding values of time after contact can be determined by numerical or graphical integration as indicated by

$$t=\int_0^{z_w}\frac{dz_w}{\dot{z}_w}$$

or

$$t=\int_{\dot{z}_{w_0}}^{\dot{z}_w}\frac{d\dot{z}_w}{\ddot{z}_w}$$

As can be seen, equations (4a) and (9a) and equations (6) and (10) have essentially the same form, as might be expected.

Although the problem treated in the present analysis involves some seven physical constants, such as β, τ, W, and the initial velocity components, it can be seen from equations (4a) and (6) and equations (9a) and (10) that the motions of the seaplane during an impact are governed by a set of three combined dimensional constants. In the x_k,z_k coordinate system, these combined constants are Γ, $\dot{z}_{k_0}$, and $\dot{x}_{k_0}\tan\tau$; in the x_w,z_w coordinate system, the constants are Λ, $\dot{z}_{w_0}$, and $\dot{x}_{k_0}\sin\tau=(\dot{x}_{w_0}\cos\tau-\dot{z}_{w_0}\sin\tau)\sin\tau$. Thus, for any given set of values of these constants, identical motions will result regardless of the individual values of the primary physical constants which comprise the combined constants.

The constants Γ and Λ are configuration factors such that $\Gamma^3\zeta_s^3$ and $\Lambda^3 z^3$ represent the instantaneous ratio of the virtual mass at any penetration to the mass of the seaplane. The quantities $\frac{\epsilon(\beta)\,\phi(A)}{3\tan\tau}$ and $\frac{\epsilon(\beta)\,\phi(A)}{3\sin\tau\cos^2\tau}$ which are contained in Γ and Λ, respectively, are shape factors determined by the geometry of the immersed part of the hull, such that $\frac{\epsilon(\beta)\,\phi(A)\,\rho}{3\tan\tau}\zeta_s^3$ and $\frac{\epsilon(\beta)\,\phi(A)\,\rho}{3\sin\tau\cos^2\tau}z_w^3$ are equal to the total virtual mass. If the virtual mass in any flow-plane element is interpreted in terms of the mass of a semicylindrical disk of fluid, as is often done, then the total virtual mass is the sum of these mass elements and may be considered as the mass contained in an equivalent half-cone of fluid. If the length of the equivalent half-cone is taken equal to the wetted keel length, then the area of the half-cone at the step is given in terms of the normal penetration of the step by $\epsilon(\beta)\,\phi(A)\,\zeta_s^2$, which includes the reduction due to end-flow losses, applied uniformly along the length.

The quantities $\dot{x}_{k_0}\tan\tau$ and $\dot{x}_{k_0}\sin\tau$ are, respectively, increments of velocity normal to the keel and normal to the water surface produced by the motion of the hull parallel to the keel. The component of velocity parallel to the keel, which is a constant during the impact, causes the immersed part of the hull, for a given displacement of the hull in the direction perpendicular to the keel, to be smaller than that which would exist if there were no longitudinal velocity component. As a result, there is a smaller virtual mass and a smaller force acting on the hull and a transfer of momentum to the downwash behind the step, as previously discussed. Consideration of the effects of the velocity component parallel to the keel in the analysis makes the foregoing equations, either in terms of the x_k,z_k coordinates or the x_w,z_w coordinates, applicable to the entire range of flight-path angles between 0° (limiting condition of planing) and 90° (resultant velocity normal to keel).

Generalized relationships.—In the preceding section, solutions for the motions of a seaplane during an impact were presented in terms of the relationships among the dimensional variables of displacement, velocity, acceleration, and time. It was also shown that the variation of these dimensional variables during an impact is governed by the values of a set of three combined dimensional constants. Since each one of these combined constants may take on any of a large range of values, depending on the geometric and mass characteristics of the seaplane and the impact conditions under consideration, a large number of solutions and graphs would be required in order to cover the complete range of seaplane and impact parameters.

In order to decrease the number of independent constants which have to be considered, the equations may be generalized by replacing the dimensional variables by suitable generalized dimensionless variables. These particular dimensionless variables are called generalized variables to distinguish them from the more restricted dimensionless variables which can be obtained by means of pure dimensionless analysis. The form of these generalized variables cannot be determined by dimensional analysis alone, since dimensional analysis without the equations of motion cannot reveal the laws of variation with those parameters, such as $\epsilon(\beta)$, τ, and γ_0, which are dimensionless quantities to begin with.

The introduction of these generalized variables permits the relationships among the motion and time variables during impacts under different sets of conditions to be reduced to a common basis; thus, fewer solutions are required to cover the entire range of seaplane and impact

parameters, and the presentation and correlation of both theoretical and experimental results is greatly simplified.

The generalized variables to be introduced are u the generalized displacement, u' the generalized velocity, u'' the generalized acceleration, and σ the generalized time.[2] The same generalized variables will be shown to apply equally to both the x_k,z_k and the x_w,z_w coordinate systems. The derivation makes use of the following relationships which have previously been determined:

$$A=\frac{\Gamma}{\cos\tau}$$

$$\zeta_s=\frac{z_w}{\cos\tau}$$

$$\dot{\zeta}_s=\dot{z}_k-\dot{x}_{k_0}\tan\tau=\frac{\dot{z}_w}{\cos\tau}$$

$$\ddot{\zeta}_s=\ddot{z}_k=\frac{\ddot{z}_w}{\cos\tau}$$

$$\dot{\zeta}_{s_0}=\dot{z}_{k_0}-\dot{x}_{k_0}\tan\tau=\frac{\dot{z}_{w_0}}{\cos\tau}$$

and

$$\dot{x}_{k_0}=\dot{x}_{w_0}\cos\tau-\dot{z}_{w_0}\sin\tau$$

In order to generalize the equations of motion, let

$$u=\zeta_s\Gamma=z_wA \tag{11}$$

and

$$\sigma=t\dot{\zeta}_{s_0}\Gamma=t\dot{z}_{w_0}A \tag{12}$$

It therefore follows that

$$u'=\frac{du}{d\sigma}=\frac{\dot{\zeta}_s}{\dot{\zeta}_{s_0}}=\frac{\dot{z}_w}{\dot{z}_{w_0}} \tag{13}$$

and

$$\left.\begin{aligned}u''&=\frac{d^2u}{d\sigma^2}\\&=\frac{\ddot{\zeta}_s}{\dot{\zeta}_{s_0}^2\Gamma}=\frac{\ddot{z}_k}{\dot{\zeta}_{s_0}^2\Gamma}=\frac{n_{t_k}g}{\dot{\zeta}_{s_0}^2\Gamma}=-\frac{F_N}{\dot{\zeta}_{s_0}^2\frac{W}{g}\Gamma}\\&=\frac{\ddot{z}_w}{\dot{z}_{w_0}^2A}=-\frac{n_{t_w}g}{\dot{z}_{w_0}^2A}=-\frac{F_V}{\dot{z}_{w_0}^2\frac{W}{g}A}\end{aligned}\right\} \tag{14}$$

where $n_{t_k}=-\frac{\ddot{z}_k}{g}$ and $n_{t_w}=-\frac{\ddot{z}_w}{g}$.

[2] The symbols and the terminology used to designate the generalized variables in the present report differ from those employed in references 2 and 3 and in a number of subsequent papers based on these references. The new system of notation has been adopted for greater clarity and convenience in the mathematical development and the terminology has been made to correspond more closely with that generally used in the field of dynamics. The symbol u in the present report corresponds to the former symbol C_d which was termed the "draft coefficient"; u' was previously designated $\dot{y}/\dot{y}_0$ and termed the "velocity ratio"; u'' corresponds to $-C_l$ where C_l was termed the "load-factor coefficient"; σ was previously designated C_t and termed the "time coefficient."

If the generalized variables u, u', u'', and σ are substituted for the dimensional variables, equations (4a) and (9a) both reduce to the same equation, namely

$$(1+u^3)u''+3u^2(u'+\kappa)^2=0 \tag{15}$$

where

$$\left.\begin{aligned}\kappa&=\frac{\dot{x}_{k_0}\tan\tau}{\dot{\zeta}_{s_0}}=\frac{\dot{x}_{k_0}\tan\tau}{\dot{z}_{k_0}-\dot{x}_{k_0}\tan\tau}\\&=\frac{\dot{x}_{k_0}\sin\tau}{\dot{z}_{w_0}}=\left(\frac{\dot{x}_{w_0}}{\dot{z}_{w_0}}\cos\tau-\sin\tau\right)\sin\tau\\&=\frac{\sin\tau}{\sin\gamma_0}\cos(\tau+\gamma_0)\end{aligned}\right\} \tag{16}$$

and

$$\gamma_0=\tan^{-1}\frac{\dot{z}_{w_0}}{\dot{x}_{w_0}}$$

Similar substitution reduces equations (6) and (10) to the following equation:

$$(1+u^3)\frac{u'+\kappa}{1+\kappa}e^{\kappa\left(u'^{+\kappa}-\frac{1}{1+\kappa}\right)}-1=0 \tag{17}$$

Equations (15) and (17) show that the motions of the seaplane, with reference to either the x_k, z_k or the x_w, z_w coordinate systems, can be expressed in terms of generalized variables which are related to one another at all instants during the course of an impact by a single dimensionless parameter κ, called the approach parameter, which is determined by the trim angle τ and the flight-path angle γ_0 at the instant of initial contact. Since all generalized variables corresponding to the same instant are uniquely related through κ, for any given value of κ there is a single relationship between any two of these variables during the impact, regardless of the individual values of the constants representing the seaplane properties, attitude, and initial velocities. Thus, the relationship between any two of the generalized variables during an impact can be represented by a single curve for each value of κ. Furthermore, a single variation with κ exists for each of the generalized variables representing the state of motion and the time corresponding to any given stage of the impact, such as the instant of maximum acceleration, maximum penetration, and so forth.

For a given value of κ, the form of each of the generalized variables shows how variations in the physical constants, such as the seaplane weight, dead-rise angle, trim angle, flight-path angle, initial velocity, and water density, affect the values of the dimensional variables at any given stage of the impact. Since the generalized treatment, by taking into account the individual effects of the various seaplane characteristics and impact conditions, in accordance with the laws governing the variation of the motion with these quantities, permits reduction of all time histories for the same value of κ to a common basis, κ may, in this sense, be considered as a criterion of impact similarity.

A graph of κ, in terms of the trim angle and the initial

flight-path angle, is presented in figure 2. For research purposes, laboratory tests may be made at values of κ ranging from zero for impacts where the resultant velocity is normal to the keel ($\gamma_0=90°-\tau$; near-vertical-drop condition) to values approaching infinity at the limiting condition of planing. In smooth water, γ_0 and τ are referred to the horizontal plane. As indicated in references 8 and 9, the motion of the seaplane in seaway may be approximated by rotating the axes and taking the initial conditions relative to the wave surface. Although statistical data showing the frequency of occurrence of the initial conditions encountered in normal seaplane operations are not available, the practical range of values of the approach parameter for conventional seaplanes is probably between $\kappa=0.2$ and $\kappa=10$.

The relationship between the generalized displacement and the generalized velocity, as obtained from equation (17), is given by

$$u=\left[\frac{1+\kappa}{u'+\kappa}e^{\kappa\left(\frac{1}{1+\kappa}-\frac{1}{u'+\kappa}\right)}-1\right]^{1/3} \tag{17a}$$

Since, from equation (15),

$$u''=-\frac{3u^2(u'+\kappa)^2}{1+u^3} \tag{15a}$$

the relationship between the generalized acceleration and the generalized velocity is given by

$$u''=-3(u'+\kappa)^2\left\{\frac{u'+\kappa}{1+\kappa}e^{\kappa\left(\frac{1}{u'+\kappa}-\frac{1}{1+\kappa}\right)}\left[1-\frac{u'+\kappa}{1+\kappa}e^{\kappa\left(\frac{1}{u'+\kappa}-\frac{1}{1+\kappa}\right)}\right]^2\right\}^{1/3} \tag{18}$$

By assuming successively smaller values of the generalized velocity $u'<1$, corresponding simultaneous values of the generalized displacement u and the generalized acceleration u'' throughout the course of an impact can be calculated from equations (17a) and (15a), respectively, for any given value of the approach parameter κ.

On the basis of the foregoing equations, figures 3 to 5 show the relationships between the generalized motion variables during impact for values of κ covering a large range of seaplane parameters and initial conditions.

Since further integration of the equations of motion in analytical form does not appear feasible, numerical or graphical integration as indicated by

$$\sigma=\int_0^u\frac{du}{u'}$$

or

$$\sigma=\int_1^{u'}\frac{du'}{u''}$$

can be employed to determine the generalized time corresponding to the instant at which any given set of the generalized motion variables exists. Figures 6 to 8 present generalized time histories of the motion variables from the instant of initial contact until the instant of exit during rebound, based on the equations presented in this section.

In applying figures 3 to 8 to particular problems involving intermediate values of κ, interpolation of the calculated curves should provide sufficient accuracy for most practical purposes. Since the generalized acceleration-time curves cross one another, interpolation of these curves may be facilitated by construction of an auxiliary graph of $\frac{u''}{u''_{max}}$ against $\frac{\sigma}{\sigma_{(u''_{max})}}$ to be used in conjunction with curves of u'' and σ corresponding to the instant of maximum acceleration.

As can be seen from figures 3 to 8, the equations of motion yield double-valued functions for $u'(u)$, $u''(u)$, and $\sigma(u)$. This result is due to the fact that each value of u is reached twice during an impact: once while the seaplane is on the way down into the water (u' positive) and once while on the way out (u' negative). The functions $u(u'')$, $u'(u'')$, and $\sigma(u'')$ are also double-valued since u'' is zero at the instant of initial contact, increases to a maximum, and then drops to zero again at the instant of exit as the seaplane rebounds from the surface of the water.

MOMENT RELATIONSHIPS

As shown by equation (1) the force contributed by a given flow-plane element may be considered to arise from two sources; namely, the rate of change of momentum accompanying the expansion of the virtual mass with penetration into the flow plane and the inertia reaction associated with the acceleration of the virtual mass. For a prismatic hull at positive trim, under the assumption of two-dimensional flow within the flow planes, the force due to the expansion of the virtual mass is linearly distributed along the keel, whereas the inertia reaction of the virtual mass follows a quadratic variation. (See fig. 1 (b).) The shape of the longitudinal distribution of the total force in each flow plane during an impact is, of course, determined by the relative magnitudes of the component distributions. For example, in the case of steady-state planing, since there is no acceleration, the total force is linearly distributed along the keel and the center of pressure is located at a distance equal to one-third the wetted length forward of the step.

Under actual three-dimensional conditions, however, as a result of the longitudinal components of flow introduced by the pressure gradient along the keel and the finite length, the theoretical distributions should be somewhat modified, probably as shown qualitatively by the broken-line curves in figure 1 (b), so that the equation for the force in a flow plane (eq. (1)) becomes

$$f=f_1(A,\xi)\frac{dm_w}{dt}\dot{\zeta}+f_2(A,\xi)m_w\ddot{\zeta}$$

$$=\epsilon(\beta)\ \rho\left[2f_1(A,\xi)\ \zeta\dot{\zeta}^2+f_2(A,\xi)\ \zeta^2\ddot{\zeta}\right]$$

where the ratio of the actual force in any flow plane to the force calculated under the assumption of two-dimensional

flow, as represented by the functions $f_1(A, \xi)$ and $f_2(A, \xi)$, is determined by the geometry of the immersed part of the hull and the station under consideration.

In order to take into account these three-dimensional effects, the total load on the seaplane, which was determined on a two-dimensional basis, was previously reduced by the application of an aspect-ratio type of correction $\phi(A)$ which depends on the immersed shape of the hull. A similar type of approximate over-all reduction factor $\phi_1(A)$ is applied herein to the hydrodynamic pitching moments calculated on the basis of two-dimensional considerations.

Instantaneous moment.—The hydrodynamic pitching moment about the step is given by

$$M_s=\int_0^{l_k} f\xi\, d\xi=\epsilon(\beta)\,\phi_1(A)\,\rho\left(2\dot{\zeta}^2\int_0^{l_k}\zeta\xi\, d\xi+\ddot{\zeta}\int_0^{l_k}\zeta^2\xi\, d\xi\right)$$

Performing the indicated integration and applying the appropriate geometric relationships gives

$$\left.\begin{aligned} M_s&=\frac{\epsilon(\beta)\,\phi_1(A)\,\rho}{3\tan^2\tau}\,\zeta_s^3\left(\dot{z}_k^2+\frac{\zeta_s\ddot{z}_k}{4}\right)\\ &=\frac{\epsilon(\beta)\,\phi_1(A)\,\rho}{3\sin^2\tau\cos^3\tau}\,z_w^3\left[(\dot{z}_w+\dot{x}_{k_0}\sin\tau)^2+\frac{z_w\ddot{z}_w}{4}\right]\end{aligned}\right\} \tag{19}$$

Generalized relationships.—With the generalized motion variables previously defined, generalized expressions can be obtained for the pitching moment, the center-of-pressure distance, and the ratio of the center-of-pressure distance to the wetted keel length:

(a) Pitching moment:

Equations (19) can be reduced to the same generalized equation by substituting for the dimensional variables the generalized variables previously defined by equations (11), (13), (14), and (16). This substitution results in the formation of a generalized pitching-moment variable for the step m_s, which, at any instant, is related to the corresponding generalized displacement, generalized velocity, and generalized acceleration by the equation

$$m_s=u^3\left[(u'+\kappa)^2+\frac{uu''}{4}\right] \tag{20}$$

where the generalized pitching moment about the step is defined by [3]

$$\left.\begin{aligned} m_s&=\frac{M_s}{\dot{\zeta}_{s_0}^2}\frac{\phi(A)}{\phi_1(A)}\frac{\tan\tau}{W/g}\\ &=\frac{M_s}{\dot{z}_{w_0}^2}\frac{\phi(A)}{\phi_1(A)}\frac{\sin\tau\cos\tau}{W/g}\end{aligned}\right\} \tag{21}$$

Introducing into equation (20) the relationships between the generalized motion variables given by equations (15a) and (17a) results in the following equations:

$$m_s=-\frac{uu''}{3}\left(1+\frac{u^3}{4}\right) \tag{22}$$

$$m_s=u^3(u'+\kappa)^2\left[1-\frac{3u^3}{4(1+u^3)}\right] \tag{23}$$

and

$$m_s=-\frac{u''}{12}\left[\frac{1+\kappa}{u'+\kappa}\,e^{\kappa\left(\frac{1}{1+\kappa}-\frac{1}{u'+\kappa}\right)}-1\right]^{1/3}\left[3+\frac{1+\kappa}{u'+\kappa}\,e^{\kappa\left(\frac{1}{1+\kappa}-\frac{1}{u'+\kappa}\right)}\right] \tag{24}$$

Substituting the relationship between u'' and u', as given by equation (18), into equation (24) provides the relationship between the generalized pitching moment and the generalized velocity:

$$m_s=\frac{(u'+\kappa)^2}{4}\left[2-3\,\frac{u'+\kappa}{1+\kappa}\,e^{\kappa\left(\frac{1}{u'+\kappa}-\frac{1}{1+\kappa}\right)}+\frac{1+\kappa}{u'+\kappa}\,e^{\kappa\left(\frac{1}{1+\kappa}-\frac{1}{u'+\kappa}\right)}\right] \tag{25}$$

From equation (25) and the definition of the generalized pitching moment, equations (21), it can be seen that, for any given stage of the impact, the dimensional pitching moment about the step is independent of the dead-rise angle.

(b) Center of pressure:

The distance of the center of pressure forward of the step is designated l_{cp}, where by definition

$$l_{cp}=\frac{M_s}{F_N} \tag{26}$$

Substituting for M_s and F_N in terms of the generalized variables permits the center-of-pressure distance to be expressed in terms of a generalized center-of-pressure distance p which is defined by [4]

$$\left.\begin{aligned} p&=l_{cp}\tan\tau\,\frac{\phi(A)}{\phi_1(A)}\,\Gamma\\ &=l_{cp}\sin\tau\,\frac{\phi(A)}{\phi_1(A)}\,\Lambda\end{aligned}\right\} \tag{27}$$

and which is related to the generalized pitching moment and the generalized acceleration by the expression

$$p=-\frac{m_s}{u''} \tag{28}$$

The combination of equation (22) with equation (28) gives the relationship between the generalized center-of-pressure distance and the generalized displacement, which applies for all values of κ:

$$p=\frac{u}{3}\left(1+\frac{u^3}{4}\right) \tag{29}$$

Combining equations (24) and (28) gives the relationship between the generalized center-of-pressure distance and the generalized velocity:

$$p=\frac{1}{12}\left[\frac{1+\kappa}{u'+\kappa}\,e^{\kappa\left(\frac{1}{1+\kappa}-\frac{1}{u'+\kappa}\right)}-1\right]^{1/3}\left[3+\frac{1+\kappa}{u'+\kappa}\,e^{\kappa\left(\frac{1}{1+\kappa}-\frac{1}{u'+\kappa}\right)}\right] \tag{30}$$

(c) Ratio of center-of-pressure distance to wetted length:

Substituting the geometric relationship between the penetration and the wetted length into equations (27) and (28)

[3] The generalized pitching moment about the step m_s was formerly designated C_{m_s} and termed the "pitching-moment coefficient."

[4] The generalized center-of-pressure distance p was formerly designated C_{cp} and termed the "center-of-pressure coefficient."

permits expressing the ratio of the center-of-pressure distance to the wetted keel length in terms of the generalized pitching-moment, acceleration, and displacement variables by

$$r=-\frac{m_s}{uu''} \tag{31}$$

where r is defined by [5]

$$r=\frac{l_{cp}}{l_k}\frac{\phi(A)}{\phi_1(A)} \tag{32}$$

Substituting in equation (31) for u, u'', and m_s in terms of u', by means of equations (17a), (18), and (25), respectively, gives the relationship between r and the generalized velocity:

$$r=\frac{1}{4}+\frac{1}{12}\frac{1+\kappa}{u'+\kappa}e^{\kappa\left(\frac{1}{1+\kappa}-\frac{1}{u'+\kappa}\right)} \tag{33}$$

Combining equations (17a) and (33) gives the relationship between r and the generalized displacement which applies for all values of κ:

$$r=\frac{1}{3}+\frac{1}{12}u^3 \tag{34}$$

As in the case of the pitching moment M_s, the ratio of the center-of-pressure distance to the wetted keel length l_{cp}/l_k at any stage of the impact is seen, from equations (32) and (33), to be independent of the dead-rise angle.

On the basis of the foregoing equations, figures 9 to 18 show the theoretical variations during impact of the generalized pitching moment about the step, the generalized center-of-pressure distance, and the ratio of the center-of-pressure distance to the wetted keel length, for a range of values of the approach parameter κ.

It is of interest to note from the form of the generalized variables that, although the pitching moment at any stage of the impact varies as the square of the initial velocity, the location of the center of pressure is independent of the velocity and is determined primarily by the wetted keel length. In fact, as shown by equation (34), the distance of the center of pressure forward of the step is generally only slightly greater than one-third the wetted keel length since $u<1$ for the practical range of impact conditions. This small difference from the one-third point is due to the quadratic nature of the longitudinal distribution of the negative (downward) increment in hydrodynamic load accompanying the deceleration of the virtual mass (see fig. 1 (b)). When this quadratic distribution is added vectorially to the linear distribution of the positive load caused by the expansion of the virtual mass, the resulting distribution of the total hydrodynamic load is not quite linear and the center of pressure is shifted slightly forward in comparison with that for a perfectly linear distribution.

The extent of this forward shift of the center of pressure depends, of course, on the relative magnitudes of the linear and quadratic distributions and increases with penetration, as shown by equation (34). Consequently, the most forward location of the center of pressure, both in an absolute sense and in relation to the wetted length, will be attained at the instant of maximum penetration. For impacts at low values of κ, this forward shift of center of pressure in terms of the wetted length may become quite large when the penetration is very deep. As the limiting condition of planing ($\kappa=\infty$) is approached, however, since there is no acceleration, the total load is linearly distributed along the keel and the center of pressure is located at a distance forward of the step equal to exactly one-third the wetted length. As shown by figures 18 and 27, for the practical range of seaplane impact conditions (values of $\kappa>0.2$), the shift of the center of pressure forward of the one-third point is small and, for practical purposes, may generally be neglected.

Transfer of moments.—The determination of the pitching moment about the step and the center of pressure readily permits the calculation of the hydrodynamic moment about any point on the seaplane. For any point a located at a distance a forward of the step (measured parallel to the keel)

$$M_a=F_N(l_{cp}-a)$$

Substituting for F_N from equation (26) gives

$$M_a=M_s\left(1-\frac{a}{l_{cp}}\right) \tag{35}$$

From equation (35) and the definitions of m_s and p, equations (21) and (27), the generalized pitching moment about the point a is given by

$$m_a=m_s\left(1-\frac{a}{l_{cp}}\right) \tag{36}$$

or

$$\left.\begin{aligned} m_a&=\frac{m_s}{p}\left[p-a\tan\tau\frac{\phi(A)}{\phi_1(A)}\Gamma\right]\\ &=\frac{m_s}{p}\left[p-a\sin\tau\frac{\phi(A)}{\phi_1(A)}\Lambda\right]\end{aligned}\right\} \tag{37}$$

where m_a is defined by

$$\left.\begin{aligned} m_a&=\frac{M_a}{\dot\zeta_{s_0}^2}\frac{\phi(A)}{\phi_1(A)}\frac{\tan\tau}{W/g}\\ &=\frac{M_a}{\dot z_{w_0}^2}\frac{\phi(A)}{\phi_1(A)}\frac{\sin\tau\cos\tau}{W/g}\end{aligned}\right\} \tag{38}$$

RELATIONSHIPS AT PARTICULAR STAGES OF THE IMPACT

The preceding section presented an analysis of the motions, hydrodynamic loads, and pitching moments encountered by a seaplane throughout the course of an impact and derived generalized relationships among the variables which are valid from the instant of initial contact until the seaplane rebounds from the water surface. The present section makes use of these results to determine the relationships which exist at particular stages of the impact, such as at the instant of maximum acceleration, the instant of maximum pitching moment, the instant of maximum penetration, and the instant of exit during rebound from the water surface. These relationships are shown in figures 19 to 31.

INSTANT OF MAXIMUM ACCELERATION

At the instant of maximum acceleration, the third derivative of the displacement is equal to zero. Therefore, differentiating equation (15) and setting $u'''=0$ gives the relationship between the generalized acceleration, the generalized

[5] The ratio of the center-of-pressure distance to the wetted length r was formerly designated C_r.

displacement, and the generalized velocity at the instant of maximum acceleration, with κ as parameter. This relationship may be written as

$$u''=-\frac{u'(u'+\kappa)(2-u^3)}{2u(1+u^3)} \tag{39}$$

Setting equation (39) equal to equation (15a), which holds throughout the impact, gives the relationship between the velocity and the displacement at the instant of maximum acceleration, namely,

$$u'=\frac{6\kappa u^3}{2-7u^3} \tag{40}$$

or

$$u^3=\frac{2u'}{7u'+6\kappa} \tag{40a}$$

Substituting in equation (39) permits the maximum acceleration to be expressed in terms of the displacement at the instant of maximum acceleration by

$$u''=-\frac{3\kappa^2u^2(2-u^3)^2}{(2-7u^3)^2(1+u^3)} \tag{41}$$

or, in terms of the velocity at the same instant, by

$$u''=-\frac{2u'(u'+\kappa)^2}{3u'+2\kappa}\left(\frac{7u'+6\kappa}{2u'}\right)^{1/3} \tag{42}$$

Combining equations (17a) and (40) results in the relationship between the displacement at the instant of maximum acceleration and the approach parameter κ:

$$\frac{u^3(6\kappa+7)-2}{(1+\kappa)(2-u^3)}=\log_e\frac{\kappa(2-u^3)(1+u^3)}{(1+\kappa)(2-7u^3)} \tag{43}$$

The relationship between the velocity at the instant of maximum acceleration and κ is obtained by setting equation (40a) equal to equation (17a):

$$\kappa\left(\frac{1}{1+\kappa}-\frac{1}{u'+\kappa}\right)=\log_e\frac{(9u'+6\kappa)(u'+\kappa)}{(7u'+6\kappa)(1+\kappa)} \tag{44}$$

If equation (43) could be solved analytically it would yield the displacement u at the instant of maximum acceleration as a function of κ. Similarly, equation (44) would yield the velocity u' at maximum acceleration as a function of κ. Substitution of $u(\kappa)$ in equation (41) or $u'(\kappa)$ in equation (42) would then give the maximum acceleration u'' as a function of κ, that is $u''(\kappa)$. However, since solution of equations (43) and (44) in closed form is not possible, recourse may be had to numerical, tabular, or graphical solutions of these equations to determine $u(\kappa)$ and $u'(\kappa)$ at the instant of maximum acceleration. With these values the maximum acceleration $u''(\kappa)$ can be determined from either equation (39), (41), or (42).

Values of u, u', and u'' at the instant of maximum acceleration, which have been determined from the foregoing equations, are listed in table I for a range of values of κ and are shown plotted against κ in figures 19 (a) to (c), as well as in figures 20, 22, and 23 where they are compared with experimental data.

For convenience in design studies where it may be desirable to have an analytical expression for the relationship between the maximum generalized acceleration and the approach parameter κ, this relationship has been approximated by fitting the following quadratic equation to the more exact results previously determined:

$$u''=-(0.61+0.92\kappa-0.016\kappa^2) \qquad (0\leqq\kappa\leqq10) \tag{45}$$

Equation (45) gives values of the maximum acceleration which agree with the more exact results within 2 percent for values of κ between 0 and 10.

Values of the generalized time corresponding to the instant of maximum acceleration, which were calculated for particular values of κ by integrating the relationship between the generalized motion variables in the manner previously discussed, are given in table I and are plotted against κ in figure 19 (d) as well as in figure 24 for comparison with experimental data.

The determination of the conditions of motion at the instant of maximum acceleration readily permits the calculation of the pitching moment about the step, the center-of-pressure distance, and the ratio of the center-of-pressure distance to the wetted keel length at the instant of maximum acceleration from the equations given in the section on pitching moments. Calculated values of these generalized variables are given in table I and are plotted against κ in figures 19 (e) to (g) and figures 25 to 27.

INSTANT OF MAXIMUM PITCHING MOMENT ABOUT THE STEP

Equation (25) provides the general relationship between the generalized pitching moment and the generalized velocity which applies at all times during the impact. The conditions of motion which exist at the instant when the maximum pitching moment about the step is reached can be determined by differentiating equation (25) with respect to σ and setting $\frac{dm_s}{d\sigma}=0$. So doing provides the relationship between the velocity at the instant of maximum pitching moment and the approach parameter κ:

$$\frac{1+\kappa}{u'+\kappa}e^{\kappa\left(\frac{1}{1+\kappa}-\frac{1}{u'+\kappa}\right)}+\frac{2(u'+\kappa)-\sqrt{13u'^2+32u'\kappa+16\kappa^2}}{u'+2\kappa}=0 \tag{46}$$

Numerical, tabular, or graphical methods can be employed to solve for u', since solution in closed form is rendered impossible by the transcendental nature of equation (46).

The substitution of values of u' obtained by the solution of equation (46) into equations (25), (30), (17a), and (18) permits the determination of the maximum pitching moment about the step and corresponding values of the center-of-pressure distance, the displacement, and the acceleration. The corresponding time may be obtained from the relationship between σ and u' previously determined by integration. Values of the generalized variables at the instant of maximum pitching moment are given in table I and are shown plotted against κ in figure 19 and figures 25 to 31.

INSTANT OF MAXIMUM PENETRATION

Explicit solutions can be obtained for the generalized variables at the instant of maximum penetration as functions

of the approach parameter κ. Since $u'=0$ at the instant of maximum penetration, making this substitution in equation (17) gives the relationship between the maximum penetration of the step-keel point and κ:

$$u=\left(\frac{1+\kappa}{\kappa}e^{-\frac{1}{1+\kappa}}-1\right)^{1/3} \tag{47}$$

Since the wetted keel length is related to the penetration by the simple trigonometric relationship $l_\kappa=\frac{\zeta_\kappa}{\tan\tau}=\frac{z_\kappa}{\sin\tau}$, equation (47) also permits the determination of the maximum wetted length.

The acceleration at the instant of maximum penetration is obtained by substituting equation (47) for u in equation (15a):

$$u''=-\frac{3\kappa^2}{1+\kappa}\left(\kappa e^{\frac{1}{1+\kappa}}\right)^{1/3}\left[(1+\kappa)-\kappa e^{\frac{1}{1+\kappa}}\right]^{2/3} \tag{48}$$

The pitching moment about the step at the instant of maximum penetration can be obtained by substituting $u'=0$ into equation (25):

$$m_s=\frac{\kappa^2}{4}\left(2-3\frac{\kappa}{1+\kappa}e^{\frac{1}{1+\kappa}}+\frac{1+\kappa}{\kappa}e^{-\frac{1}{1+\kappa}}\right) \tag{49}$$

The same substitution in equation (30) gives the center-of-pressure distance at the instant of maximum penetration:

$$p=\frac{1}{12}\left(\frac{1+\kappa}{\kappa}e^{-\frac{1}{1+\kappa}}-1\right)^{1/3}\left(\frac{1+\kappa}{\kappa}e^{-\frac{1}{1+\kappa}}+3\right) \tag{50}$$

Similarly, the ratio of the center-of-pressure distance to the wetted length can be determined by means of equation (33):

$$r=\frac{1}{4}+\frac{1}{12}\frac{1+\kappa}{\kappa}e^{-\frac{1}{1+\kappa}} \tag{51}$$

The time corresponding to the instant of maximum penetration can be obtained from the variations of the generalized variables with σ during the impact, the determination of which has been previously discussed.

Calculated generalized values of the displacement, the acceleration, the time, the pitching moment about the step, the center-of-pressure distance, and the ratio of the center-of-pressure distance to the wetted keel length at the instant of maximum penetration are given in table I and are shown as functions of the approach parameter κ in figure 19 and in figures 21 and 23 to 28.

INSTANT OF EXIT DURING REBOUND

The impact process is completed when the seaplane finally leaves the water surface and rebounds into the air. At the instant of exit $u=0$ and, if the wing lift is still assumed to be equal to the weight, $u''=0$. Therefore, the relationship between the generalized velocity at the instant of exit and the approach parameter κ can be obtained by setting equation (17a) equal to zero, which gives

$$(u'+\kappa)e^{\frac{\kappa}{u'+\kappa}}=(1+\kappa)e^{\frac{\kappa}{1+\kappa}} \tag{52}$$

It can be seen from equation (52) that the generalized velocity at the instant of exit depends only on the approach parameter κ and is independent of the mass and geometric characteristics of the seaplane. The transcendental form of equation (52) prevents solution for $u'(\kappa)$ in closed form. However, values of u' can be readily determined for any given values of κ by numerical, tabular, or graphical means; these values in conjunction with the relationship between u' and σ previously discussed permit the determination of the time at the instant of exit.

It is evident from physical considerations, also from equations (23) and (29), that the pitching moment about the step and the center-of-pressure distance are both equal to zero at the instant of exit; the ratio of the center-of-pressure distance to the wetted keel length becomes equal to 1/3 at the instant of exit, regardless of the value of κ, as can be seen from equation (34).

Calculated values of the generalized velocity and the generalized time corresponding to the instant of exit are given in table I and are shown plotted against κ in figures 19 (b) and (d) and in figures 22 and 24 where they are compared with experimental data.

LIMITING CONDITIONS

Since the approach parameter κ may have any of a large range of values between 0 and ∞, it is desirable to determine the limiting values between which the generalized variables can vary.

RESULTANT VELOCITY NORMAL TO KEEL: $\kappa=0$

The condition $\kappa=0$ is obtained when the direction of the flight path at contact is normal to the keel. This condition is often attained in laboratory testing and may be approached in impacts of water-based helicopters.

General relationships during impact.—For the condition $\kappa=0$ the equations of motion, equations (15) and (17), reduce to the following relationships which hold throughout the course of the impact:

$$(1+u^3)u''+3u^2u'^2=0 \tag{53}$$

and

$$(1+u^3)u'-1=0 \tag{54}$$

or

$$u''=-\frac{3u^2u'^2}{1+u^3} \tag{53a}$$

and

$$u^3=\frac{1-u'}{u'} \tag{54a}$$

Since u^3 represents the ratio of the virtual mass to the total mass of the seaplane, it can be seen from equation (54a) that the sum of the instantaneous momentum of the seaplane and the momentum of the virtual mass of the water directly beneath the keel is constant throughout the impact and equal to the initial momentum of the seaplane. As has been previously discussed, this equality of momentum exists only when the resultant velocity at contact is normal to the keel; that is, $\kappa=0$. Since the deceleration of the seaplane is in the direction normal to the keel and in the same direction as the resultant velocity, the seaplane continues along its original path of motion. Thus, only the flow planes directly beneath

the keel an be affected by the immersion and only these flow planes can absorb the total momentum lost by the seaplane. For values of κ other than 0, this situation does not exist since part of the momentum lost by the seaplane will be contained in the downwash created behind the step by the component of velocity parallel to the keel, as previously discussed.

For $\kappa=0$, combining equations (53a) and (54a) permits the generalized acceleration to be written in terms of the generalized velocity or the generalized displacement as follows:

$$u''=-3u'^{7/3}(1-u')^{2/3} \tag{55}$$

and

$$u''=-\frac{3u^{2/3}}{(1+u^3)^3} \tag{56}$$

The generalized time may be expressed in terms of the generalized displacement by direct quadrature of equation (54):

$$\sigma=u\left(1+\frac{u^3}{4}\right) \tag{57}$$

It can be seen from equation (57) that the displacement increases without limit for $\kappa=0$. Thus although the downward velocity grows continually smaller as the impact progresses, a maximum penetration is never reached. This situation is further evident from the fact that, since the momentum lost by the seaplane is completely contained in the virtual mass alone, an infinite virtual mass, or infinite penetration, is required to satisfy the condition of zero velocity. (See also eq. (54a)). This result stems from neglect of the buoyant forces which, because of the large penetrations involved, become important toward the later stages of the impact, particularly when $\kappa=0$. These bouyant forces are of relatively little importance in the range of κ for practical seaplane landing conditions.

Combining equations (54a) and (57) gives the relationship between the time and the velocity for $\kappa=0$:

$$\sigma=\left(\frac{1-u'}{u'}\right)^{1/3}\left(1+\frac{1-u'}{4u'}\right) \tag{58}$$

The relationship between the pitching moment about the step and the velocity is obtained by substituting $\kappa=0$ into equation (25):

$$m_s=\frac{u'}{4}(3u'+1)(1-u') \tag{59}$$

Combining equations (54a) and (59) gives the relationship between the pitching moment and the displacement:

$$m_s=\frac{u^3(4+u^3)}{4(1+u^3)^3} \tag{60}$$

The relationship between the center-of-pressure distance and the velocity is obtained by substituting $\kappa=0$ into equation (30):

$$p=\frac{(1-u')^{1/3}(3u'+1)}{12u'^{4/3}} \tag{61}$$

The relationship between the center-of-pressure distance and the displacement is given by equation (29) which is valid for all values of κ.

The variation of the ratio of the center-of-pressure distance to the wetted keel length with the velocity is obtained from equation (33):

$$r=\frac{1}{4}+\frac{1}{12u'} \tag{62}$$

The preceding generalized equations apply at all instants during an impact where the resultant velocity is normal to the keel. The values of the generalized variables at particular stages of the impact are presented in the following section.

Values of generalized variables for particular stages of the impact.—From the foregoing general relationships may be determined the particular relationships which exist at the instant of maximum acceleration and at the instant of maximum pitching moment about the step when $\kappa=0$:

(a) Instant of maximum acceleration:

The value of the generalized displacement at the instant of maximum acceleration for $\kappa=0$ is obtained from equation (40a):

$$u=\left(\frac{2}{7}\right)^{1/3}=0.6586 \tag{63}$$

The ratio of the virtual mass to the mass of the seaplane has previously been shown to be equal to u^3, this ratio at the instant of maximum acceleration is therefore

$$u^3=\frac{\text{Virtual mass}}{\text{Seaplane mass}}=\frac{2}{7} \tag{64}$$

The value of the velocity at this instant is obtained by substituting for u in equation (54a):

$$u'=\frac{7}{9} \tag{65}$$

The corresponding value of the acceleration (maximum acceleration) is obtained by substituting in equation (53a):

$$u''=-3\left(\frac{2}{7}\right)^{2/3}\left(\frac{7}{9}\right)^3=-0.6123 \tag{66}$$

The corresponding value of the time is obtained by substituting in equation (57):

$$\sigma=\left(\frac{2}{7}\right)^{1/3}\left(1+\frac{1}{14}\right)=0.7057 \tag{67}$$

The corresponding value of the pitching moment about the step is obtained by substituting in equation (59):

$$m_s=\frac{1}{4}\frac{7}{9}\left(\frac{21}{9}+1\right)\left(1-\frac{7}{9}\right)=0.1440 \tag{68}$$

The corresponding value of the center-of-pressure distance is obtained by substituting in equation (61):

$$p=\frac{\left(1-\frac{7}{9}\right)^{1/3}\left(\frac{21}{9}+1\right)}{12\left(\frac{7}{9}\right)^{4/3}}=0.2352 \tag{69}$$

The corresponding value of the ratio of the center-of-pressure distance to the wetted length is obtained by substituting in equation (62):

$$r=\frac{1}{4}+\frac{9}{84}=0.3571 \tag{70}$$

(b) Instant of maximum pitching moment about the step:

Equation (46) gives the relationship between the generalized velocity at the instant of maximum pitching moment about the step and the approach parameter κ. For $\kappa=0$, the velocity at this instant is given by

$$u'=\frac{1}{\sqrt{13}-2}=0.6228 \tag{71}$$

The corresponding value of the displacement is obtained by substituting in equation (54a):

$$u=(\sqrt{13}-3)^{1/3}=0.8460 \tag{72}$$

The corresponding value of the acceleration is obtained by substituting in equation (55):

$$u''=-\frac{3(\sqrt{13}-3)^{2/3}}{(\sqrt{13}-2)^3}=-0.5187 \tag{73}$$

The corresponding value of the time is obtained from equation (58):

$$\sigma=(\sqrt{13}-3)^{1/3}+\frac{1}{4}(\sqrt{13}-3)^{4/3}=0.9741 \tag{74}$$

The maximum value of the pitching moment about the step is obtained by substituting in equation (59):

$$m_s=\frac{(\sqrt{13}+1)(\sqrt{13}-3)}{4(\sqrt{13}-2)^3}=0.1685 \tag{75}$$

The corresponding value of the center-of-pressure distance is obtained by substituting in equation (61):

$$p=\frac{1}{12}(\sqrt{13}-3)^{1/3}(\sqrt{13}+1)=0.3247 \tag{76}$$

The corresponding value of the ratio of the center-of-pressure distance to the wetted length is obtained by substituting in equation (62):

$$r=\frac{\sqrt{13}+1}{12}=0.3838 \tag{77}$$

The foregoing values of the generalized variables apply only for $\kappa=0$ and at the particular instants of maximum acceleration and maximum pitching moment about the step, as noted. As previously mentioned, for $\kappa=0$ a maximum penetration is never reached and therefore there is no rebound from the water surface.

RESULTANT VELOCITY PARALLEL TO WATER SURFACE: $\kappa=\infty$

At values of κ other than 0, because of the loss of downward momentum to the downwash resulting from the velocity component parallel to the keel, a finite maximum penetration will be attained and the seaplane will rebound from the water in a finite time. For steep impacts—that is, small values of κ—the difference in the time between the occurrence of the various stages of the impact, such as the instants of maximum acceleration, maximum pitching moment, maximum penetration, and exit, will be relatively large. As the flight path becomes flatter and κ becomes larger, these differences in the conditions of motion at the various stages of the impact diminish, and, as the flight path becomes parallel to the water surface and the planing condition is approached as a limit ($\kappa=\infty$), these differences completely disappear. For the latter condition, the generalized variables approach the following limiting values:

$$\lim_{\kappa\to\infty} u=0$$

$$\lim_{\kappa\to\infty} u'=1$$

$$\lim_{\kappa\to\infty} u''=-\infty$$

$$\lim_{\kappa\to\infty} \sigma=0$$

$$\lim_{\kappa\to\infty} m_s=\infty$$

$$\lim_{\kappa\to\infty} p=0$$

$$\lim_{\kappa\to\infty} r=\frac{1}{3}$$

The foregoing results are for the case where the wing lift is equal to the weight.

For pure planing with partial wing lift, the generalized displacement may be determined as a function of seaplane characteristics, trim angle, and velocity by setting F_V in equation (9) equal to the load on the water Δ and letting $\dot{z}_w=\ddot{z}_w=0$. These substitutions give

$$u_{planing}=\sqrt{\frac{C_\Delta\rho}{3\frac{W}{g}\Delta}}\frac{b}{C_V\sin\tau\cos\tau} \tag{78}$$

where

$$C_\Delta=\frac{\Delta}{\rho g b^3}=\text{Load coefficient}$$

$$C_V=\frac{\dot{x}_w}{\sqrt{gb}}=\text{Speed coefficient}$$

The wetted keel length can be easily determined from u by employing the simple trigonometric relationship

$$l_k=\frac{\zeta_s}{\tan\tau}=\frac{z_w}{\sin\tau}$$

EFFECTS OF CHINE IMMERSION

In the foregoing analysis it has been assumed that the width (beam) of the V-shaped hull bottom is sufficiently large that the chines do not become immersed at any time during the impact. This assumption is generally valid for

the values of beam loading employed in conventional seaplane design practice and for the flight-path angles encountered in normal seaplane operations. Even in the case of some of the most recent seaplanes which employ somewhat higher than average values of beam loading, any chine immersion which might be experienced would be expected to occur during the later stages of the impact subsequent to the attainment of the maximum load and, thus, should have relatively little effect on the over-all behavior of the seaplane. However, since the trend in water-based aircraft is toward increased beam loading, some mention should be made of the effects of chine immersion which may be encountered with long, narrow (high length-beam ratio) hulls or other hydrodynamic-load supporting devices having considerably higher than conventional beam loading, or which may be experienced in water landings at unusually high flight-path angles (small values of κ).

PHYSICAL CONSIDERATIONS

In the foregoing analysis the force exerted by the water on any cross section of the hull was considered to arise from two actions; namely, the rate of increase of the virtual mass accompanying the enlarging flow pattern and the reaction to the acceleration of the virtual mass. For a V-shaped cross section, if the wetted width is considered to be a measure of the virtual mass, then immersion of the chines in any given flow plane terminates the expansion of the wetted width and, therefore, the growth of the virtual mass. On this basis, further immersion of a chine-immersed cross section would take place with constant virtual mass and would result in a smaller total force on the seaplane subsequent to chine immersion than that which would exist if the beam were greater and the wetted width had continued to increase.

These simplified concepts, if applied to a hull in pure planing, would indicate, rather absurdly, the complete absence of any force on the chine-immersed areas. It is clear, then, that equation (1) is, by itself, not adequate for cross sections with immersed chines if the virtual mass is defined in terms of the wetted width. Instead, it appears more reasonable to assume that the chine-immersed areas are subject to forces similar to the steady-state profile-drag forces for two-dimensional separated flow. It might be expected that such drag forces would be proportional to the square of the velocity component normal to the keel and considerably smaller than the forces due to the continued expansion of the virtual mass. In reference 10 results calculated by assuming the force on the chine-immersed cross sections to be given by Bobyleff's solution for the force on a bent lamina (see ref. 11, pp. 104 and 105) were compared with planing data for chine-immersed conditions and appeared to indicate that the chine-immersed portions of the hull may be treated in this manner.

For a hull at a positive trim angle, any reductions in total force resulting from chine immersion should occur gradually as successive stations along the keel become immersed beyond the chines. For conventional values of beam loading, since chine immersion, if encountered at all, would be expected to occur considerably after the maximum load has been reached, any reductions in total force due to chine immersion should have no effect on the maximum load, as previously indicated. With increasing beam loading, however, chine immersion will occur at increasingly earlier stages of the impact until, for very high values of beam loading, chine immersion will take place before the maximum load would have been reached if the chines had not become immersed; a reduction in the maximum load will then occur, the amount of the reduction depending on the beam loading, that is, on how soon after initial contact chine immersion occurs.

SIMPLIFIED ANALYSIS

The simplified treatment presented in this section is a first approach toward the determination of the effects of chine immersion on the maximum load and is intended to apply only to moderate degrees of chine immersion. With this qualification, it is assumed that the forces on the areas subject to chine immersion are small enough in comparison with the forces on the larger nonchine-immersed areas to be neglected. On this basis, since the total virtual mass is constant after chine immersion occurs, the total force should not increase subsequent to this instant; thus, the maximum force should be equal to the force at the instant of initial chine immersion, as determined in accordance with the theory for impacts with no chine immersion. This assumption is not intended to apply to heavily loaded, extremely narrow, hydrodynamic-load supporting devices which may experience very large degrees of penetration, in which case the force on the chine-immersed area can become a major portion of the total hydrodynamic force. In such cases the maximum force can very well occur considerably after the chines are first immersed, when the chine-immersed area becomes large relative to the nonchine-immersed area.

In order to evaluate the effects of chine immersion, it is first necessary to determine when the disturbed water surface reaches the chines. For a V-section hull, because of geometric similarity of the flow patterns at all degrees of penetration prior to chine immersion, the penetration at the instant of chine immersion is directly proportional to the beam. The constant of proportionality is some function of the dead-rise angle β which, for the present, is denoted by $\psi(\beta)$. With this notation the normal penetration of the step at the instant of chine immpersion ζ_{s_c} is expressed by

$$\zeta_{s_c}=\psi(\beta)\, b \tag{79}$$

In accordance with equation (11), the displacement at the instant of chine immersion can be written as

$$\left.\begin{aligned} u_c&=\zeta_{s_c}\Gamma=\psi(\beta)\, b\Gamma \\ &=\frac{\Pi}{C_{\Delta_0}^{1/3}} \end{aligned}\right\} \tag{80}$$

where

$$\Pi=\left\{\frac{[\psi(\beta)]^3\,\epsilon(\beta)\,\phi(A)}{3\tan\tau}\right\}^{1/3}$$

and

$$C_{\Delta_0}=\frac{W}{\rho g b^3}$$

The importance of chine immersion during an impact at a given value of κ can be evaluated with the aid of figure 4 by comparing the displacement at the instant of chine immersion with the maximum value of the displacement u_{max} and with the displacement $u_{(u''_{max})}$ corresponding to the maximum acceleration when the chines are not immersed. If $\frac{\Pi}{C_{\Delta_0}^{1/3}}$ is greater than u_{max}, chine immersion will not occur during the impact. If $\frac{\Pi}{C_{\Delta_0}^{1/3}}$ is less than u_{max} but greater than $u_{(u''_{max})}$, chine immersion will occur during the impact, after the maximum acceleration has been attained, but will have no effect on the maximum acceleration (or load). On the other hand, if $\frac{\Pi}{C_{\Delta_0}^{1/3}}$ is less than $u_{(u''_{max})}$, chine immersion will occur prior to the instant of maximum acceleration in the case of no chine immersion and, in accordance with the previous assumptions, the maximum load will be limited (reduced) to the value corresponding to $u_c=\frac{\Pi}{C_{\Delta_0}^{1/3}}$. For values of $\frac{\Pi}{C_{\Delta_0}^{1/3}}<u_{(u''_{max})}$, therefore, the greater the beam loading the smaller the maximum load; for values greater than $u_{(u''_{max})}$, the beam loading has no effect on the maximum load.

Equation (43), with the substitution $u=u_c=\frac{\Pi}{C_{\Delta_0}^{1/3}}$, permits the determination of the largest values of the approach parameter κ for which a reduction in the maximum load due to chine immersion can be obtained; that is, the values of κ required to cause the chines to become immersed, for given values of $\frac{\Pi}{C_{\Delta_0}^{1/3}}$, at the same instant that the maximum acceleration is reached when there is no chine immersion. For all smaller values of κ (steeper impacts), the variation with κ of the maximum acceleration, as reduced by chine immersion, can be determined by application of equations (17a) and (15a). Combining these two equations and setting $u=u_c$ gives the following transcendental relationship between the reduced maximum acceleration u_c'' and the parameters u_c and κ:

$$\kappa\left[\frac{1}{1+\kappa}-\frac{u_c}{\sqrt{-\frac{u_c''}{3}(1+u_c^3)}}\right]+\log_e\frac{(1+\kappa)u_c}{\sqrt{-\frac{u_c''}{3}(1+u_c^3)^3}}=0 \quad (81)$$

The effect of chine immersion on the maximum generalized acceleration is shown in figure 20 by the broken-line curves which have been calculated by means of the aforementioned procedure for a number of values of $u_c=\frac{\Pi}{C_{\Delta_0}^{1/3}}$ corresponding to a wide range of beam loadings extending from conventional values to values considerably higher than those employed in present-day seaplane design practice. The solutions for the highest beam loadings are presented in order to make available theoretical results which will be required to evaluate the limits of applicability of the present simplified analysis when experimental data for very high beam loading become available.

DEAD-RISE-ANGLE AND ASPECT-RATIO FUNCTIONS

In the foregoing development of the generalized relationships which apply during a seaplane impact, the variation of the two-dimensional virtual mass with the dead-rise angle and the corrections for the effects of the finite aspect ratio of the submerged portion of the hull on the virtual mass, the total force on the seaplane, and the pitching moment were not specified explicitly but were represented by undefined functions of the pertinent variables, such as $\epsilon(\beta)$, $f(\beta)$, $\psi(\beta)$, $\phi(A)$, and $\phi_1(A)$. Although the equations relating the generalized variables are valid regardless of what these functions actually are, the functions must be defined explicitly in order to permit conversions to be made between generalized and dimensional variables if the theoretical results are to be used in seaplane design, or if the theory is to be compared with experiment. The practical usefulness of the theoretical results is therefore dependent to a great extent on the correctness of the functions used.

VIRTUAL MASS

Although existing information is still rather limited and the current state of knowledge yields only relatively rough approximations to the actual functions, sufficient theoretical and empirical information is available at present to permit practical application of the theoretical results to seaplanes having conventional dead-rise angles. Analytically, the virtual mass in any flow plane may be evaluated approximately from the results of an iterative flow analysis made by Wagner to calculate the force on a two-dimensional V-shape of 18° angle of dead rise during immersion at constant velocity. Wagner extended the theoretical results for this particular case to other dead-rise angles by employing a parabolic variation of force with dead-rise angle which satisfies the solution for 18° as well as the end points of zero force at 90° and infinite force at 0°. This relationship is given by equation (78) of reference 5 and, in the notation of the present report, may be written as

$$f=\left(\frac{\pi}{2\beta}-1\right)^2\rho\pi\zeta\dot{\zeta}^2$$

The virtual mass corresponding to this force equation may be evaluated by recognizing that, for constant velocity penetration, the force in a given flow plane is due solely to the rate of increase of the virtual mass associated with the enlarging flow pattern. For this condition, equation (1) becomes

$$f=\frac{dm_w}{dt}\dot{\zeta}$$

Equating the preceding two equations and integrating gives the following expression for the virtual mass corresponding to Wagner's force equation:

$$m_w=\left(\frac{\pi}{2\beta}-1\right)^2\frac{\rho\pi}{2}\zeta^2 \quad (82)$$

If the virtual mass is defined as $m_w=\epsilon(\beta)\,\rho\zeta^2$, as in equation (2), then

$$\epsilon(\beta)=\left(\frac{\pi}{2\beta}-1\right)^2\frac{\pi}{2} \quad (83)$$

If the virtual mass is interpreted in terms of an equivalent semicylinder of water with radius equal to $f(\beta)\ \zeta$, then, $m_w=[f(\beta)]^2\frac{\rho\pi}{2}\zeta^2$, as in equation (2a), and

$$f(\beta)=\frac{\pi}{2\beta}-1 \tag{83a}$$

Equations (82), (83), and (83a) are valid only as long as the immersed cross section in any flow plane is a V-shape and do not apply after the chines become immersed. In the case of V-shaped cross sections with chine flare, equation (82) holds until the flared portion reaches the water surface, after which point Wagner's expanding-plate analogy, as given in references 5 and 6 or as modified in reference 8, may be applied to determine the equation for the shape of the free surface at the instant the flared portion reaches the water surface and to calculate the increase in virtual mass with further penetration. An example of the procedure for determining the variation of the virtual mass of curved cross sections with penetration is given in reference 8, with particular application to the case of a float with a scalloped (fluted) bottom.

WETTED WIDTH

In the preceding study of the effects of chine immersion it was pointed out that, because of geometric similarity of the flow patterns at all degrees of penetration prior to chine immersion, the normal penetration of the keel at the instant of chine immersion is directly proportional to the beam, the ratio of the normal penetration to the beam (or the wetted width) being some unknown function of the dead-rise angle, designated $\psi(\beta)$; thus, $\zeta_{s_c}=\psi(\beta)\ b$. By means of the expanding-plate analogy previously mentioned, Wagner, in references 5 and 6, concluded that the wetted width for a V-shaped cross section is $\pi/2$ times as great as the width of the cross section in the plane of the undisturbed water surface and used this wetted width as the diameter of the semicylinder of water representing the virtual mass. If this result is accepted, $b=\pi\cot\beta\ \zeta_{s_c}$ and $\psi(\beta)$ becomes equal to $\frac{1}{\pi\cot\beta}$.

However, the simplifying assumptions inherent to the expanding-plate approach are such as to make these results questionable for finite angles of dead rise. For example, it has been shown in reference 1 that the virtual mass corresponding to Wagner's iterative solution is in much closer agreement with experiment than is the virtual mass determined by application of his expanding-plate analogy. As a result it has been proposed herein that the virtual mass and the functions $\epsilon(\beta)$ and $f(\beta)$ be defined to correspond with the results of Wagner's iterative solution, rather than with the results of his expanding-plate analysis, and equations (82), (83), and (83a) have been written accordingly. It is also proposed, for the time being, that the effective wetted width be taken equal to the diameter of the semicylinder of water equivalent to the virtual mass determined from Wagner's iterative solution. With this assumption, $b=2\ f(\beta)\ \zeta_{s_c}$ and

$$\psi(\beta)=\frac{1}{2\ f(\beta)}=\frac{1}{2\left(\frac{\pi}{2\beta}-1\right)} \tag{84}$$

The definition of $\psi(\beta)$ given by equation (84) is suggested as an interim approximation to be used until a better understanding of the flow phenomenon permits a more rational function to be specified.

ASPECT RATIO

An approximate correction for the end-flow losses due to finite aspect ratio in the three-dimensional case may be obtained from the results of Pabst's experiments with vibrating plates in water (ref. 7). These tests showed that the reduction in virtual mass due to finite aspect ratio is closely given by the expression

$$\phi(A)=1-\frac{1}{2A}\qquad(A\geqq 1)$$

where A is the aspect ratio of the vibrating plate.

For V-bottom seaplanes, if it is assumed that the primary flow occurs in transverse flow planes and that the end-flow loss is determined by the shape of the intersected area in the plane of the water surface, then

$$A=\frac{\tan\beta}{\tan\tau}$$

and the application of Pabst's results to the keeled seaplane gives

$$\phi(A)=1-\frac{\tan\tau}{2\tan\beta} \tag{85}$$

In view of the fact that no information is available regarding the aspect-ratio correction to the pitching moments determined on the basis of two-dimensional considerations, it may be assumed for the time being that $\phi(A)$ applies uniformly to all flow planes; that is,

$$\phi_1(A)=\phi(A) \tag{86}$$

From the nature of this approximation it would appear that this assumption should be adequate for most practical purposes.

Although it is known from studies of planing data that the dead-rise-angle and aspect-ratio functions given by equations (83) and (85) are questionable for very low angles of dead rise, in references 12 and 13 these functions have been found to be in rather good agreement with experimental data obtained in the Langley impact basin with seaplane hull models of 22½°, 30°, and 40° angles of dead rise. Present indications lead to the belief that these functions may be adequate for angles of dead rise as low as 15°, but more definite conclusions in this respect must await the results of further investigation.

It would appear, then, that for practical purposes the functions given in this section should be adequate for the range of dead-rise angles most likely to be encountered in conventional seaplane design practice. In the derivation of the generalized relationships which apply during an impact, the dead-rise-angle and aspect-ratio variations were represented in functional notation in order to permit incorporation of improved functions into the definitions of the generalized variables as additional theoretical and experimental results are obtained.

APPLICABILITY AND LIMITATIONS OF THE THEORY

In view of the fact that the foregoing analysis considers a hull of constant cross section, there may be some question regarding the effects of the pulled-up (warped) bow and the afterbody in applications to conventional seaplanes. Although the longitudinal warping of the hull may be taken into account by more complicated equations, it appears that, since conventional floats and hulls are essentially prismatic for a considerable distance forward of the step, the bow will not cause any important deviation of the loads from those calculated on the basis of constant cross section for normal impacts at positive trim (ref. 14).

The afterbody, on the other hand, may exert a much more pronounced influence on the motion of the seaplane, particularly in certain types of laboratory tests where, as is sometimes the case, the trim of the model may be fixed at high positive angles. Under such conditions the load is taken almost entirely by the afterbody whereas the forebody may not become immersed to any appreciable degree until after the maximum acceleration has been attained. At the lower trims associated with step impacts, on the other hand, the depth of step, the keel angle of the afterbody, and the relatively high longitudinal velocity apparently combine to shield the afterbody so that it carries very little load in comparison with the forebody.

In flight impacts, even though the landing approach may be made at high trim, the initial contact rearward of the step generally results in a downward pitching of the seaplane to the extent that the main impact occurs at reduced trim and corresponds to a forebody impact. The equations presented may thus be considered to represent approximately free-flight impacts at high trim if the initial conditions are taken to correspond with those at the beginning of the main impact. Since the distance between the step and the center of gravity of the seaplane is generally small in comparison with the radius of gyration in pitching, the effects of freedom in pitching should be relatively unimportant in main step impacts. This hypothesis appears to be substantiated fairly well by limited analytical and experimental results presented in reference 15.

As a first approach toward the calculation of the behavior of seaplanes during landings in seaway, the preceding analysis may be applied to rough-water impacts if the initial conditions are defined relative to the wave surface. For trochoidal waves with large length-amplitude ratio, the wave profile may be simulated by an inclined plane tangent to the surface at the point of contact, which serves as the effective frame of reference for the foregoing equations. The effective trim angle τ_e and the effective approach parameter κ_e are then determined with respect to the wave slope. These assumptions fail to consider the internal orbital velocities and displacements of the fluid particles within the wave and are therefore approximate. At best, the procedure should be applied only to impacts where the float contacts the wave about halfway between trough and crest for those cases where the trim is equal to or greater than the slope of the wave. In reference 8, the application of these approximations to several rough-water impacts of a scalloped-bottom float yielded calculated results which were in fairly good agreement with experimental data obtained in the Langley impact basin. Comparisons with more extensive experimental data in reference 9 also indicated reasonably good agreement. This simplified approach can probably be improved by vectorially combining the initial velocity of the seaplane with the wave-particle velocity (see ref. 11, pp. 366–369) at the point of contact for determining the effective initial flight-path angle relative to the wave surface, as in reference 16.

DISCUSSION OF GENERALIZED RESULTS

The foregoing analysis showed that all the quantities which characterize a seaplane impact can be represented in terms of generalized variables which are related to one another during an impact through the approach parameter κ, and figures 3 to 18 present the theoretical relationships among these generalized variables which apply from the instant of initial contact until the seaplane rebounds from the water surface. It was also shown that a single variation exists between each of the generalized variables corresponding to any particular stage of the impact and the approach parameter κ, and figures 19 to 31 show the generalized variables at the instant of maximum acceleration, the instant of maximum pitching moment about the step, the instant of maximum penetration, and the instant of exit during rebound from the water surface, all as functions of κ.

Although the generalized curves permit the complete determination of the behavior of the seaplane during an impact, some physical interpretations of these results in terms of the corresponding dimensional variables may be desirable, particularly with regard to the laws of variation indicated by the form of the generalized variables and as concerns the effects of κ on the dimensional variables.

The definitions of the generalized variables clearly show how the seaplane characteristics and the initial downward velocity affect the dimensional variables at any given stage of an impact at a particular value of κ. As an example, it can be seen from the form of the generalized-acceleration variable that the maximum acceleration (or load factor) for a given value of κ varies as the square of the downward velocity, inversely with the cube root of the mass of the seaplane, and so forth. It can also be seen that, for constant κ, the penetration at any stage of the impact is independent of the initial velocity and that the pitching moment about the step is independent of the angle of dead rise. Similar observations from the form of the generalized variables can be readily made for all other dimensional variables.

With regard to the effects of κ on the dimensional variables, since all the generalized variables are based on the initial downward velocity (either vertical or normal to the keel, depending on which coordinate system is employed), curves showing the relationships between any two dimensional variables for different values of κ will have the same relative shapes as the generalized curves if the downward velocity is the same for each value of κ. Thus, the generalized curves shown in figures 3 to 31 may be interpreted as corresponding to dimensional curves for impacts with the same downward velocity but different flight-path angles and, therefore, different forward velocities. In this case the effect of κ on the dimensional

variables is the same as on the generalized variables; that is, an increase in κ, which corresponds to an increase in the resultant velocity or a decrease in the flight-path angle, results in an increase in the maximum acceleration, an increase in the maximum pitching moment about the step, a decrease in the time to reach any given stage of the impact, and so forth.

On the other hand, a somewhat different interpretation of the generalized curves may be given if the resultant velocity is considered to be constant and the flight-path angle or downward velocity is assumed to vary. This situation corresponds to landings of a given seaplane at a more or less constant resultant velocity but with different downward velocities as determined largely by piloting technique. In this case the dimensional curves for different values of κ will not have the same relative shapes as the generalized curves since the generalized variables are based on the downward velocity rather than on the resultant velocity. The effect of κ on the dimensional variables may be evaluated by considering, for example, the acceleration-time relationship. As can be seen from the definitions of the generalized variables, for any given value of κ, the dimensional acceleration at any proportional stage of the impact process varies as the square of the downward velocity, as previously noted; whereas, the corresponding time is inversely proportional to the downward velocity. If the resultant velocity and the trim angle are both held constant, higher flight-path angles are associated with smaller values of κ. As κ becomes smaller, the resulting increase in downward velocity more than offsets the corresponding reduction in the generalized acceleration and the increase in the generalized time. As a result, the maximum acceleration (dimensional) obtained with constant velocity and trim angle will be greater at the higher flight-path angles (smaller values of κ) than at the smaller flight-path angles and will be reached in a shorter time after contact. These results as well as interpretations of the effect of κ on the relationships between the other dimensional variables when the resultant velocity is considered to be constant can be easily seen if the generalized curves are converted to dimensional curves for constant resultant velocity. This type of presentation has the disadvantage that separate curves are required for each trim angle.

With regard to the sequence of events during an impact, it can be seen from figure 19 that the various stages of the impact are reached in the following order: maximum acceleration, maximum pitching moment about the step, maximum penetration, and exit during rebound. It can also be seen that the state of motion at the instant of maximum pitching moment about the step is only slightly different from that at the instant of maximum acceleration. As might reasonably be expected, for a given sinking speed, the time required to reach a given stage of the impact is greatest at the high flight-path angles (small values of κ) where the planing forces due to forward speed are smallest. Similarly, the differences in the state of motion and in the times corresponding to the various stages of the impact are large for high flight-path angles and become very small as the limiting condition of planing is approached.

COMPARISON OF THEORETICAL RESULTS WITH EXPERIMENTAL DATA

In this section, theoretical and experimental time histories of the draft, vertical velocity, vertical acceleration, and pitching moment, as well as the values of these variables at particular stages of the impact, such as the instant of maximum acceleration, the instant of maximum penetration, and the instant of exit during rebound, are correlated in figures 6 to 8, 20 to 24, and 32 to 37 by comparing theoretical values of the generalized variables with corresponding experimental values. The theoretical values have been determined from the solutions of the generalized equations for the system, whereas the experimental values have been obtained by substituting measured values of the dimensional variables and the appropriate physical constants into the definitions of the generalized variables.

As previously discussed, although the theoretical equations relating the generalized variables are valid regardless of how the dead-rise-angle and aspect-ratio functions are defined, it is necessary to specify these functions explicitly in order to convert the experimental data into generalized variables. For this purpose, the dead-rise-angle and aspect-ratio functions have been taken in accordance with equations (83) to (86). Thus, the comparisons between theoretical and experimental results do not show only the validity of the equations relating the generalized variables, but rather the validity of these equations in conjunction with the particular dead-rise-angle and aspect-ratio functions used in the determination of the experimental values of the generalized variables.

SOURCE OF EXPERIMENTAL DATA

The applicability of the theory to seaplane impacts is illustrated by comparisons with a large quantity of experimental data which has been obtained over a period of time in the Langley impact basin. The tests included a much wider range of trim and flight-path angles than is usually encountered in normal seaplane operations. Although most of the experimental results have been presented in earlier papers (refs. 12 to 14 and 17 to 20), some of the data included in the present report have not been previously available. A tabulation of the detailed test conditions and the most important experimental results is given in tables II to IV.

A description of the impact basin and its equipment is presented in reference 17. The test data were obtained in smooth water at fixed trim with three hull forebody models, M–1, M–2, and M–3, which are described in references 14 and 17, 12, and 13, respectively. These models, which are of all-metal construction, have lines generally similar to the hulls of conventional flying boats except for the absence of chine flare. Model M–1 has an angle of dead rise of 22½° at the step, model M–2 has 30° dead rise, and model M–3 has 40° dead rise. The tests were run at a number of weights between 1,000 and 2,700 pounds and include trim angles ranging from 3° to 15°. The range of flight-path angles investigated included virtually all conditions between planing and vertical drop. Wing lift was simulated by the action of a pneumatic cylinder and cam device which was designed

to apply a constant upward force to the model equal to the total weight.

During an impact, the motion of the hull normal to the water surface was determined by independent time-history measurements of the vertical acceleration, vertical velocity, and draft at the step. Several different NACA accelerometers were used in the course of the testing. These ranged in natural frequency from 12.5 to 26 cycles per second. The velocity and displacement measurements were made by means of variable-resistance slide wires whose response characteristics have not been completely determined. Measurements of the pitching moment were obtained by means of the strain-gage dynamometer truss schematically illustrated in figure 38 and are referred to the front hull attachment point as shown in the figure. A typical oscillograph record obtained in the tests is shown, greatly reduced, in figure 39.

Estimates of the precision of the experimental data are tabulated in references 12, 13, 17, 18, 19, and 20. On the basis of these values, most of the basic measurements are believed to be correct within the following limits:

Horizontal velocity, feet per second	±0.5
Vertical velocity, feet per second	±0.2
Vertical displacement (draft), feet	±0.02
Vertical acceleration, g, percent of reading	+5 to −10
Pitching moment, pound-feet, percent of reading	±10

It should be noted that the accuracies quoted refer to measurements of the maximum values attained by the variables during an impact. On the other hand, measurements of instantaneous values which require the use of more than one record trace, such as the acceleration at the instant of maximum draft, involve additional errors due to instrument response (primarily lag) and time-correlation difficulties.

COMPARISONS OF LOADS AND MOTIONS

Comparisons between theoretical and experimental time histories of the vertical displacement, velocity, and acceleration are presented in figures 6, 7, and 8, respectively, for hull models of 22½° and 30° angles of dead rise and a range of contact conditions extending from very shallow flight paths ($\kappa=10$) up to extremely steep flight paths ($\kappa\approx0.5$). A typical seaplane impact in smooth water at, for instance, 6° trim, vertical velocity of 3 feet per second, and horizontal velocity of 80 miles per hour would correspond to a value of κ of 4.05. For a high-speed landing at 150 miles per hour, for example, and the same vertical velocity, the flight-path angle is reduced and gives a value of κ of 7.6. A landing into the flank of an oncoming wave, on the other hand, might correspond to a value of κ as low as 0.2.

It can be seen from figures 6 to 8 that the agreement between the experimental and calculated time histories is fairly good throughout almost the entire immersion process. Near the very end of the impact, however, just before the hull rebounds from the water surface, there is a deviation from the theoretical results which indicates the application of an external downward force on the model that causes the rebound to be slightly delayed. In figure 7, where this effect is most clearly visible, the test points corresponding to the instant of exit have been differentiated by the addition of a flag (⟍). The extraneous force is apparently contributed by the test equipment and has been attributed to two factors which take effect after the maximum draft has been reached and the model has begun its upward travel; namely, leakage in the pneumatic "lift" cylinder which balances the weight, and friction in the dropping mechanism. As a result of the reduction in hydrodynamic force accompanying the decrease in draft, the effect of the extraneous force on the motion of the hull is proportionately greatest just before the model leaves the water surface. On the whole, it may be said that the discrepancies between theory and test data evident from the figures are within the limits of the experimental accuracy provided by the equipment and instrumentation.

Figures 20 to 23 show how the state of motion corresponding to the instants of maximum acceleration, maximum penetration, and exit varies with κ. A comparison between the theoretical and experimental times at which these events occur is given in figure 24. The test data cover a wide range of weights, velocities, and flight-path angles. A flag (⟋) attached to an experimental point signifies that chine immersion has occured previous to the instant represented by the point. Logarithmic scales have been used in figures 20 to 24 in order to spread out the test data and emphasize the differences in the states of motion and times corresponding to the various stages of the impact. The extent of this expansion of the data can be evaluated by a comparison with figure 19 which shows the theoretical curves plotted on uniform coordinates.

Figure 20 shows the variation of the maximum generalized acceleration with the approach parameter and compares the theoretical results with experimental data obtained with hull models of 22½°, 30°, and 40° angles of dead rise The reduced scatter in the data for 40° angle of dead rise is due to the improved instrumentation used in these tests. The solid-line curve represents the theoretical results for the case in which the beam of the seaplane is large enough that the chines are not immersed at the instant of maximum acceleration. As can be seen, there is relatively good agreement with experiment.

The effect of chine immersion in reducing the maximum acceleration is shown by the broken-line curves, which have been calculated by the method previously discussed, for several values of $u_c=\frac{\Pi}{C_{\Delta_0}^{1/3}}$ (equal to the generalized displacement at the instant of chine immersion) corresponding to a wide range of beam loadings. For a given beam loading, the intersection of the broken-line curve, corresponding to the proper value of $\frac{\Pi}{C_{\Delta_0}^{1/3}}$, with the solid-line curve determines the value of κ above which there is no reduction in load due to chine immersion. For values of beam loading which have been in the past commonly used in American seaplane design practice ($C_{\Delta_0}<1$) and normal flight-path angles, the theory indicates that the reduction in maximum acceleration due to chine immersion is small.

With higher beam loadings, on the other hand, the theory indicates that appreciable reductions in load may be obtained. For a given seaplane weight, a decrease in beam of 45 percent

increases the gross-load coefficient six times. For a seaplane with C_{Δ_0} of 6, β of 22½°, τ of 6°, and an initial flight-path angle γ_0 of 5°, κ=1.18 and $\frac{\Pi}{C_{\Delta_0}^{1/3}}$=0.311. As may be seen by comparing the appropriate broken-line curve with the solid-line curve in figure 20, the maximum load for the foregoing impact conditions should be about 30 percent less than that in a corresponding impact of a wide hull not subject to chine immersion. With still higher beam loadings, even greater reductions in maximum load are indicated by the curves.

For more conventional values of beam loading, a considerable amount of experimental data, extending over a 2½-to-1 range of beam loading and including values somewhat greater than those currently employed, is presented in figure 20. As can be seen, the reductions in the maximum load due to chine immersion appear to be in fairly good agreement with the theoretical results. For the great majority of the test conditions investigated, however, the load reductions, as indicated by both theory and experiment, are either relatively small or entirely absent. A more detailed investigation of the effects of chine immersion for extremely high beam loadings, where the force on the chine-immersed areas becomes too large to be neglected, is given in reference 21.

Figure 21 shows the variation with κ of the generalized acceleration corresponding to the instant of maximum penetration. From the figure it is seen that the acceleration at this instant is always less than the maximum acceleration, which occurs at an earlier time after contact. (See fig. 24.) As might reasonably be expected, the difference in the acceleration at these two instants is greatest at the high flight-path angles and decreases as the planing condition is approached. Because of lag in the slide-wire measurements which were used to determine the instant of maximum draft, the recorded time at which this stage of the impact occurs is slightly greater than the actual time. As a result, the accelerations corresponding to the recorded time of maximum draft are somewhat lower than the true values. At the low values of κ, the experimental accelerations at the instant of maximum draft are considerably greater than the theoretical values as a combined result of the immersion of the nonprismatic bow section of the hull and the action of the buoyant forces, caused by the large penetrations associated with the high flight-path angles. This effect is most pronounced beyond the range of conditions applicable to conventional seaplanes. The importance of the buoyant forces will be discussed subsequently in more detail.

The vertical velocities at the instants of maximum acceleration and exit are presented in figure 22. The positive velocities corresponding to the occurrence of maximum acceleration show that the motion of the seaplane is still downward at this instant and that the maximum draft has not yet been attained. At the instant of exit, the seaplane is traveling upward—hence, the negative velocities. The scatter evident in the test data is largely due to the previously mentioned lag in the slide-wire system as well as to the difficulties encountered in correlating the various independent measurements of the motion which are required to establish the time at which each event occurs.

Figure 23 shows the draft at the instant of maximum acceleration as well as the maximum draft. As might be reasonably expected, all other conditions being equal, the greater drafts occur at the higher flight-path angles. Similarly, the difference between the maximum draft and the draft at the instant of maximum acceleration is greatest at the low values of κ and decreases as the flight-path angle is reduced. As indicated by the form of the generalized displacement, for a given value of κ, the absolute draft at any stage of the impact is independent of the magnitude of the initial velocity. This fact is borne out by the test data which include an 8-to-1 velocity range.

Figure 24 shows the time corresponding to the instants of maximum acceleration, maximum penetration, and exit. In conformity with the results shown in the preceding figures, for the same vertical velocity, a longer time is required to reach a given stage of the impact process at the high flight-path angles than for the flatter-approach conditions. In a similar manner, the differences in time between the occurrence of the various stages are greatest for the low values of κ and become very small as the limiting condition of planing is approached. The experimental factors which cause the recorded time of maximum draft and exit to be slightly delayed have been previously enumerated.

An examination of figure 23 reveals that the maximum draft at low values of κ tends to be slightly less than that specified by the theory. This result is apparently due to the combined effects of immersion of the upswept bow section and the action of the buoyant (gravity) forces which cause the downward motion of the seaplane to be arrested at an earlier time. The buoyant forces are, of course, larger at the instant of maximum draft than at any other time during the impact and are of greatest importance at the high flight-path angles because of the greater drafts reached. In addition, because the vertical velocities are subject to physical and operational limitations, the resultant velocities at the high flight-path angles are so small as to emphasize still further the importance of the buoyant forces in comparison with the inertia forces for such approach conditions. As a result, the experimental accelerations at maximum draft for the high flight-path angles are greater than the theoretical values. Furthermore, the effect of buoyancy at the instant of maximum draft more than overcomes the reduction in force due to chine immersion, which would otherwise result in slightly greater drafts than would be experienced if the beam of the seaplane were large enough to prevent the chines from reaching the water surface.

For the practical range of flight-path angles applicable to conventional seaplanes, on the other hand, the agreement between the theoretical results and the experimental data indicates that the buoyant forces are relatively insignificant and that the theory is generally applicable.

COMPARISONS OF PITCHING MOMENTS

The applicability of the theoretical pitching-moment results is illustrated by comparisons with experimental data obtained with two hull forebodies having angles of dead rise of 30° and 40° at the step. The total weights in the pitching-moment tests ranged between approximately 1,200 and 1,350 pounds. The detailed test conditions are presented in figures 32 to 35 and in table IV.

Experimental pitching-moment time histories, as derived from the oscillograph records, are shown in figures 32 to 35. These data are compared with theoretical time histories of the total pitching moment about the front attachment point as well as with theoretical time histories of the hydrodynamic pitching moment about this point.

The time histories of the hydrodynamic pitching moment about the front attachment point were calculated by application of equations (36) and (38) in conjunction with the analytical results plotted in figures 12 and 17. The dimension a in equation (36), which represents the distance from the step to the front attachment point, was measured as 2.89 feet for the two hull models used in the pitching-moment tests.

In order to compare the theoretical and experimental results properly, the inertia and static moments about the front attachment point, introduced by the fact that the center of gravity of the model did not coincide with the center of moments, must be added to the hydrodynamic moment about the front attachment point. The increment in pitching moment arising from this source is given by the equation

$$\Delta M_a = W_h\left[\frac{\ddot{z}_w}{g}\frac{d}{\cos\tau} - (d\cos\tau + c\sin\tau)\right] \tag{87}$$

Thus, the total pitching moment referred to the point a is expressed by

$$M_{a_T} = \frac{\dot{z}_{w_0}^2}{g\cos\tau}\left[\frac{m_s W}{\sin\tau}\frac{\phi_1(A)}{\phi(A)} + u''\Lambda(aW + dW_h)\right] - W_h(d\cos\tau + c\sin\tau) \tag{88}$$

where the dimensions d and c define the location of the center of gravity relative to the center of moments, as shown in figure 38. Values of d and c for each of the configurations tested are given in table IV.

Figure 32 shows the results of three tests of the hull model with 30° angle of dead rise at 12° trim. All three tests were made at approximately the same flight-path angle of about 5° and, therefore, closely correspond to a single value of the approach parameter κ equal to about 2.2. Two of the tests were made with almost identical resultant velocities. The third test was made at a velocity approximately 60 percent greater than that for the first two runs. The theoretical results were calculated for values of the initial vertical velocity measured in the tests and for a value of $\kappa=2.0$, which approximately corresponds to the magnitude of the approach parameter associated with the tests. The theoretical total pitching moments appear to be in substantial agreement with the results measured in the tests.

Figure 33 is a composite plot of the quantity

$$\frac{M_{a_T} + W_h(d\cos\tau + c\sin\tau)}{\frac{W}{g}\dot{z}_{w_0}^2} = \left[\frac{m_s}{\sin\tau}\frac{\phi_1(A)}{\phi(A)} + u''\Lambda\left(a + d\frac{W_h}{W}\right)\right]\frac{1}{\cos\tau} \tag{88a}$$

against the variable $t\dot{z}_{w_0}$. For the three tests previously discussed, since all parameters except the resultant velocity were held constant, equation (88a) and the form of the generalized time show that the results of all three tests should be reduced to the single theoretical variation given by the solid-line curve. As is evident from the figure, this result is closely attained. The extent of the deviations which do exist may be taken as a direct indication of the consistency of the experimental data. The oscillatory nature of the results of some of the tests (see, for example, fig. 32 (c)) is attributed to structural vibrations induced in the equipment by the magnitude of the catapulting accelerations required to produce the relatively high horizontal velocities attained in the tests.

Figures 34 and 35 show comparisons of theoretical and experimental pitching-moment time histories for typical impacts of a float with a 40° angle of dead rise at trim angles of 9° and 6° and values of the approach parameter κ approximately equal to 1. Comparisons between theoretical and experimental maximum total pitching moments for this hull model are presented in figures 36 (a), (b), and (c) for trim angles of 12°, 9°, and 6°, respectively. In order to reduce the increment in pitching moment due to the displacement of the center of gravity from the center of moments, another set of tests was made, at 12° trim, with the hull model weighted to move the center of gravity rearward to a position vertically in line with the front attachment fitting. The results of these tests are shown in figure 37. As is evident from the figures, the theoretical results appear to be in good agreement with the experimental data. A more exact evaluation of the end-flow correction to the pitching moment $\phi_1(A)$, which in this comparison has been taken equal to the end-flow correction to the total load $\phi(A)$, should result in even better agreement between the calculated and experimental results. In the absence of suitable pressure-distribution data, the favorable results of this comparison may be considered an indirect indication of the validity of the longitudinal distribution of the hydrodynamic load (running load) specified by the theory.

CONCLUDING REMARKS

A theoretical study has been made to determine the motions, hydrodynamic loads, and pitching moments experienced by V-bottom seaplanes during step-landing impacts, and the equations relating the displacement, velocity, acceleration, pitching moment, and time throughout the course of the impact have been derived. In order to decrease the number of independent constants which have to be considered, the relationships during impact have been generalized by the introduction of suitable dimensionless variables which take into account the effects of such factors as the weight of the seaplane, the dead-rise angle, the trim angle, the flight-path angle, and the initial velocity, in accordance with the laws governing the variation of the behavior of the seaplane with these quantities.

It is shown that all generalized variables are related to one another during the impact by a single parameter, called the approach parameter κ, which is determined by the trim angle and the flight-path angle at initial contact. Thus, the relationship between any two of the generalized variables during an impact can be represented by a single curve for each value of κ. Furthermore, a single variation with κ exists for each of the generalized variables corresponding to any particular stage of the impact.

In order to permit convenient use of the theoretical results in the design of seaplanes, charts are presented showing the relationships among the generalized variables during the impact for values of κ corresponding to a wide range of impact conditions; charts are also presented which show the variations with κ of the generalized variables corresponding to the instant of maximum acceleration, the instant of maximum pitching moment about the step, the instant of maximum penetration, and the instant of exit during rebound. In addition, charts are presented which show the effects on the maximum load produced by chine immersion due to increased beam loading or unusually high flight-path angles. These theoretical results are shown to be generally in good agreement with extensive test data obtained in the Langley impact basin over a period of years.

Although the generalized relationships are independent of the definition of the virtual mass, simplified equations for the dead-rise-angle and aspect-ratio functions which govern the virtual mass are suggested, on the basis of previous work, for use in making conversions between generalized and dimensional variables. Even though these approximations permit relatively good agreement between theory and experiment to be obtained and should be adequate for the design of conventional seaplanes, a need for additional research to define more rationally the virtual mass for three-dimensional bodies is indicated, particularly for conditions where the chines are deeply immersed due to unusually large beam loading.

LANGLEY AERONAUTICAL LABORATORY,
NATIONAL ADVISORY COMMITTEE FOR AERONAUTICS,
LANGLEY FIELD, VA., *October 30, 1952.*

REFERENCES

1. Mayo, Wilbur L.: Analysis and Modification of Theory for Impact of Seaplanes on Water. NACA Rep. 810, 1945. (Supersedes NACA TN 1008.)
2. Milwitzky, Benjamin: A Generalized Theoretical and Experimental Investigation of the Motions and Hydrodynamic Loads Experienced by V-Bottom Seaplanes During Step-Landing Impacts. NACA TN 1516, 1948.
3. Milwitzky, Benjamin: A Generalized Theoretical Investigation of the Hydrodynamic Pitching Moments Experienced by V-Bottom Seaplanes During Step-Landing Impacts and Comparisons With Experiment. NACA TN 1630, 1948.
4. Von Kármán, Th.: The Impact of Seaplane Floats During Landing. NACA TN 321, 1929.
5. Wagner, Herbert: Über Stoss- und Gleitvorgänge an der Oberfläche von Flüssigkeiten. Z.f.a.M.M., Bd. 12, Heft 4, Aug. 1932, pp. 193–215.
6. Wagner, Herbert: Landing of Seaplanes. NACA TM 622, 1931.
7. Pabst, Wilhelm: Theory of the Landing Impact of Seaplanes. NACA TM 580, 1930.
8. Milwitzky, Benjamin: A Theoretical Investigation of Hydrodynamic Impact Loads on Scalloped-Bottom Seaplanes and Comparisons With Experiment. NACA Rep. 867, 1947. (Supersedes NACA TN 1363.)
9. Miller, Robert W.: Hydrodynamic Impact Loads in Rough Water for a Prismatic Float Having an Angle of Dead Rise of 30°. NACA TN 1776, 1948.
10. Steiner, Margaret F.: Analysis of Planing Data for Use in Predicting Hydrodynamic Impact Loads. NACA TN 1694, 1948.
11. Lamb, Horace: Hydrodynamics. Sixth ed., Cambridge Univ. Press, 1932.
12. Miller, Robert W., and Leshnover, Samuel: Hydrodynamic Impact Loads in Smooth Water for a Prismatic Float Having an Angle of Dead Rise of 30°. NACA TN 1325, 1947.
13. Edge, Philip M., Jr.: Hydrodynamic Impact Loads in Smooth Water for a Prismatic Float Having an Angle of Dead Rise of 40°. NACA TN 1775, 1949.
14. Mayo, Wilbur L.: Theoretical and Experimental Dynamic Loads for a Prismatic Float Having an Angle of Dead Rise of 22½°. NACA RB L5F15, 1945.
15. Miller, Robert W.: Theoretical Analysis of Hydrodynamic Impact of a Prismatic Float Having Freedom in Trim. NACA TN 2698, 1952.
16. Hedrick, I. G., and Siebert, E. G.: Water Loads Investigation—Airplane Model XJR2F–1. Rep. No. 2003.41, Grumman Aircraft Eng. Corp., May 19, 1946.
17. Batterson, Sidney A.: The NACA Impact Basin and Water Landing Tests of a Float Model at Various Velocities and Weights. NACA Rep. 795, 1944. (Supersedes NACA ACR L4H15.)
18. Batterson, Sidney A.: Variation of Hydrodynamic Impact Loads With Flight-Path Angle for a Prismatic Float at 12° Trim and With a 22½° Angle of Dead Rise. NACA RB L5K21a, 1946.
19. Batterson, Sidney A.: Variation of Hydrodynamic Impact Loads With Flight-Path Angle for a Prismatic Float at 3° Trim and With a 22½° Angle of Dead Rise. NACA RB L5A24, 1945
20. Batterson, Sidney A., and Stewart, Thelma: Variation of Hydrodynamic Impact Loads With Flight-Path Angle for a Prismatic Float at 6° and 9° Trim and a 22½° Angle of Dead Rise. NACA RB L5K21, 1946.
21. Schnitzer, Emanuel: Theory and Procedure for Determining Loads and Motions in Chine-Immersed Hydrodynamic Impacts of Prismatic Bodies. NACA TN 2813, 1952.

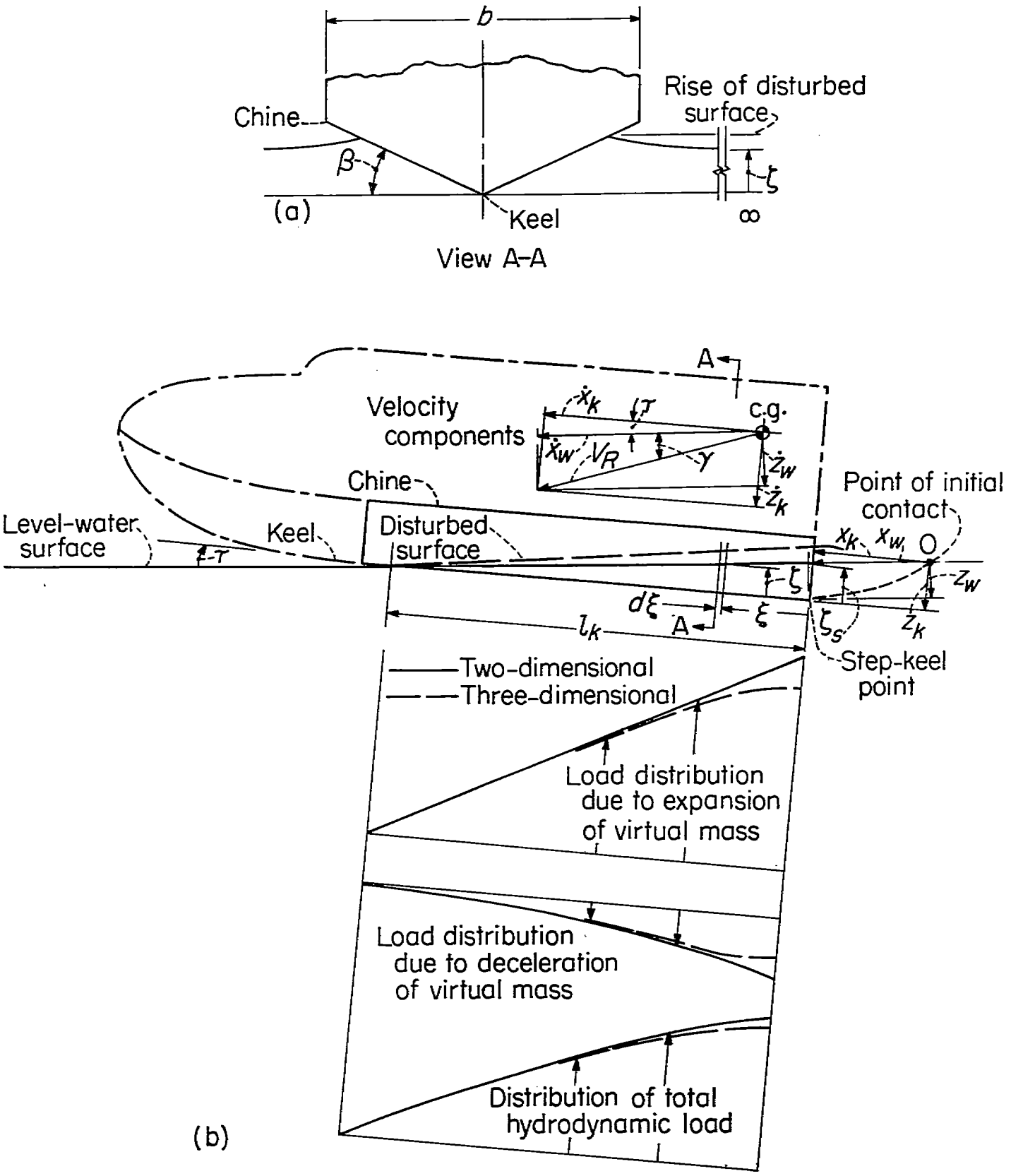

(a) View in transverse section.
(b) Side view

FIGURE 1.—Schematic representation of the impact of a seaplane with a prismatic bottom.

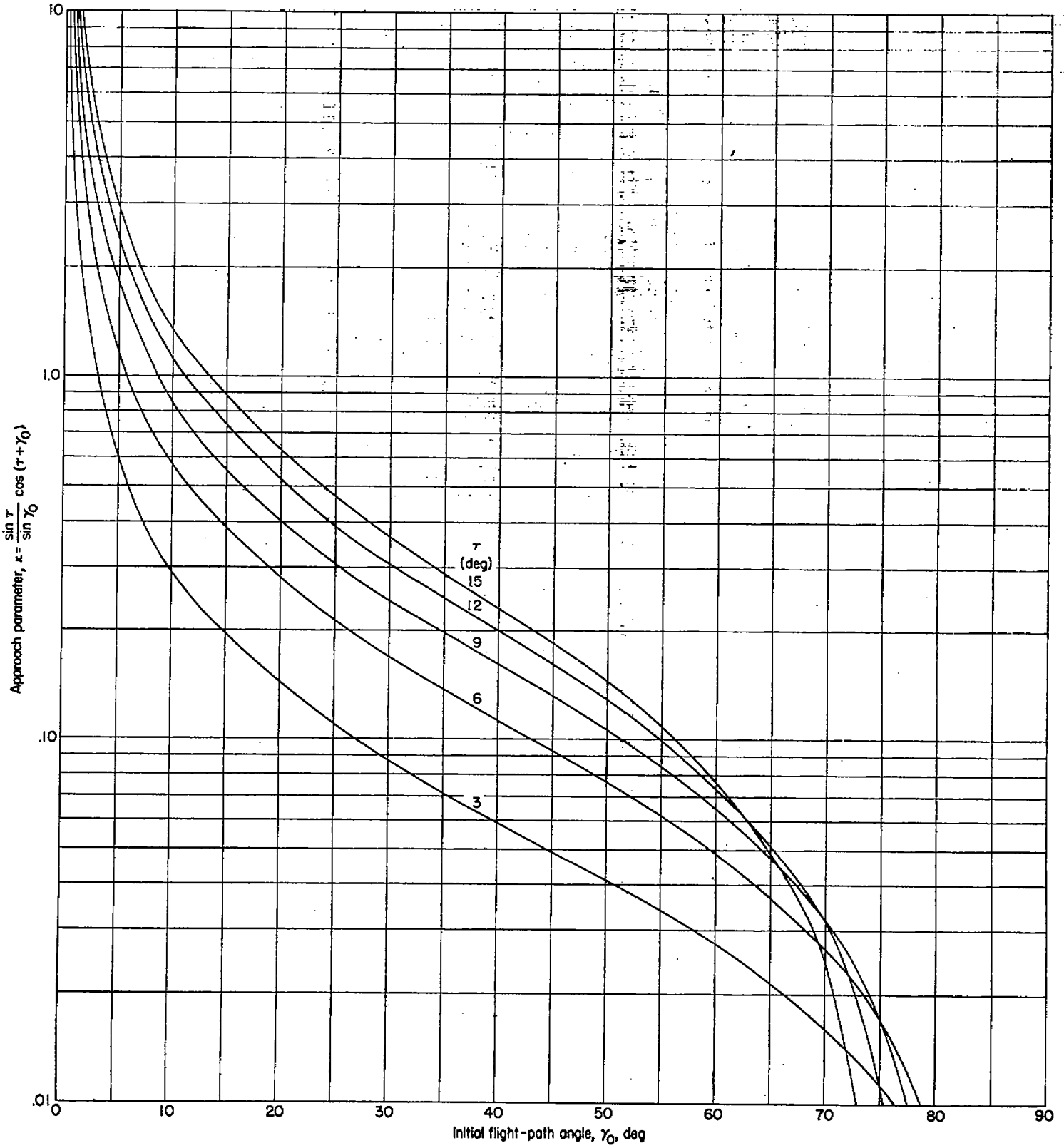

FIGURE 2.—Variation of approach parameter with trim angle and initial flight-path angle.

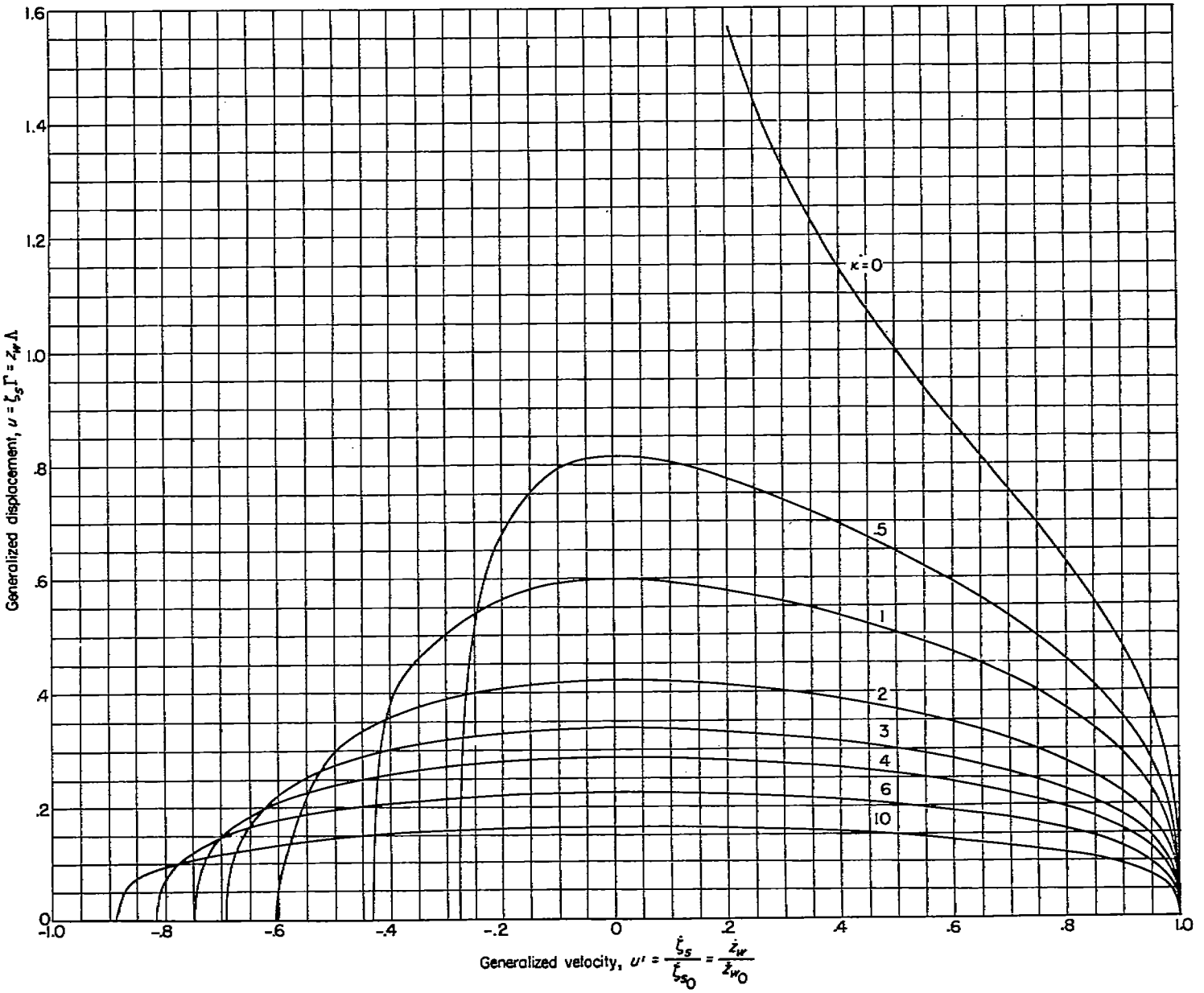

FIGURE 3.—Theoretical variation of displacement with velocity during impact.

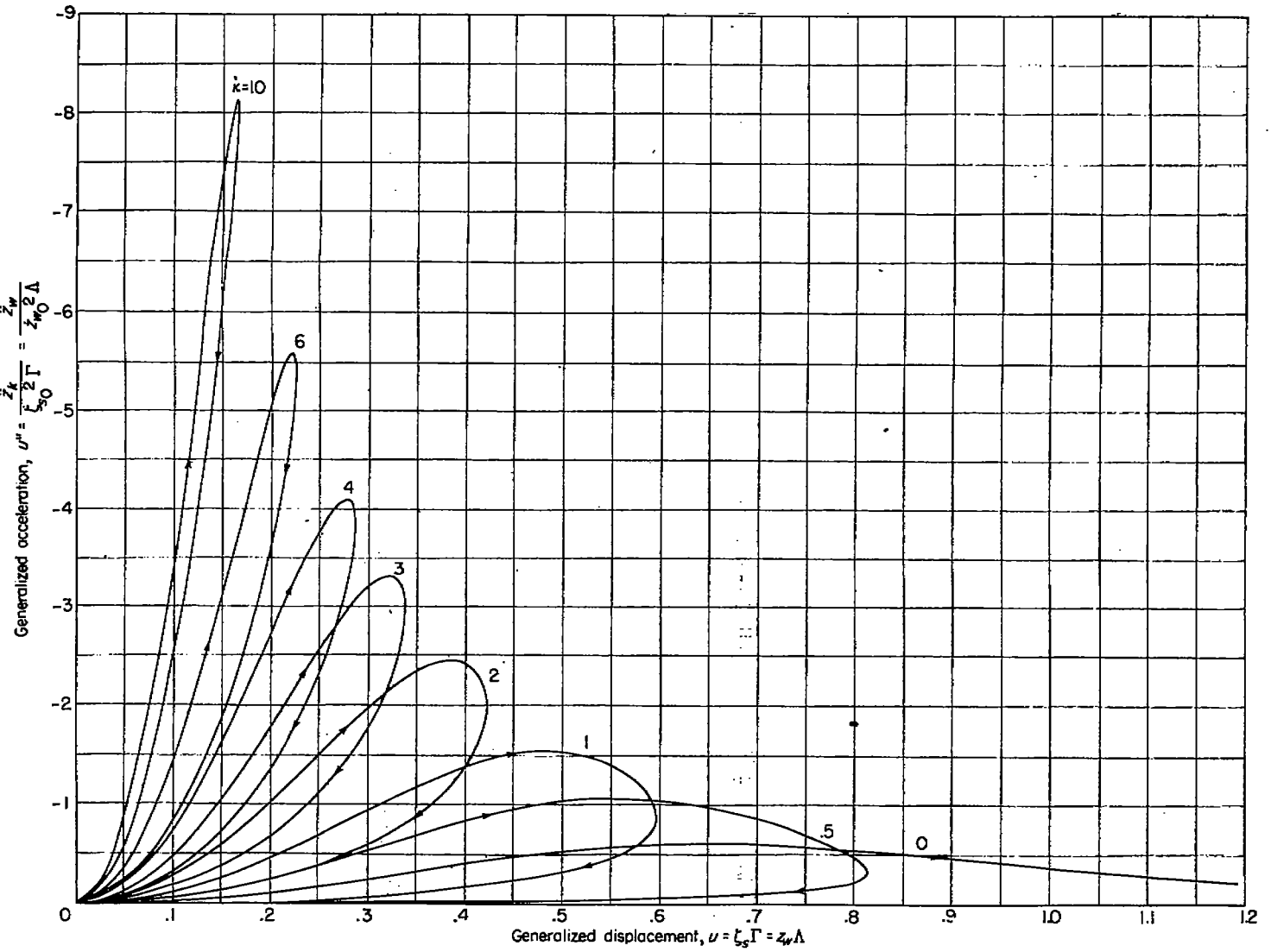

FIGURE 4.—Theoretical variation of acceleration with displacement during impact.

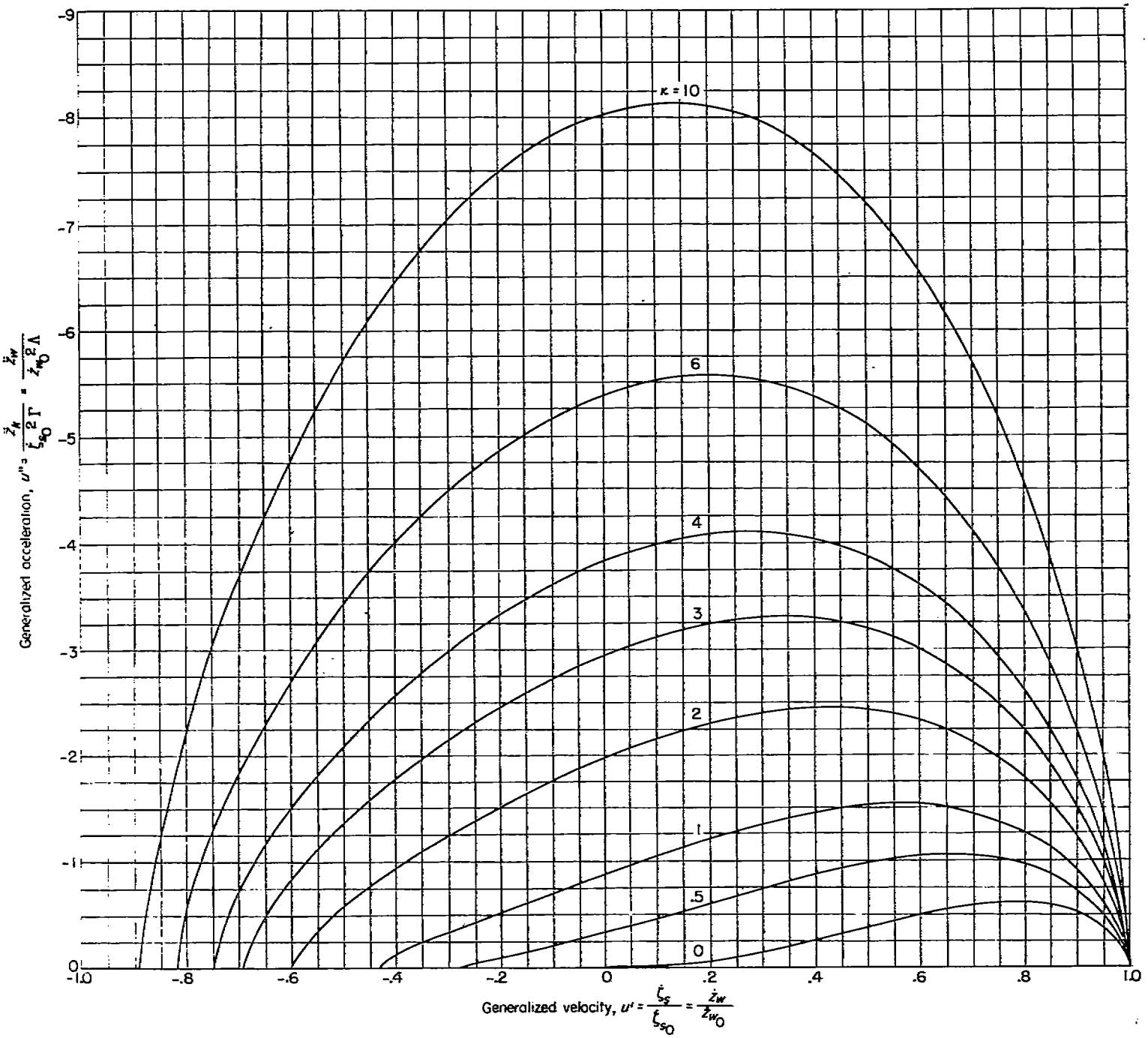

FIGURE 5.—Theoretical variation of acceleration with velocity during impact.

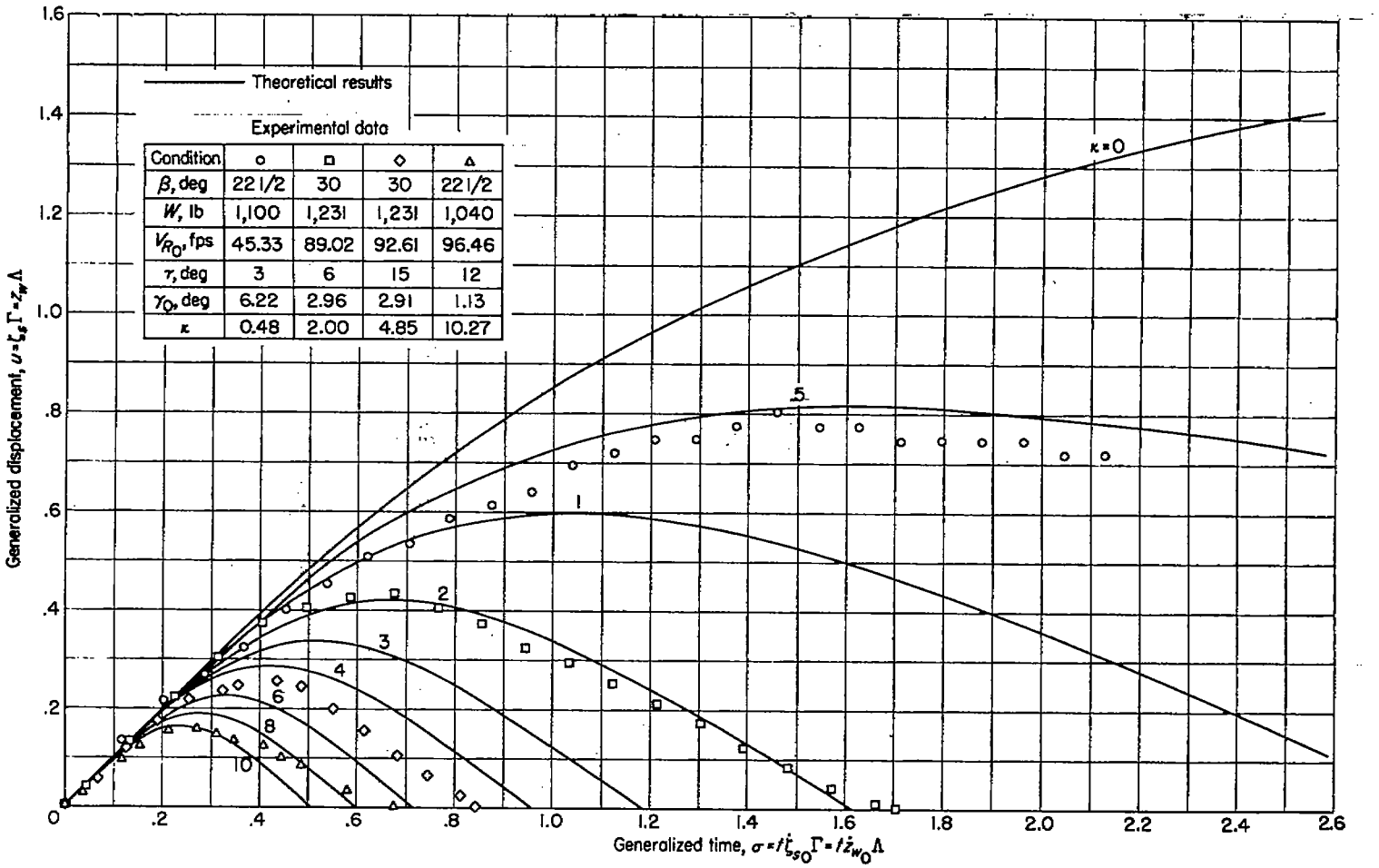

FIGURE 6.—Comparison between theoretical and experimental time histories of displacement during impact.

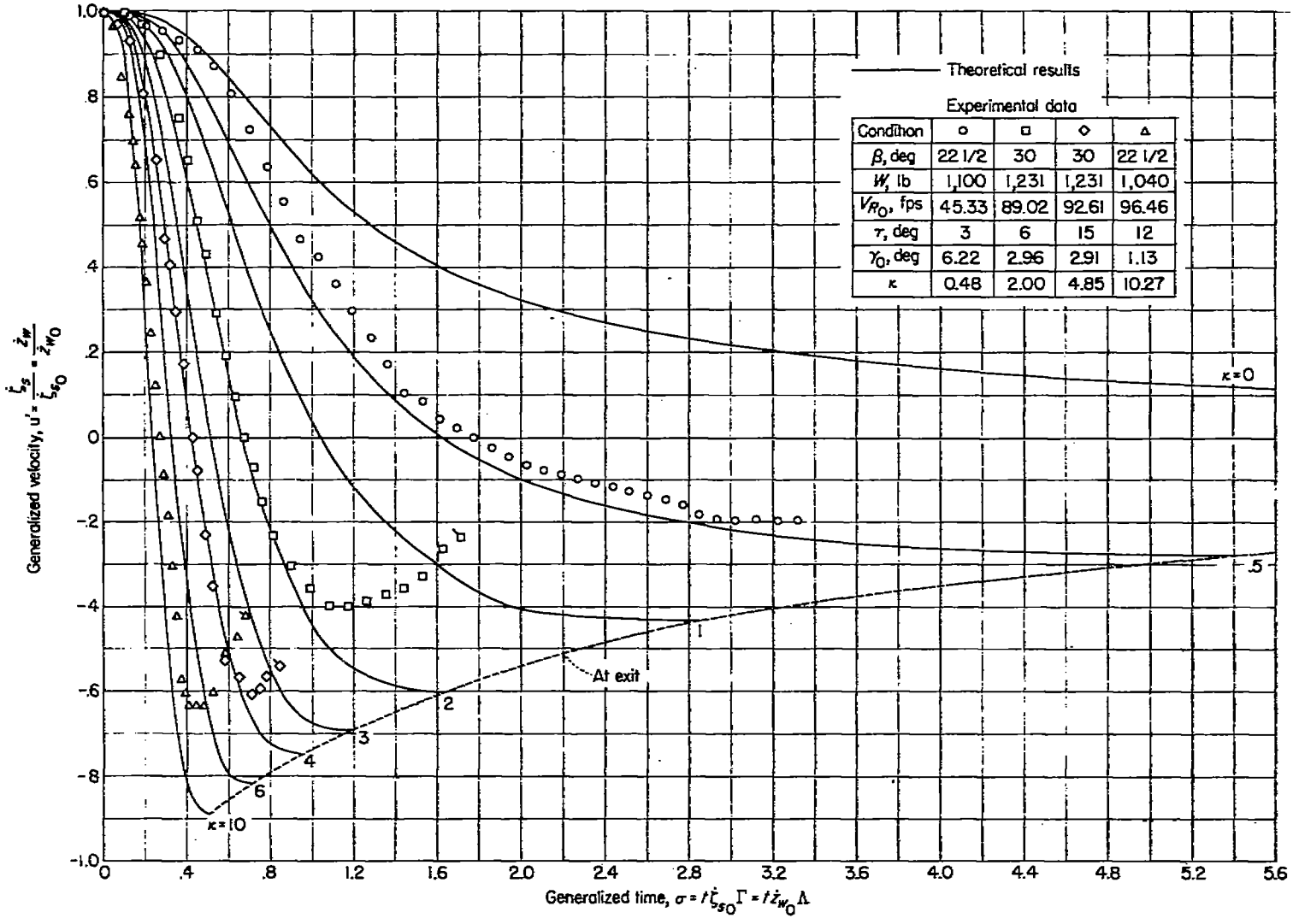

FIGURE 7.—Comparison between theoretical and experimental time histories of velocity during impact.

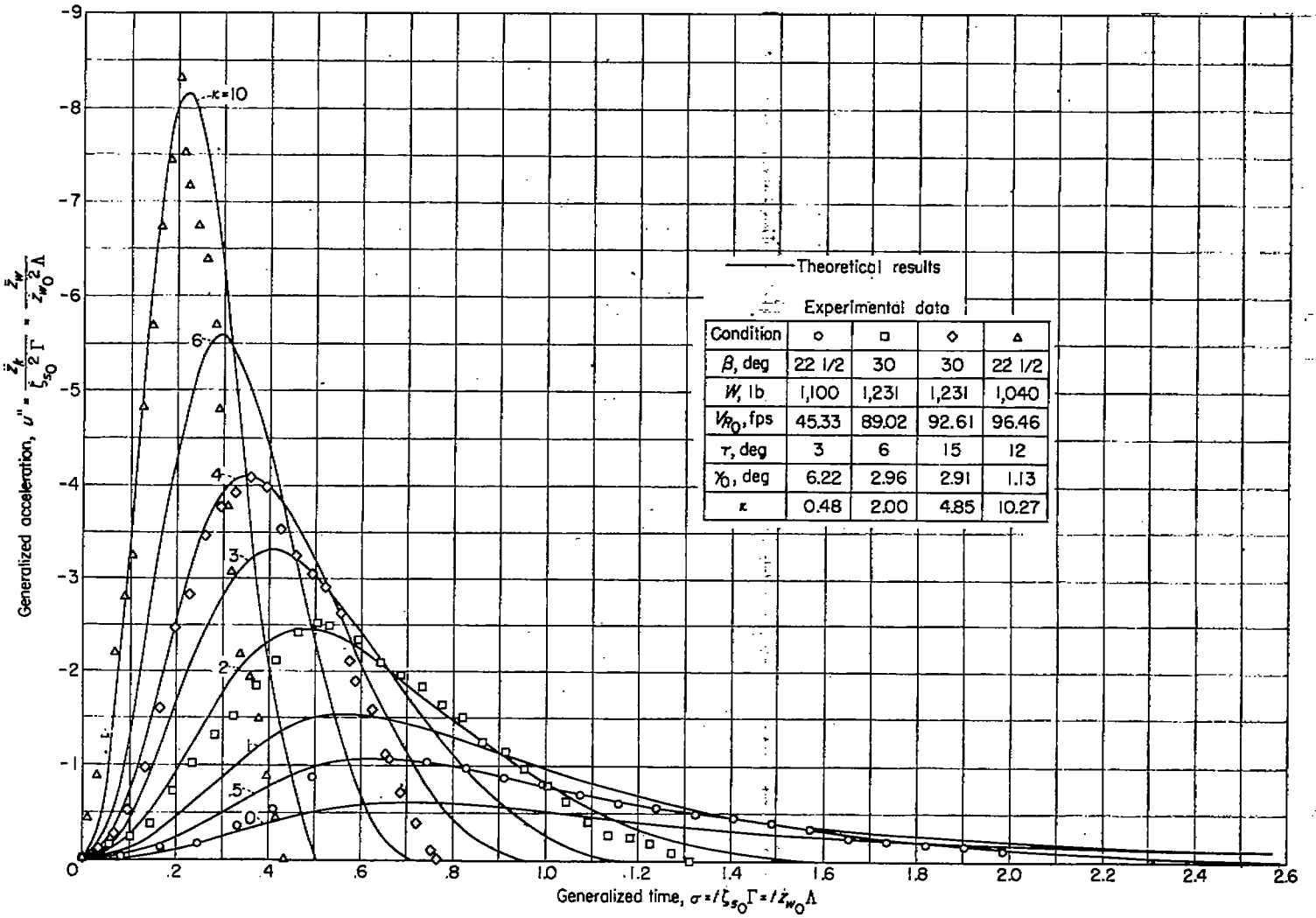

FIGURE 8.—Comparison between theoretical and experimental time histories of acceleration during impact.

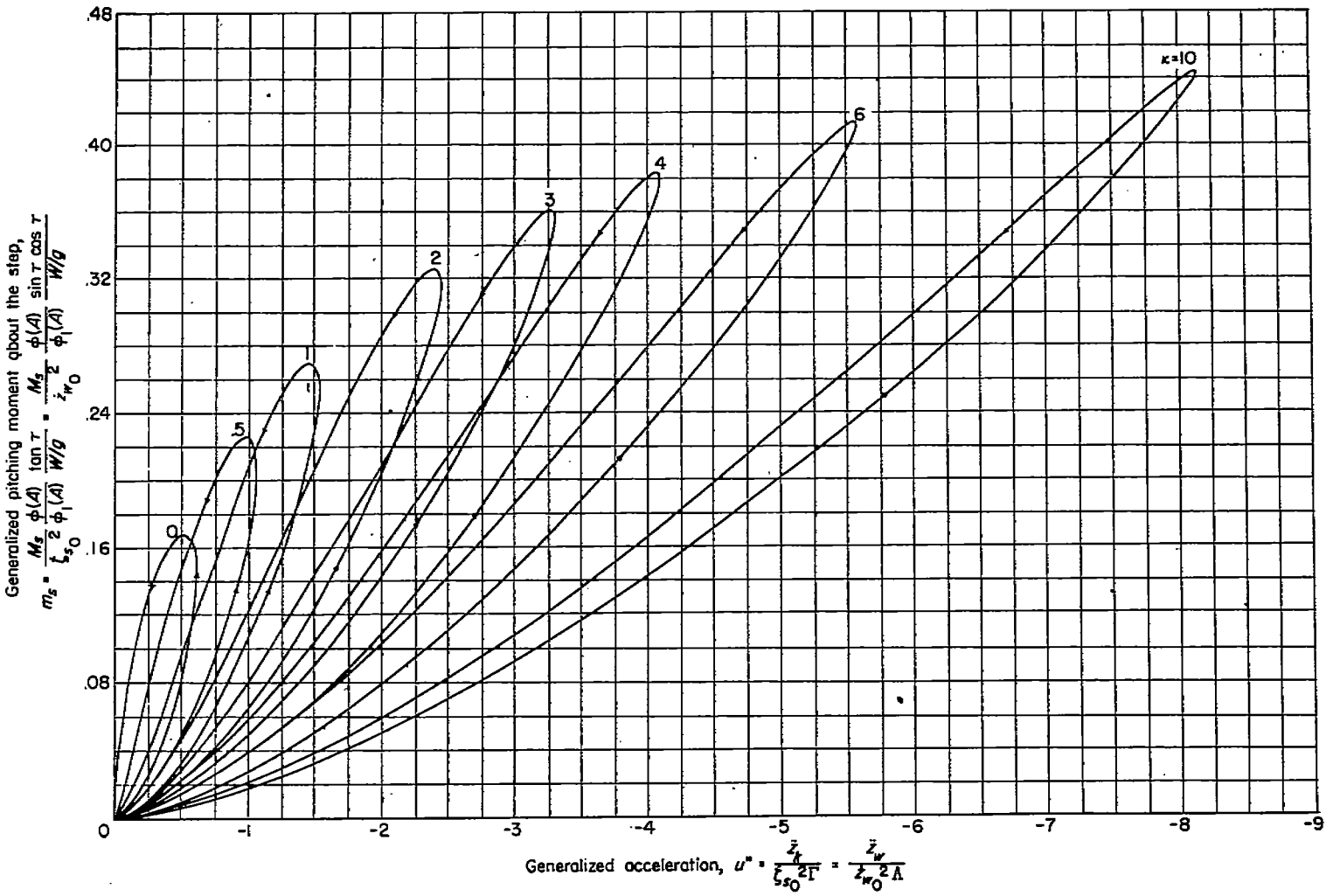

FIGURE 9.—Theoretical variation of pitching moment with acceleration during impact.

272183—54——63

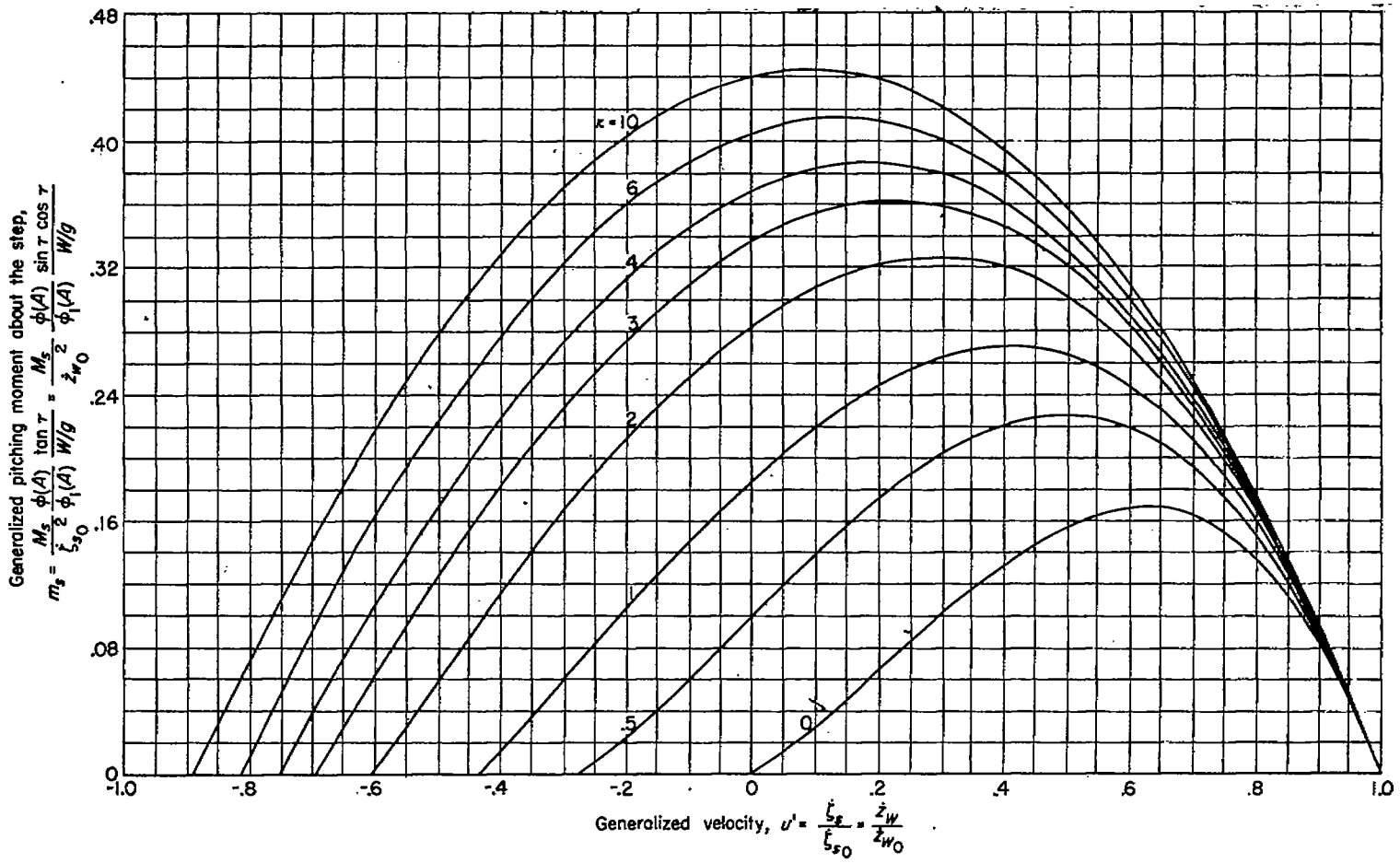

FIGURE 10.—Theoretical variation of pitching moment with velocity.

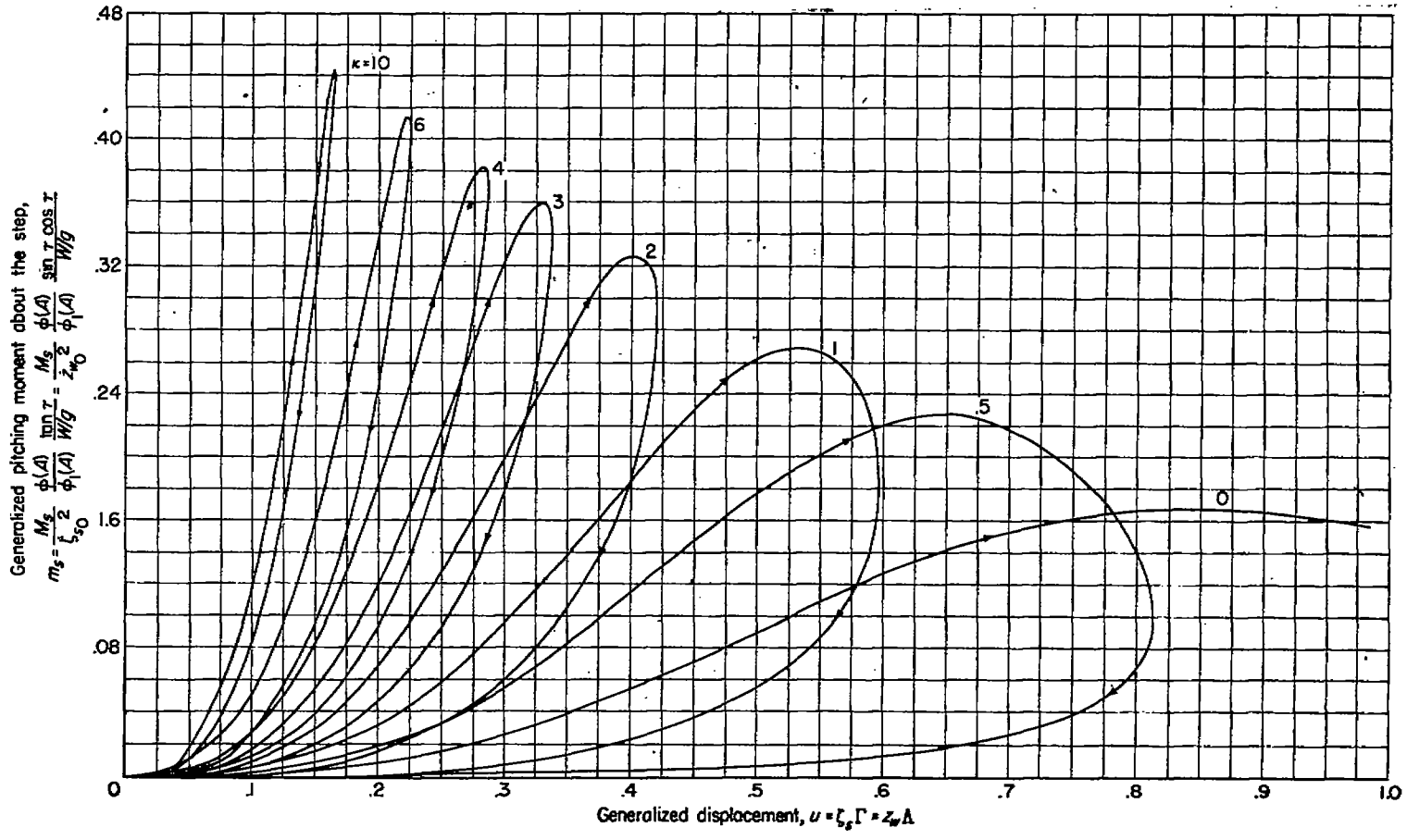

FIGURE 11.—Theoretical variation of pitching moment with displacement during impact.

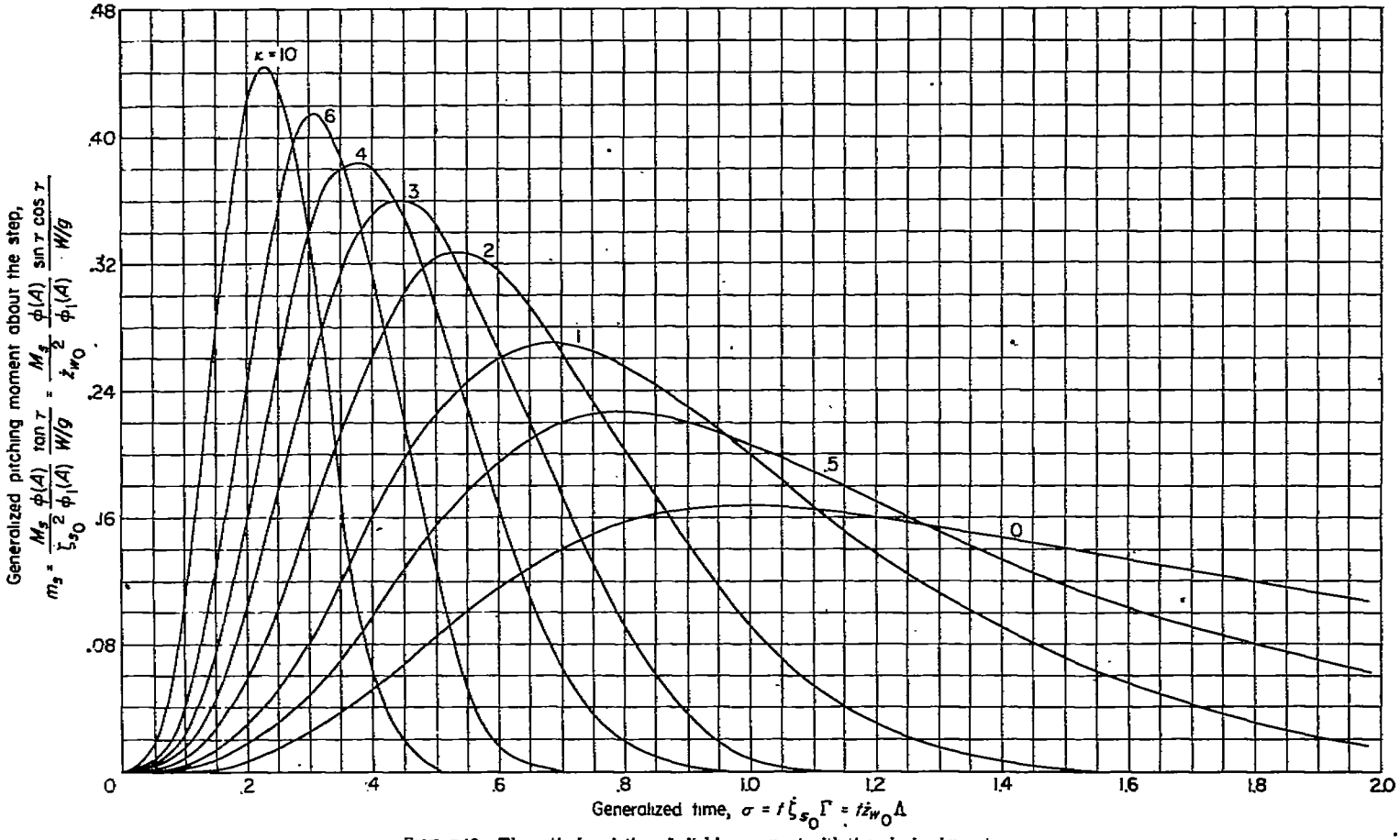

FIGURE 12.—Theoretical variation of pitching moment with time during impact.

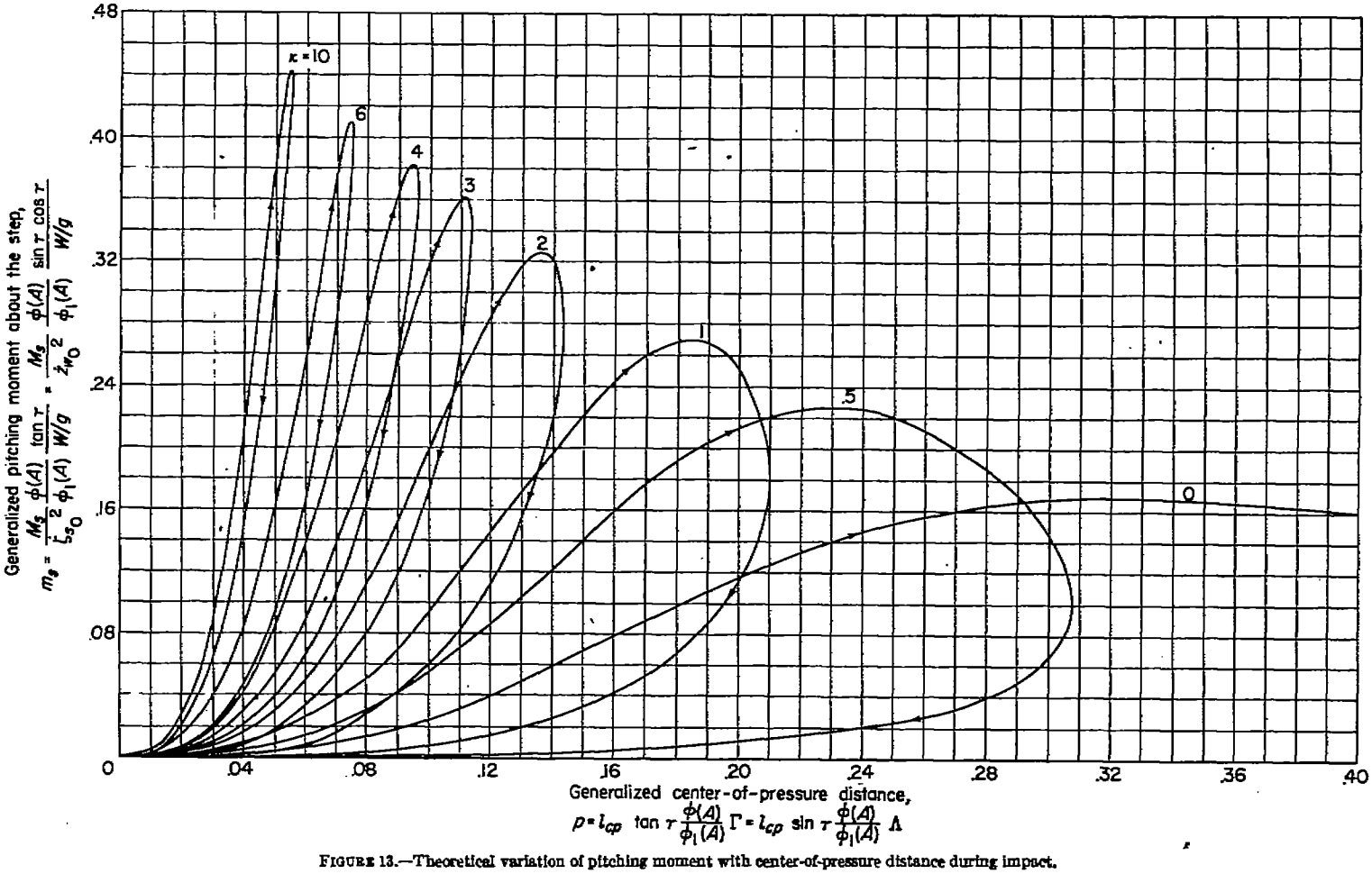

FIGURE 13.—Theoretical variation of pitching moment with center-of-pressure distance during impact.

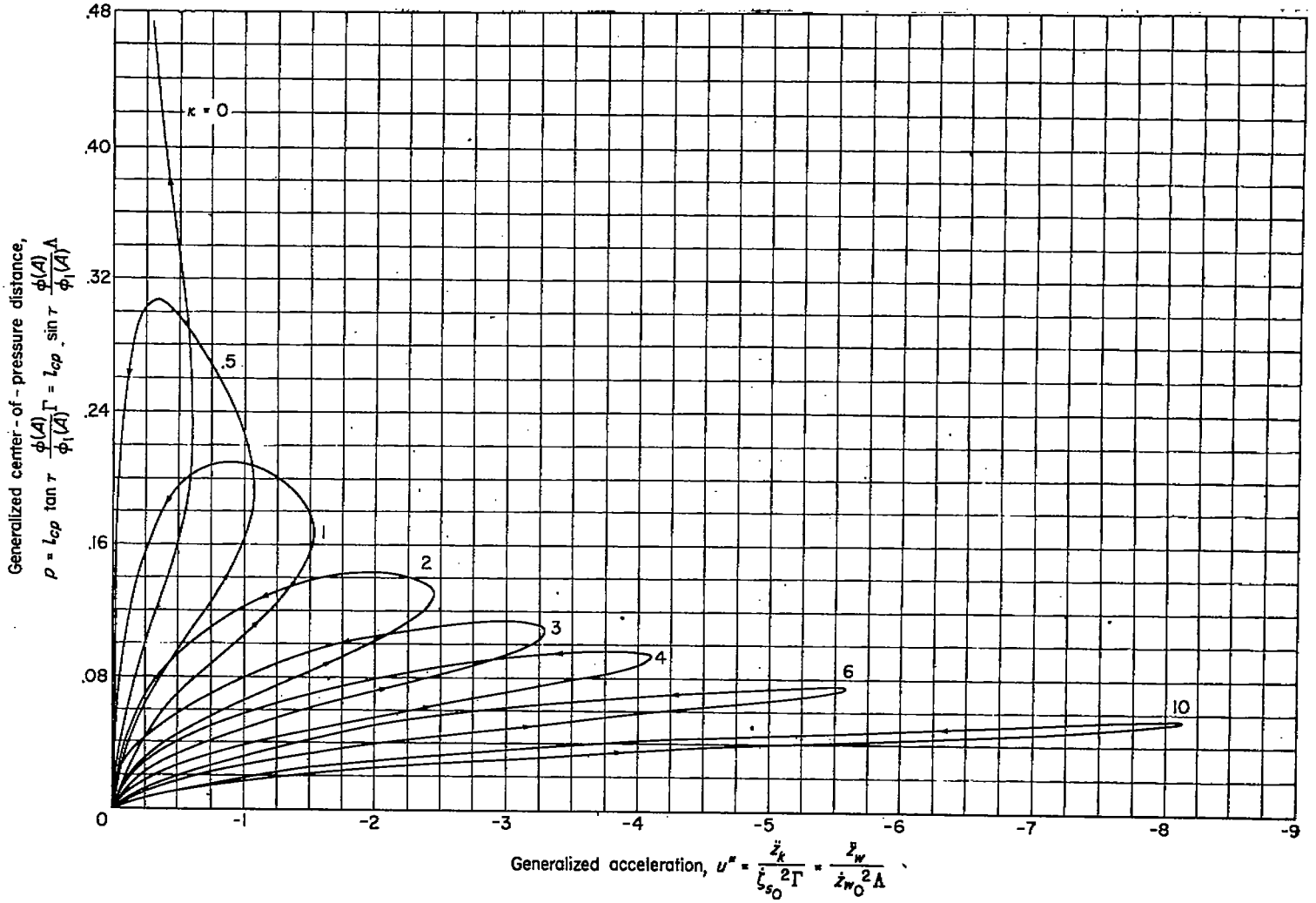

FIGURE 14.—Theoretical variation of center-of-pressure distance with acceleration during impact.

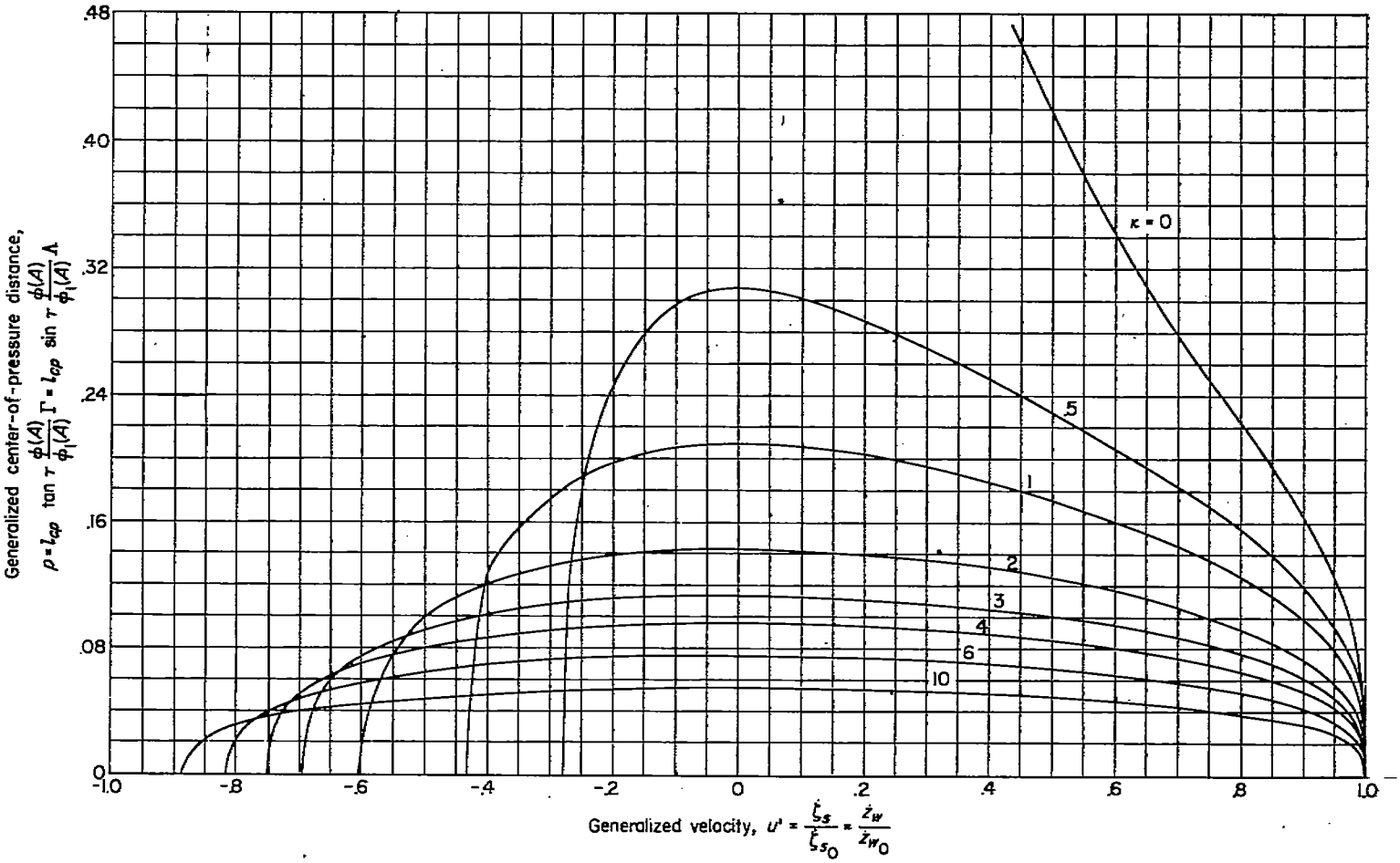

FIGURE 15.—Theoretical variation of center-of-pressure distance with velocity during impact.

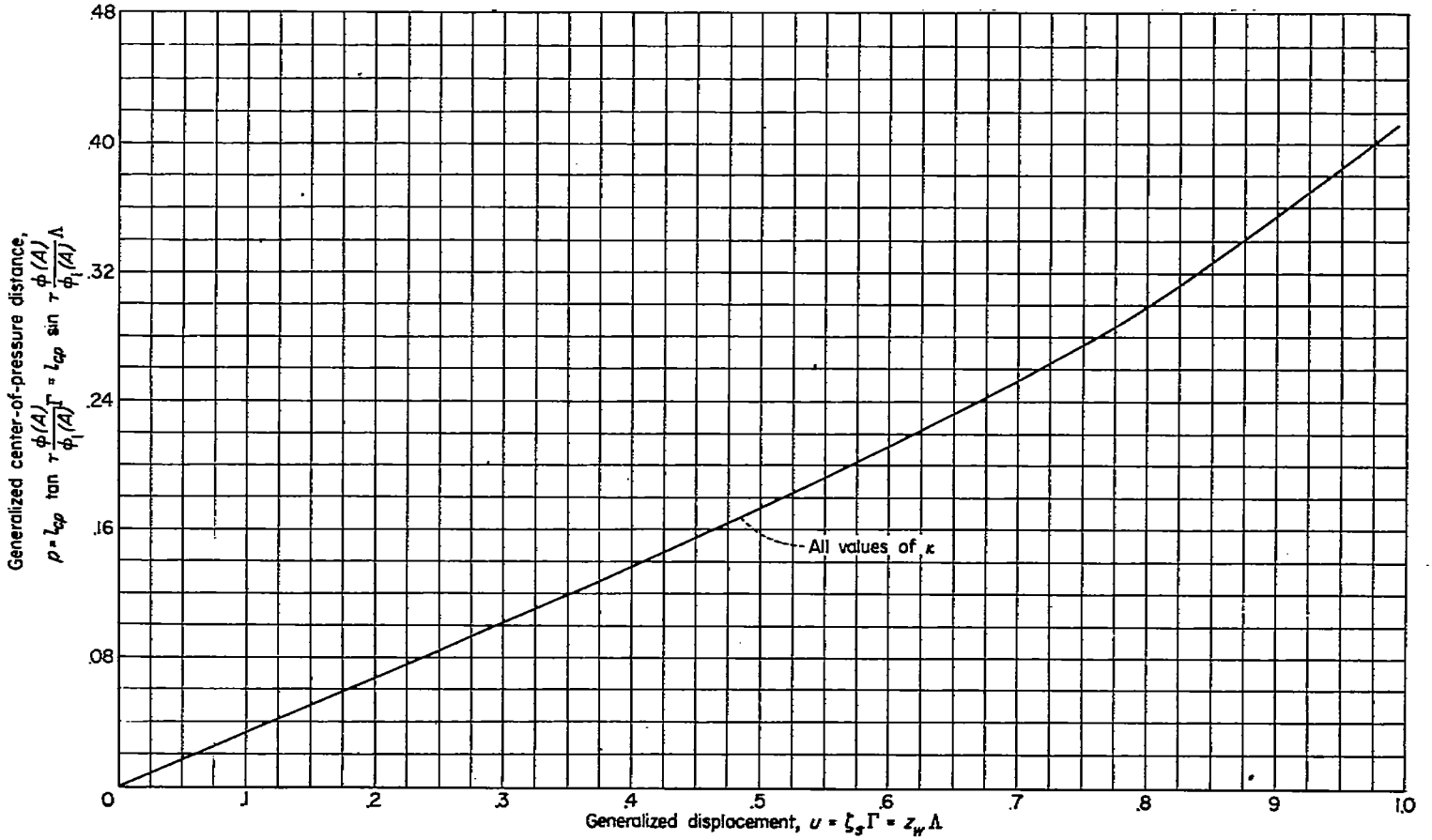

FIGURE 16.—Theoretical variation of center-of-pressure distance with displacement during impact.

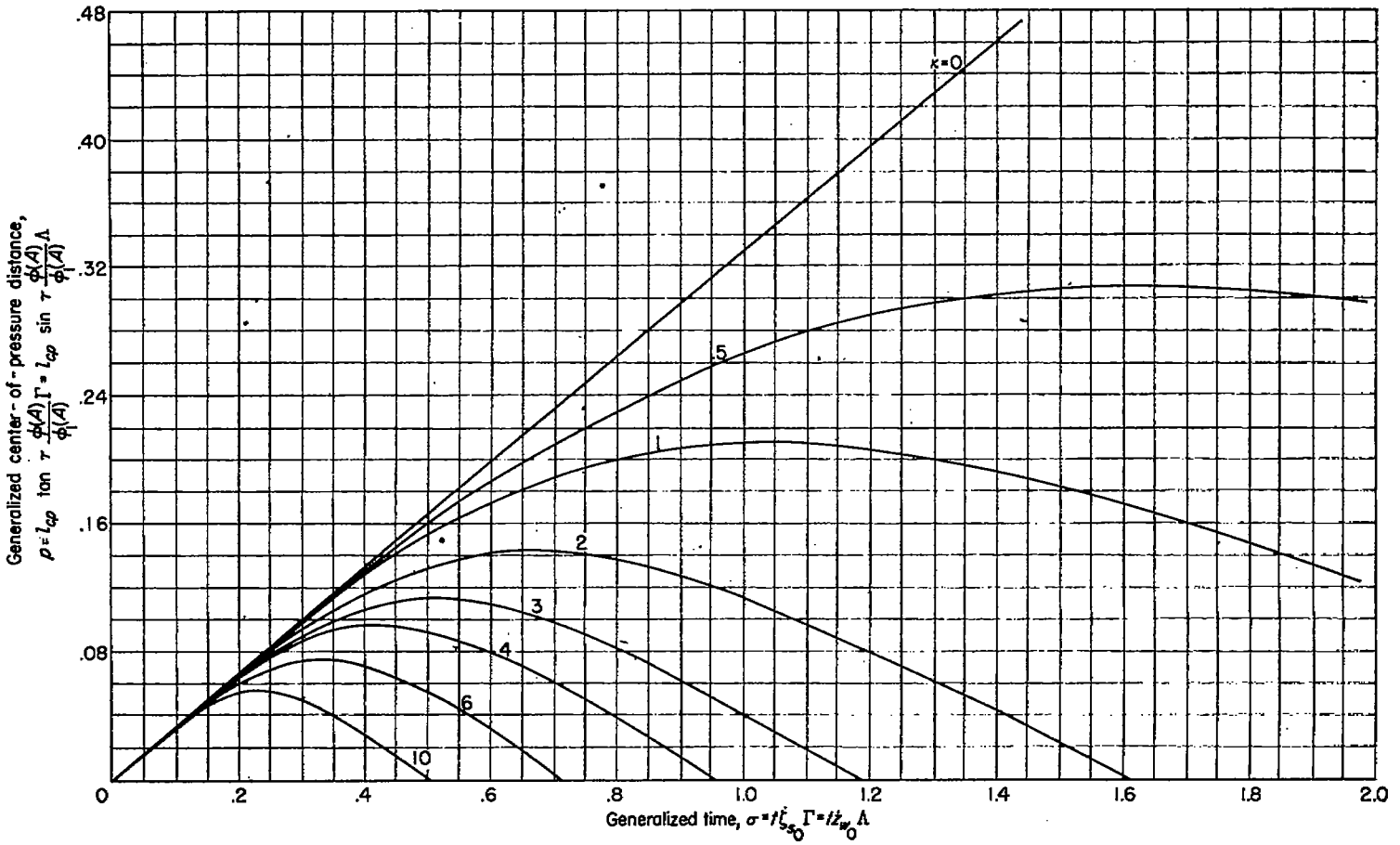

FIGURE 17.—Theoretical variation of center-of-pressure distance with time during impact.

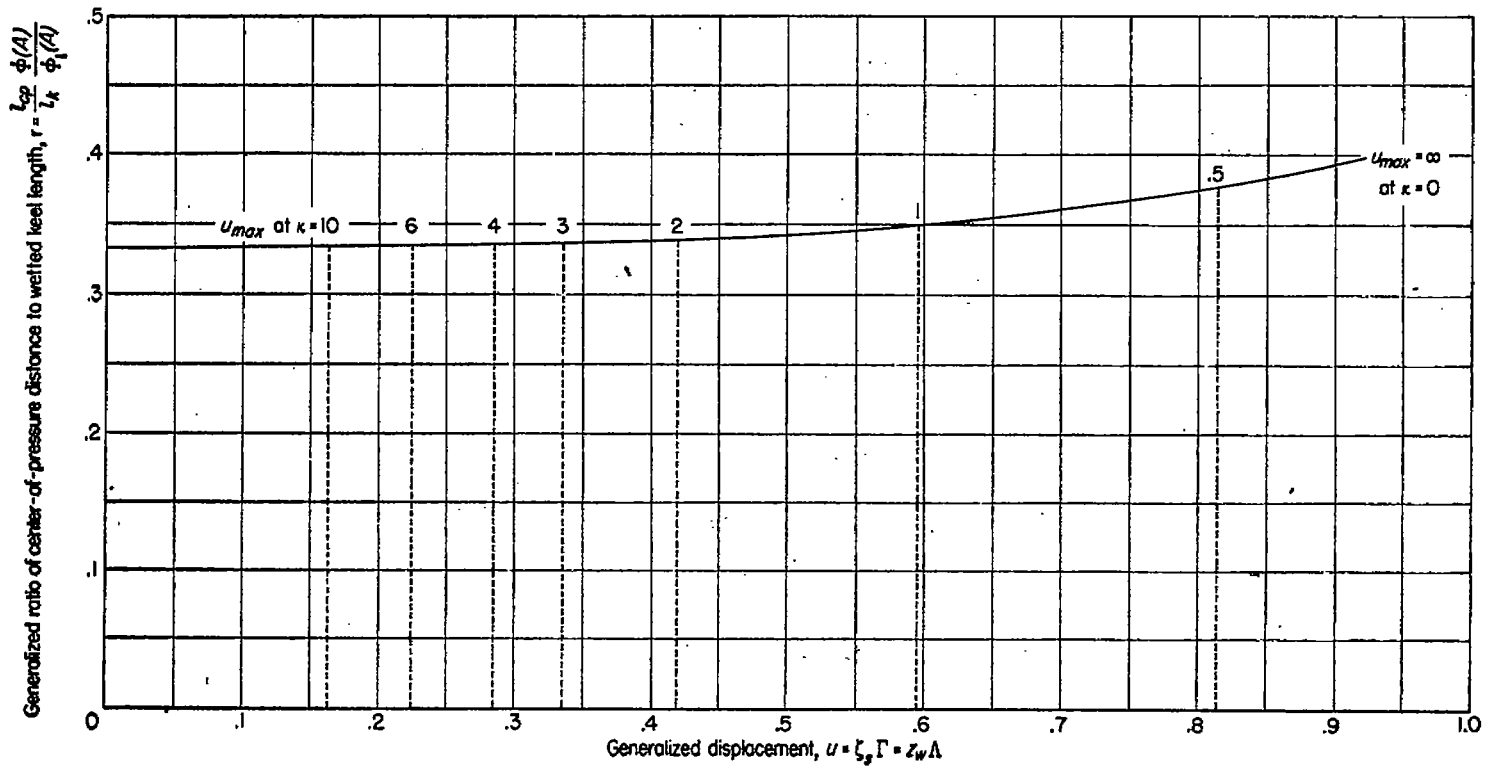

FIGURE 18.—Theoretical variation of ratio of center-of-pressure distance to wetted length with displacement during impact.

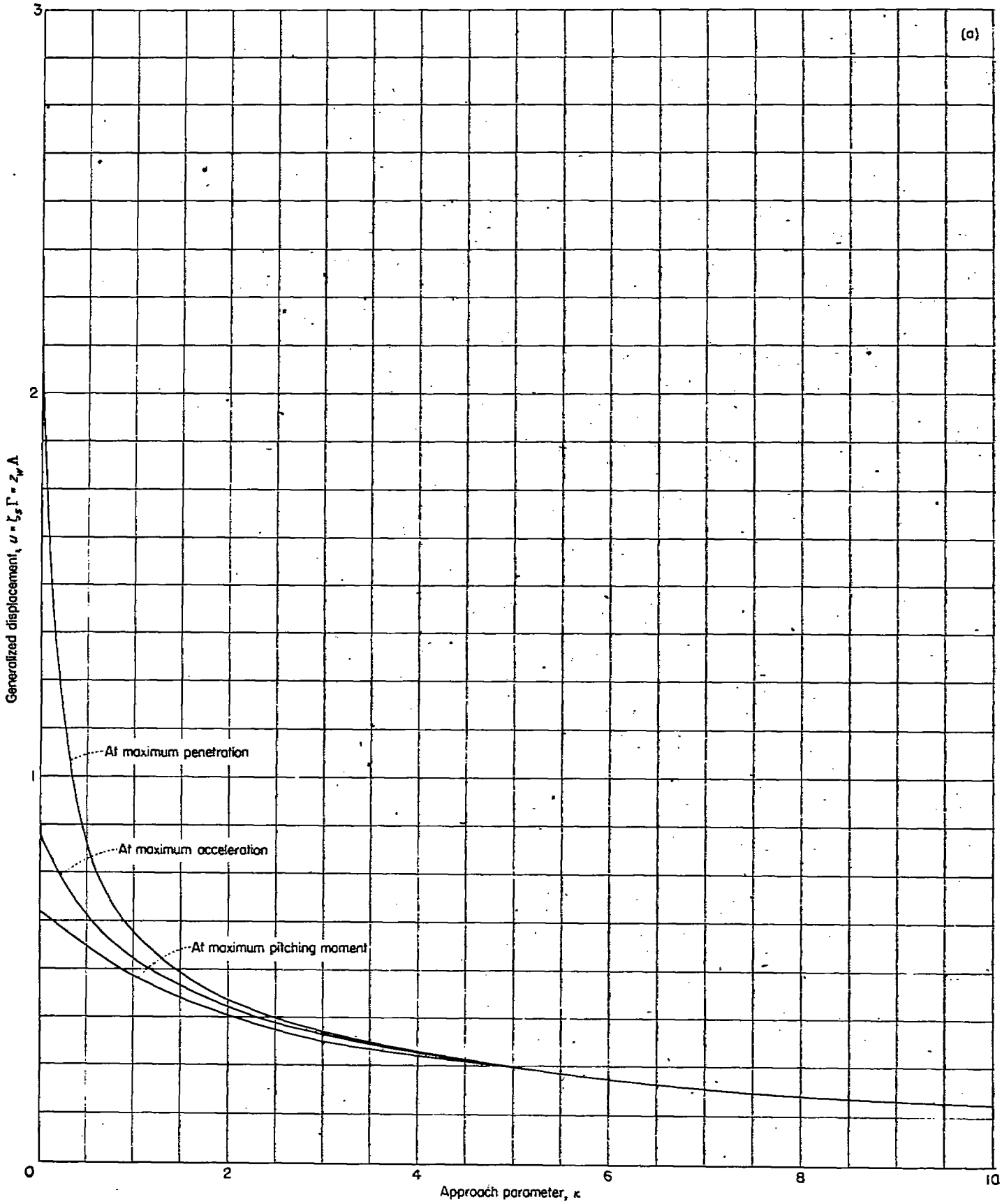

(a) Generalized displacement

FIGURE 19.—Theoretical variation of the generalized variables at particular stages of the impact with the approach parameter.

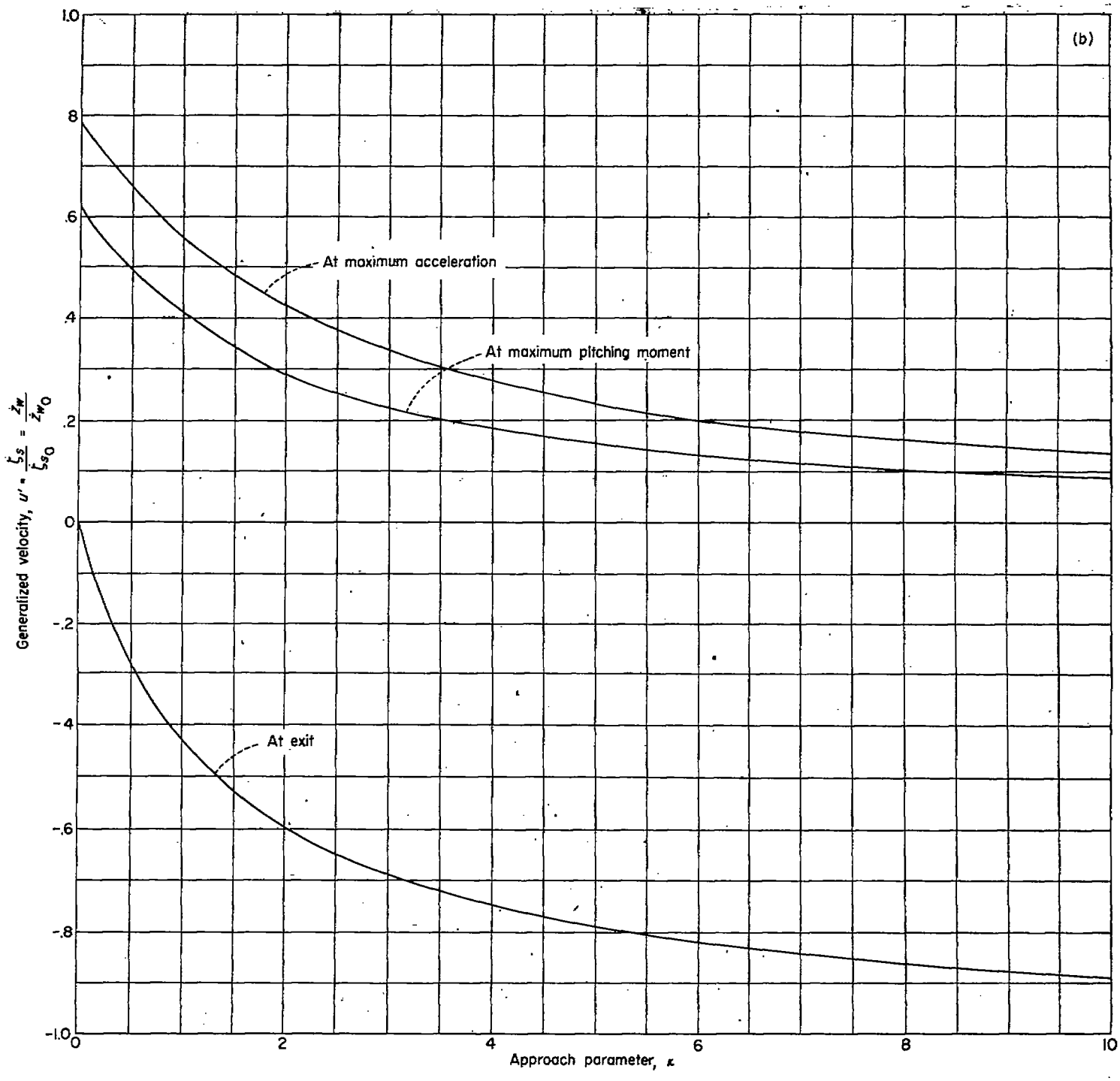

(b) Generalized velocity.

FIGURE 19.—Continued.

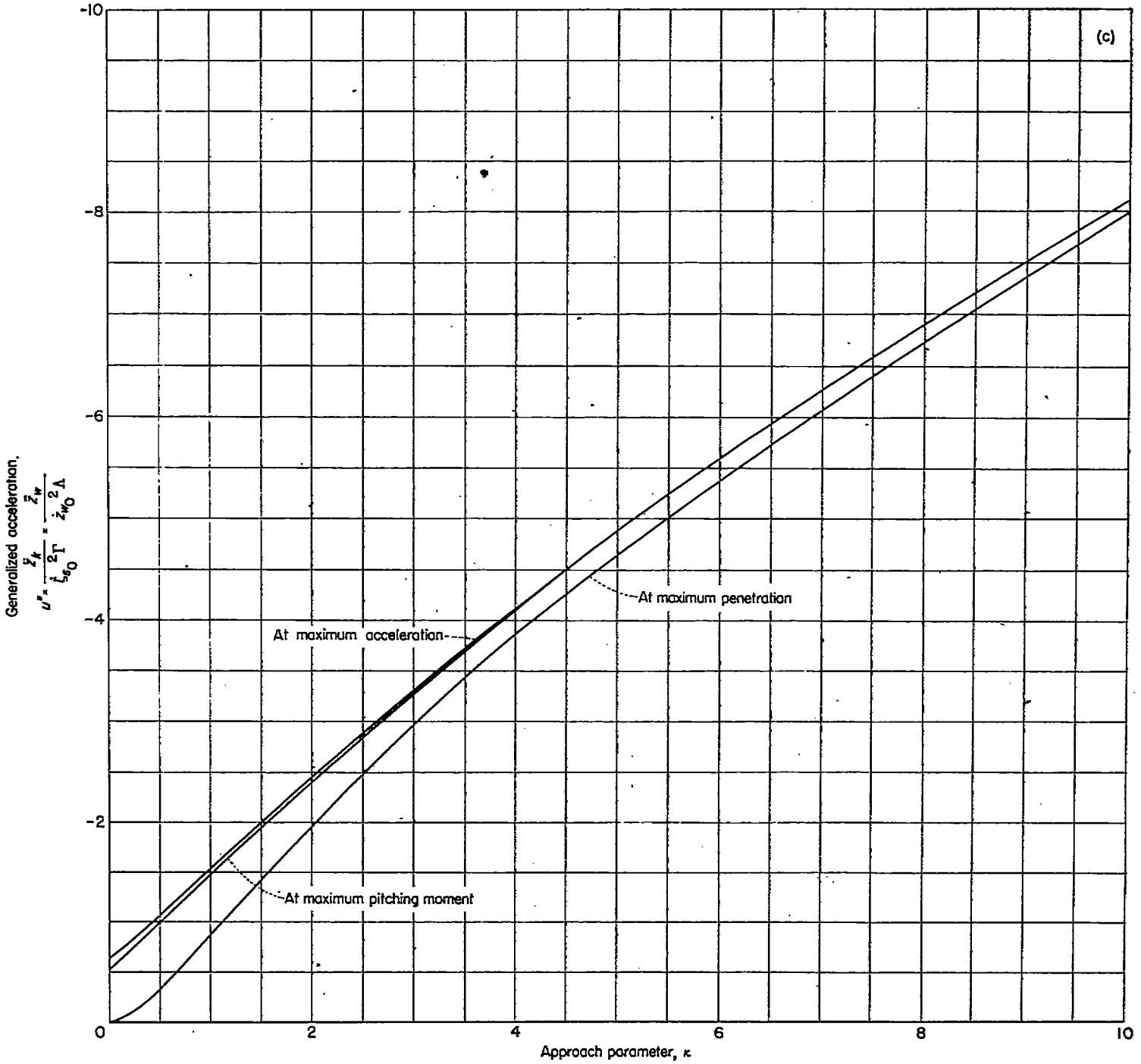

(c) Generalized acceleration.

FIGURE 19.—Continued.

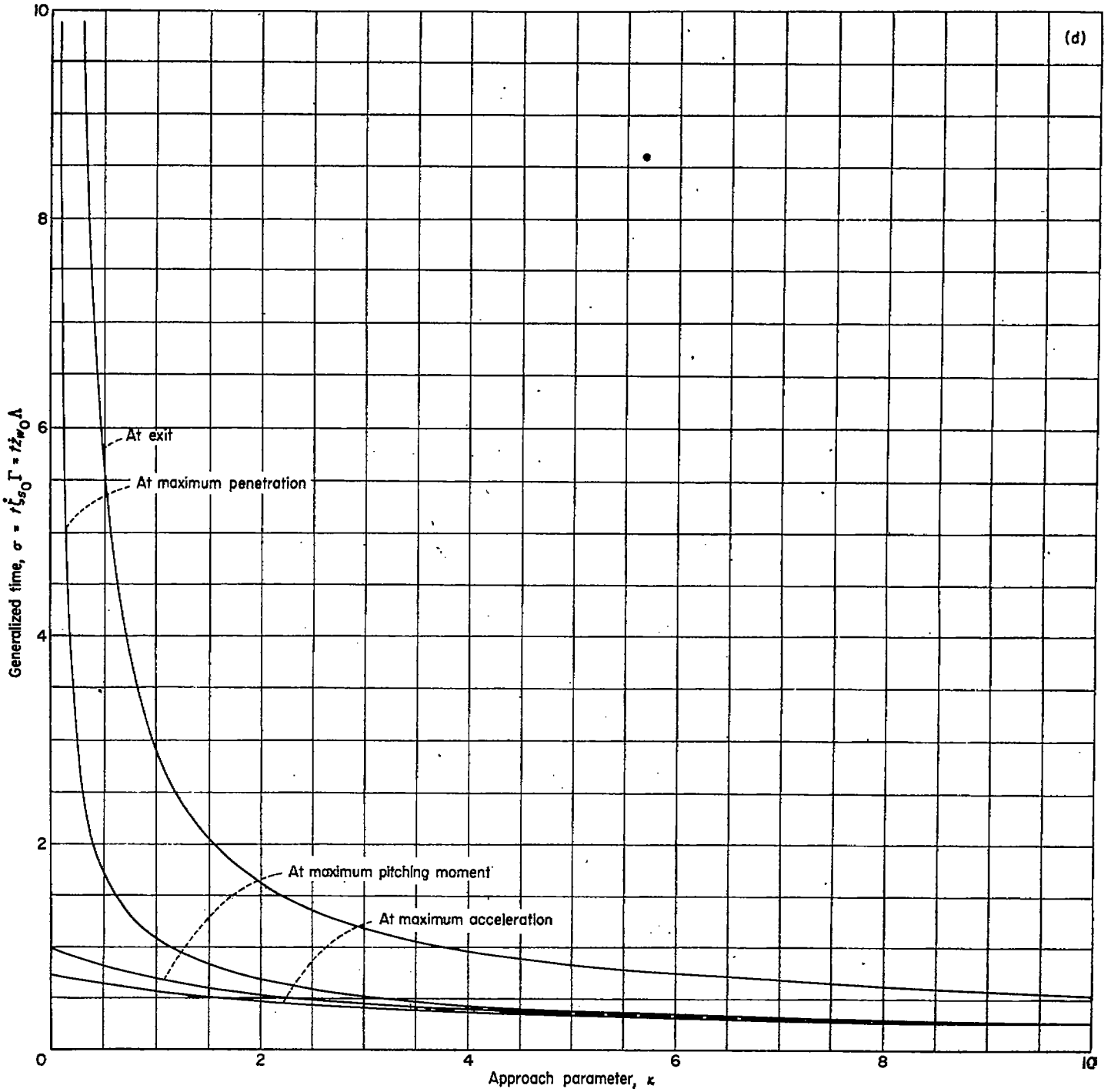

(d) Generalized time.

FIGURE 19.—Continued.

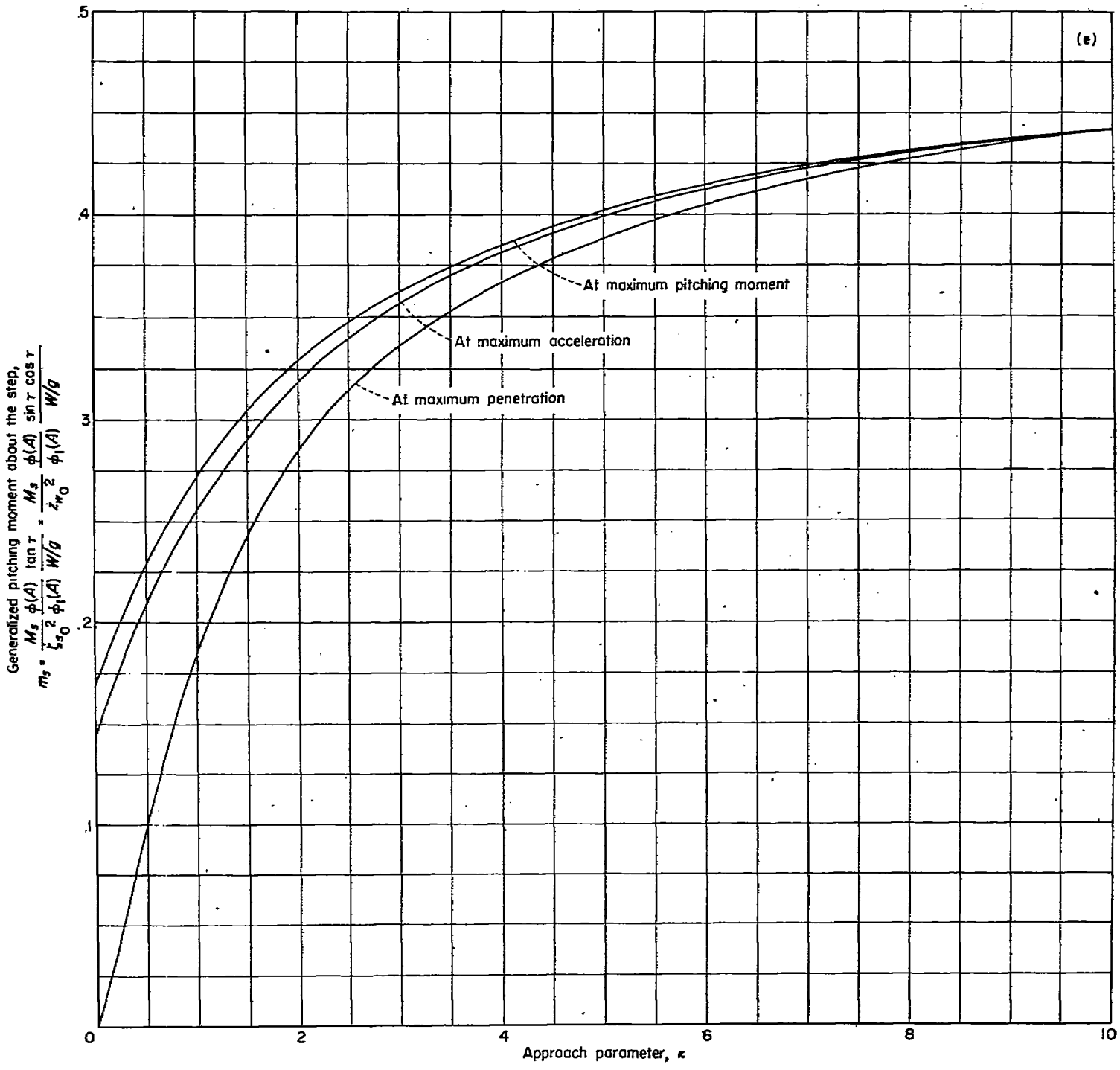

(e) Generalized pitching moment.

FIGURE 19.—Continued.

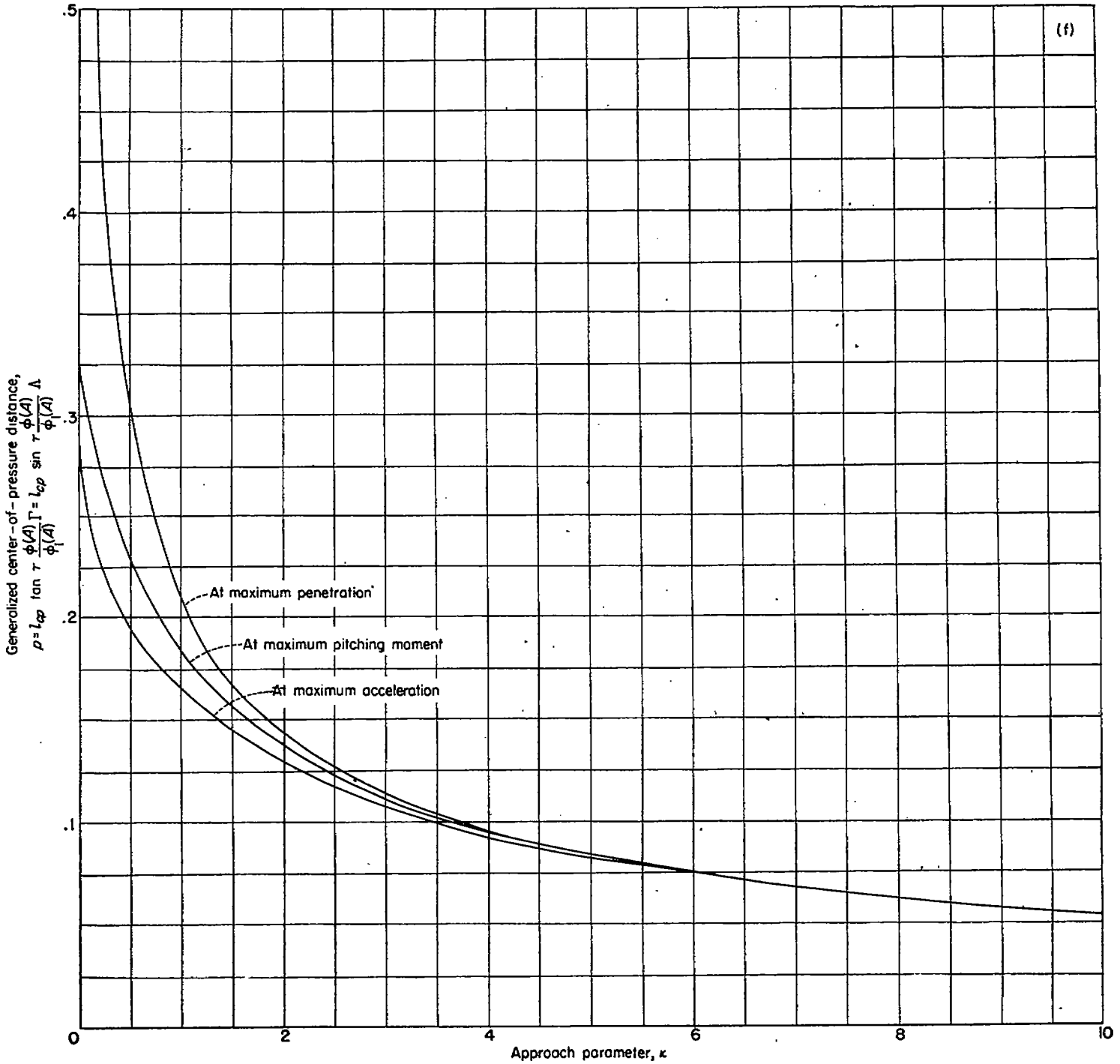

(f) Generalized center-of-pressure distance.

FIGURE 19.—Continued.

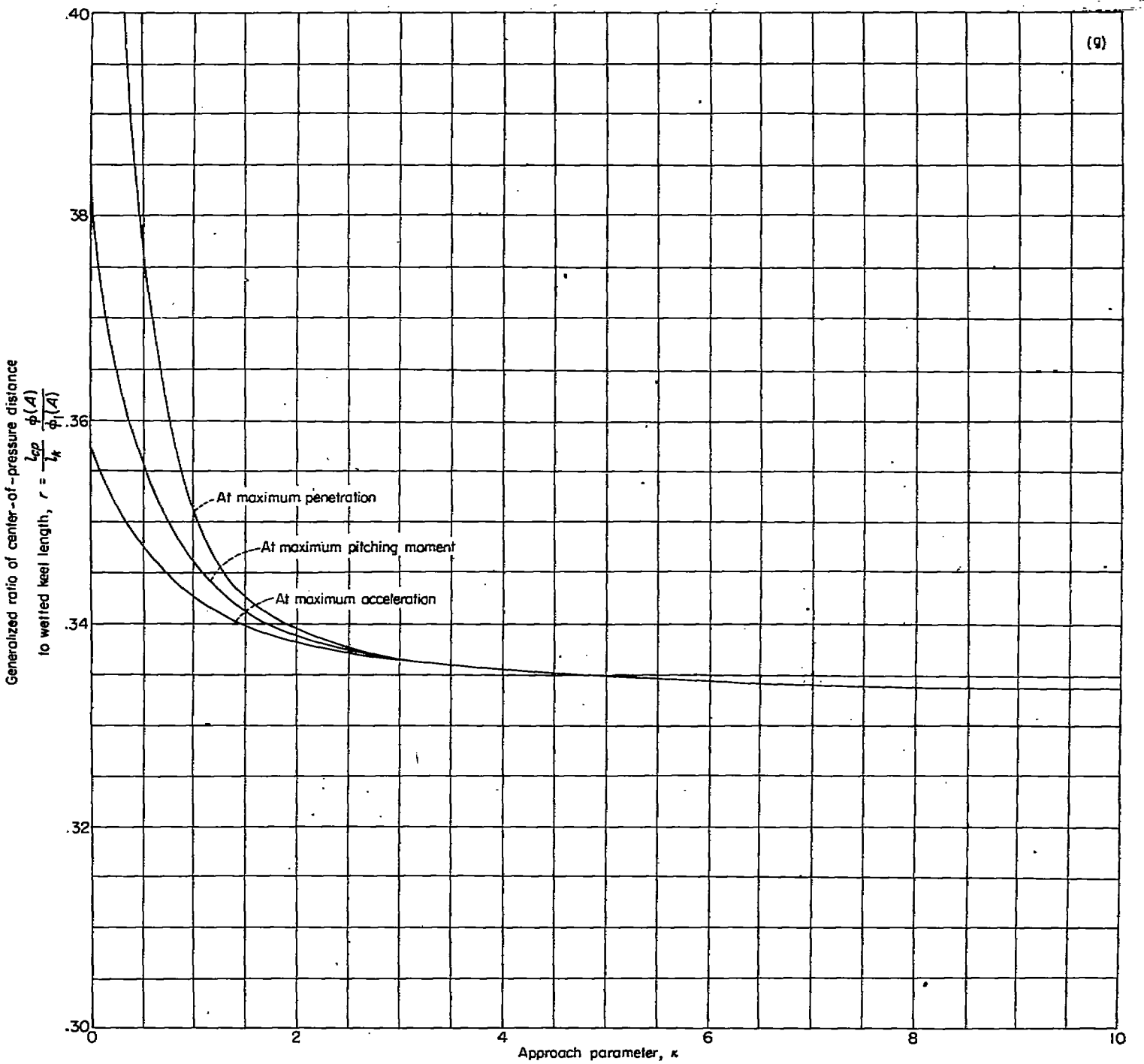

(g) Ratio of center-of-pressure distance to wetted length.

FIGURE 19.—Concluded.

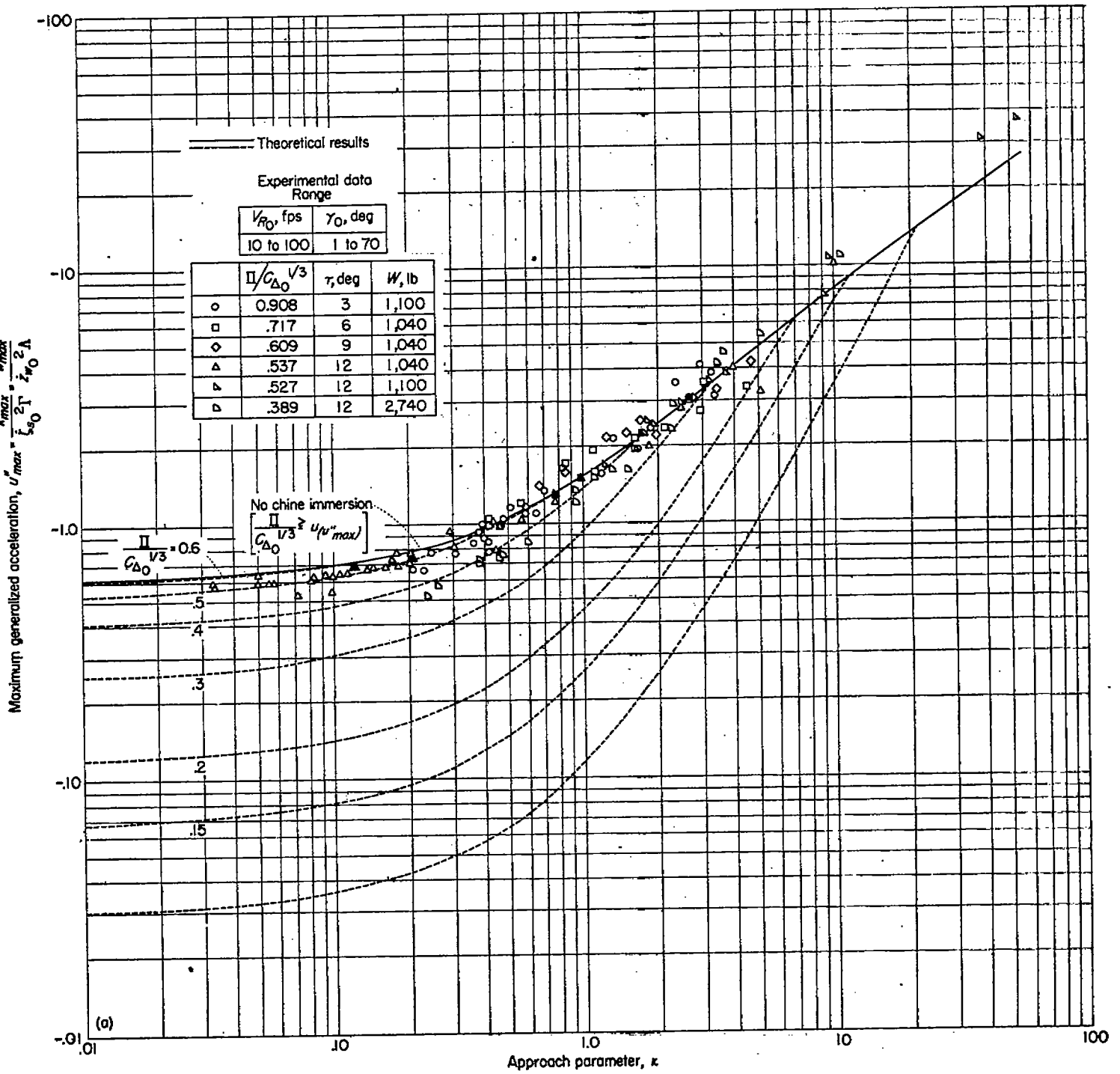

(a) Comparisons for $\beta = 22\frac{1}{2}°$.

FIGURE 20.—Comparison of theoretical and experimental variation of the maximum acceleration with the approach parameter, including the effects of chine immersion.

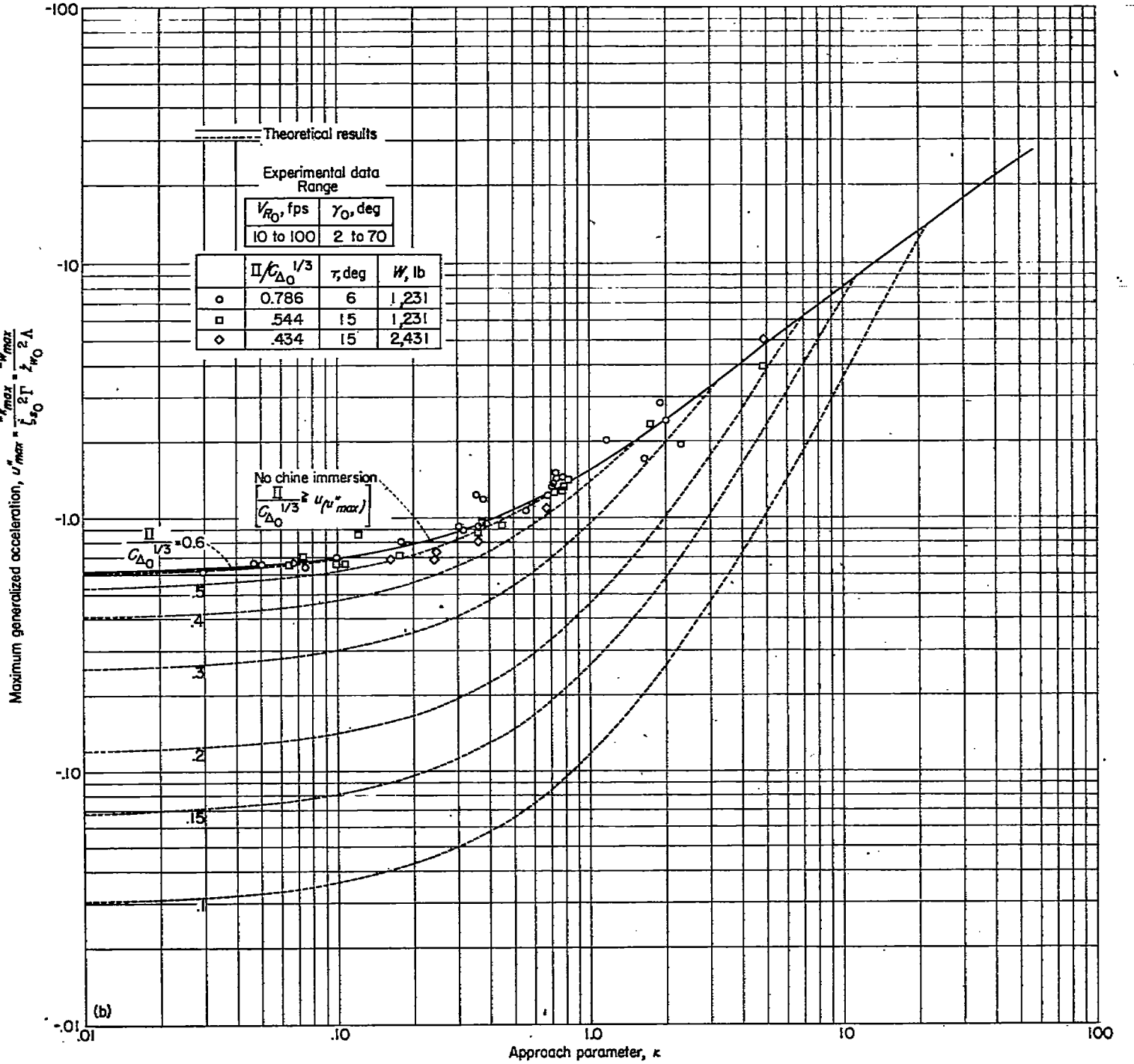

(b) Comparisons for β=30°.

FIGURE 20.—Continued.

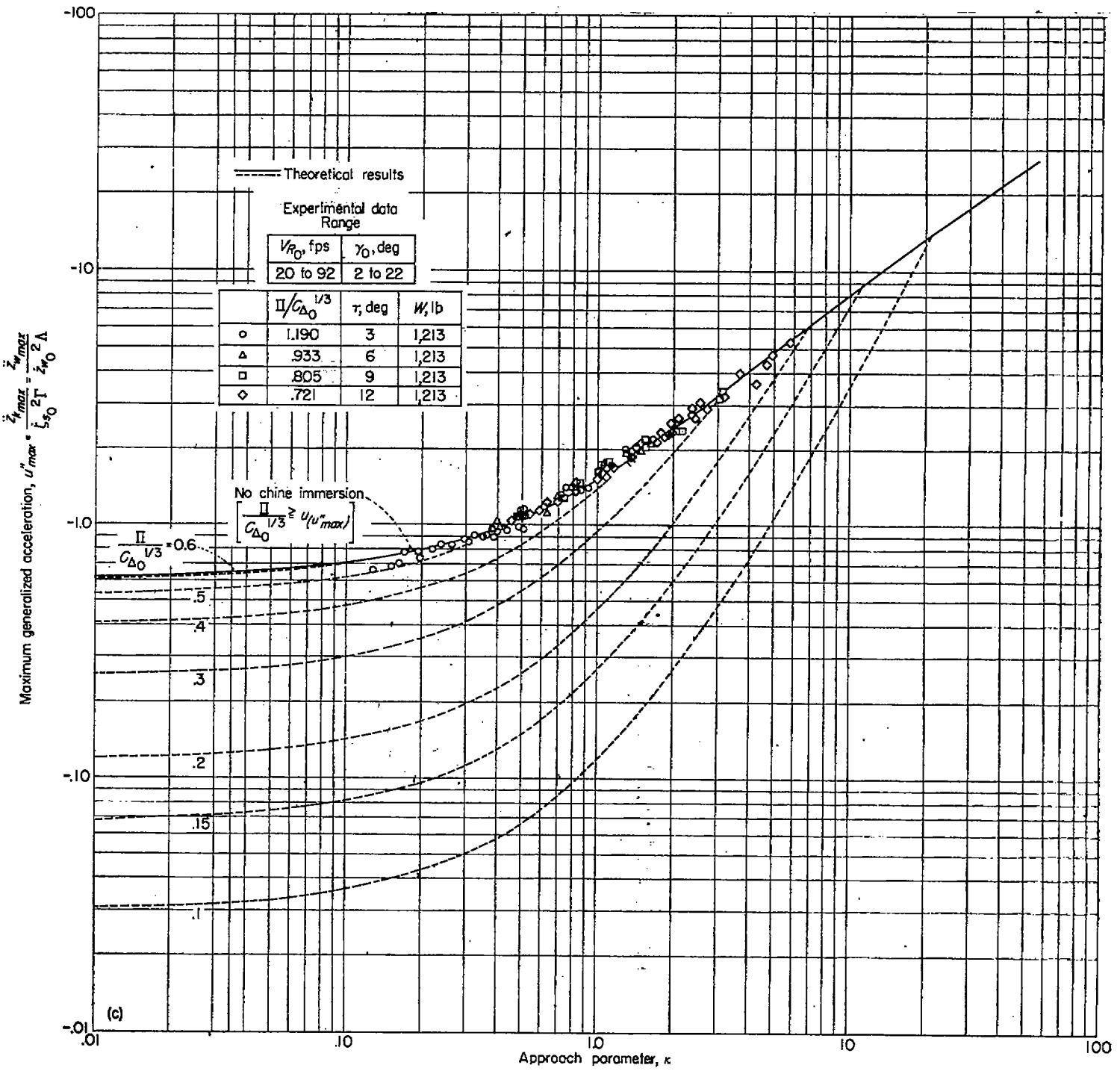

(c) Comparisons for $\beta = 40°$.

FIGURE 20.—Concluded.

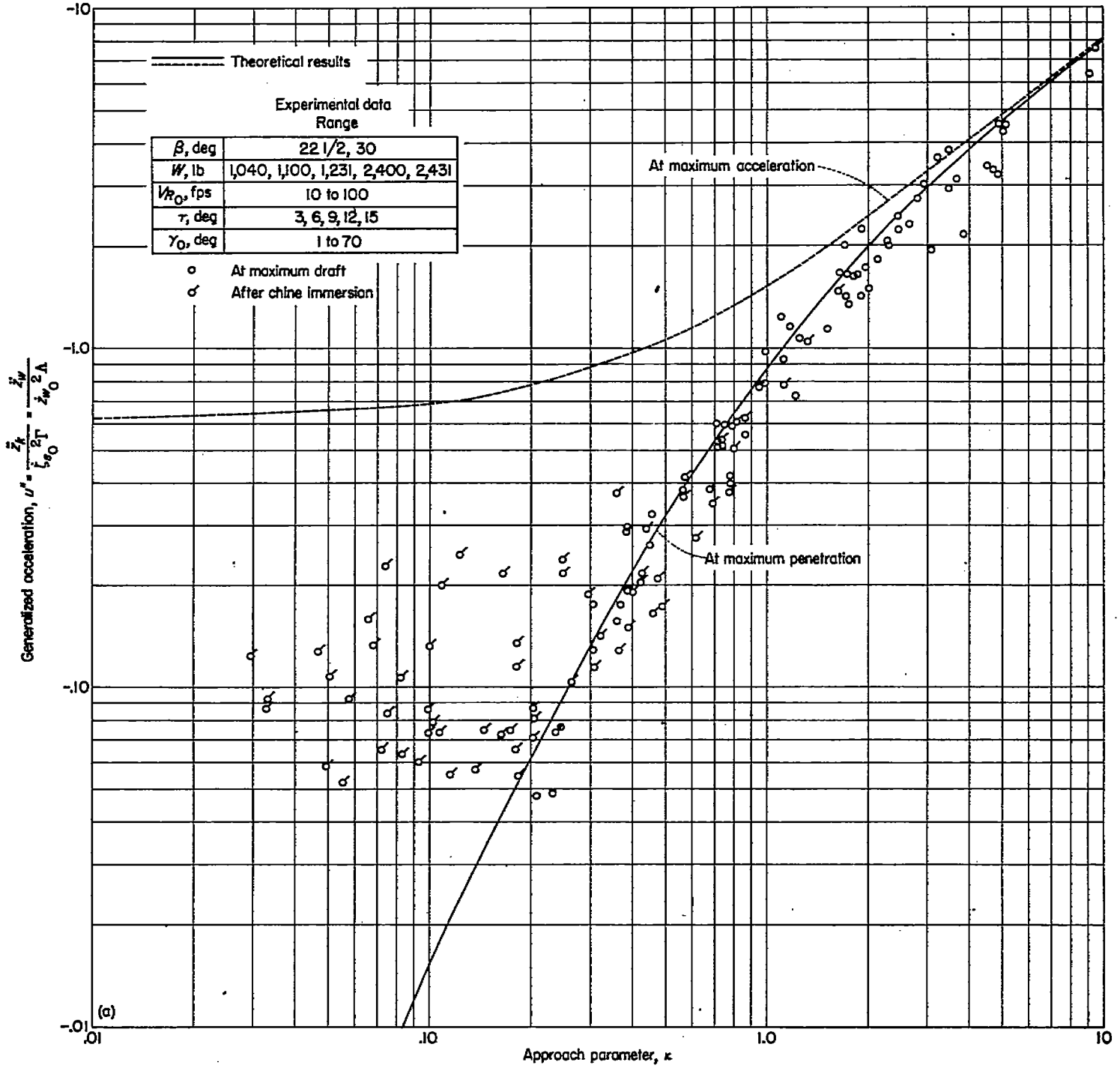

(a) Comparisons for $\beta = 22\frac{1}{2}°$ and $\beta = 30°$.

FIGURE 21.—Comparison between theoretical and experimental variations of the acceleration at the instant of maximum penetration with the approach parameter.

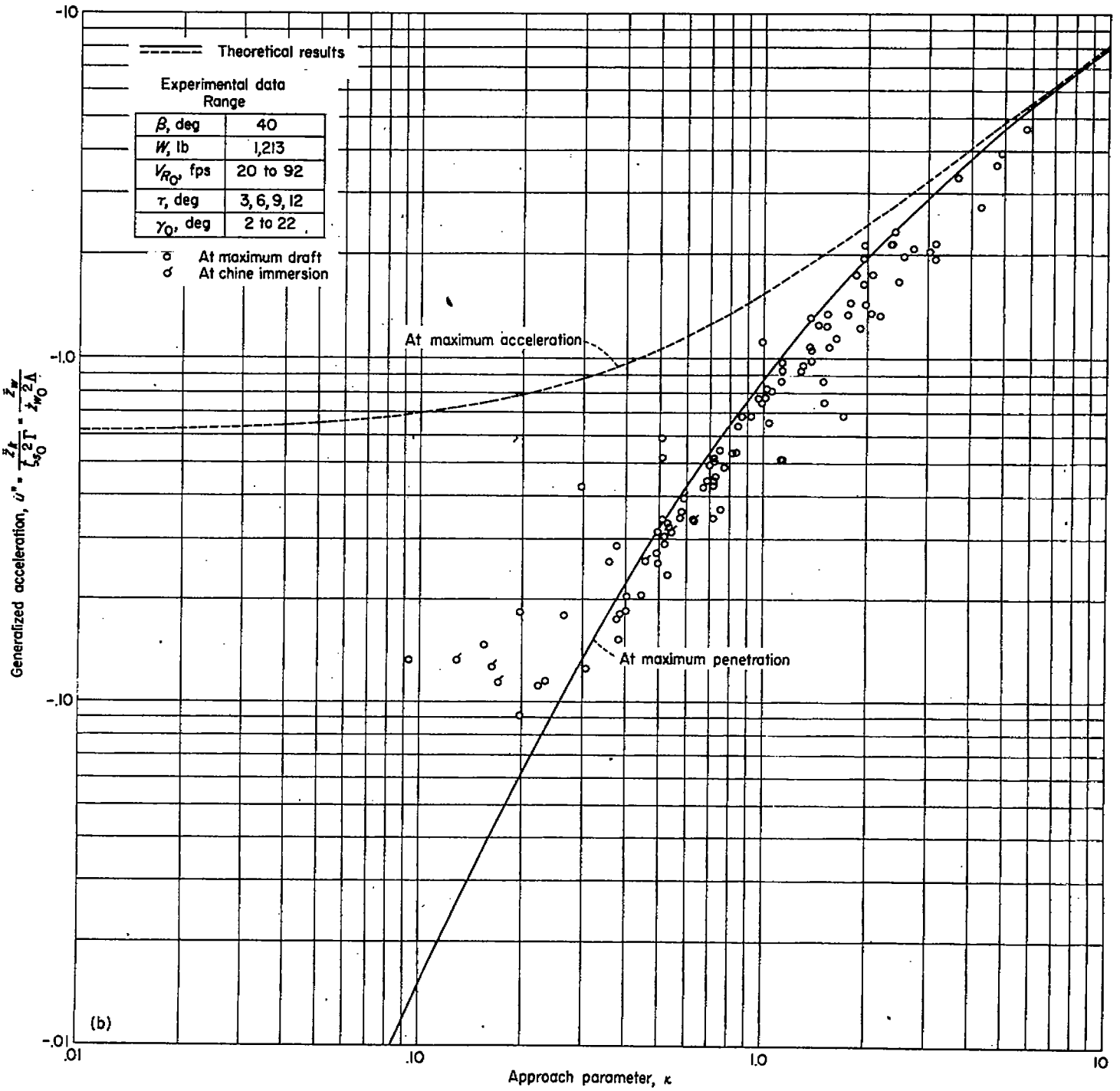

(b) Comparisons for $\beta = 40°$.

FIGURE 21.—Concluded.

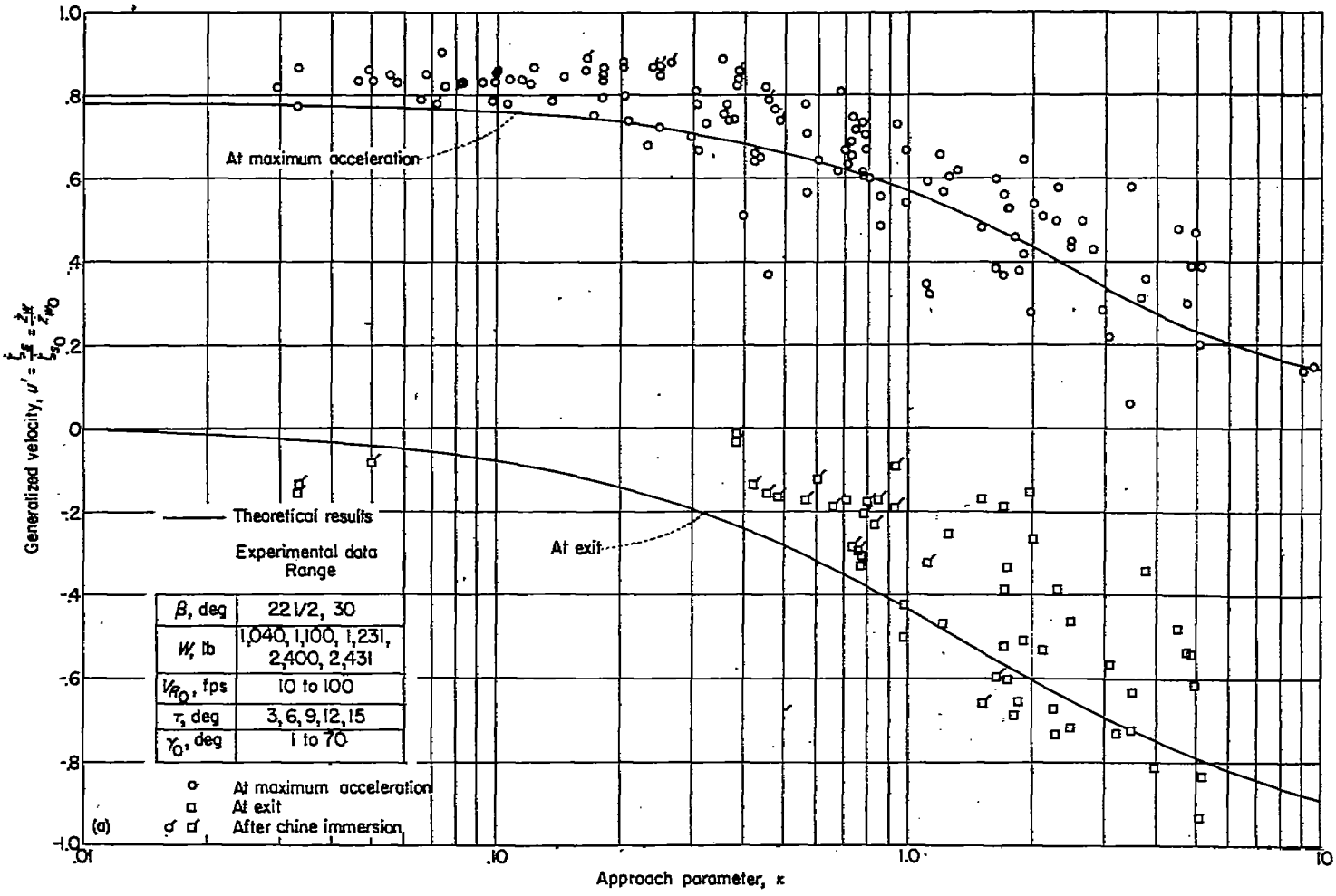

(a) Comparisons for $\beta = 22\frac{1}{2}°$ and $\beta = 30°$.

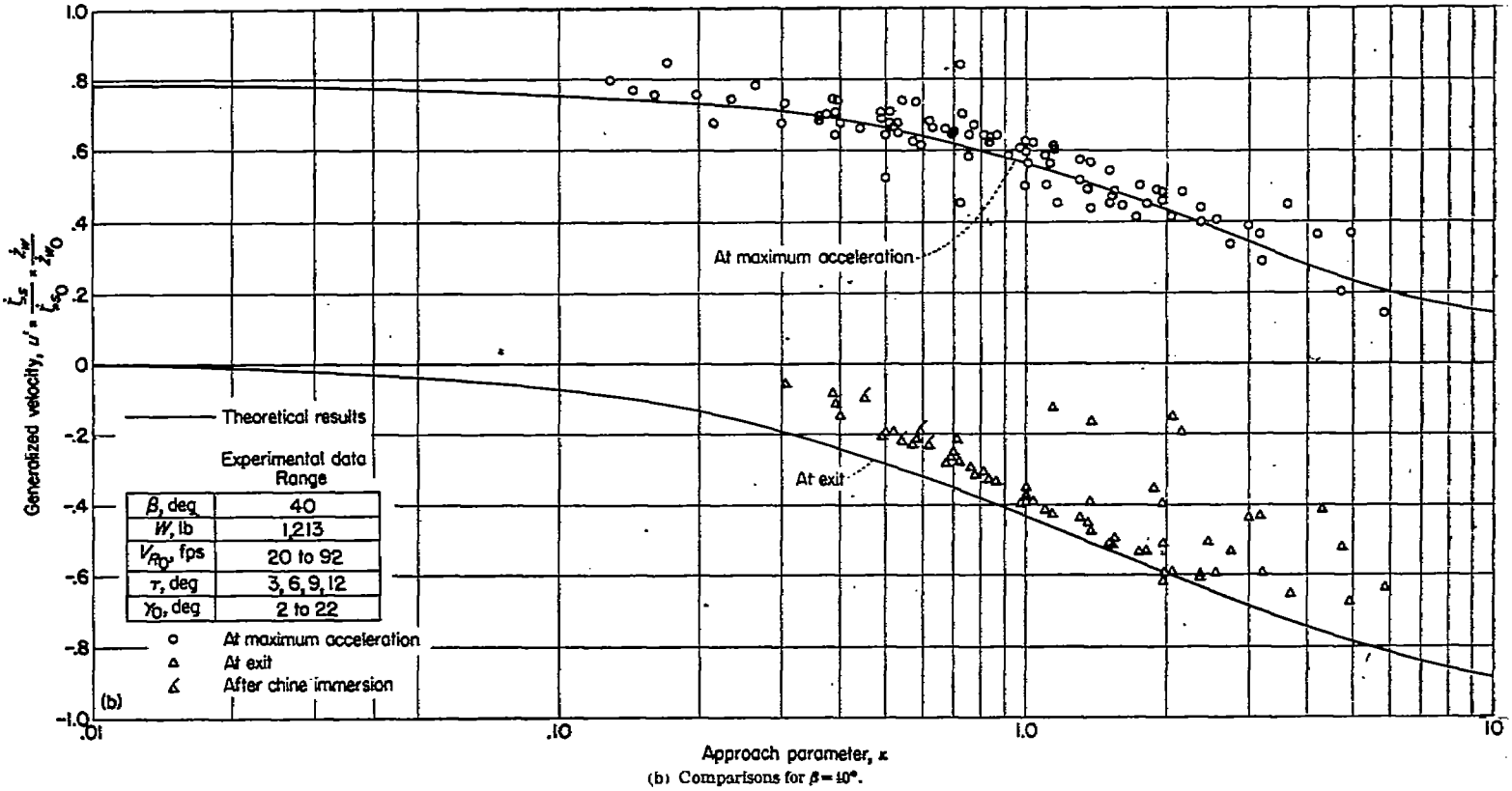

(b) Comparisons for $\beta = 40°$.

FIGURE 22.—Comparison between theoretical and experimental variations of the velocity at particular stages of the impact with the approach parameter.

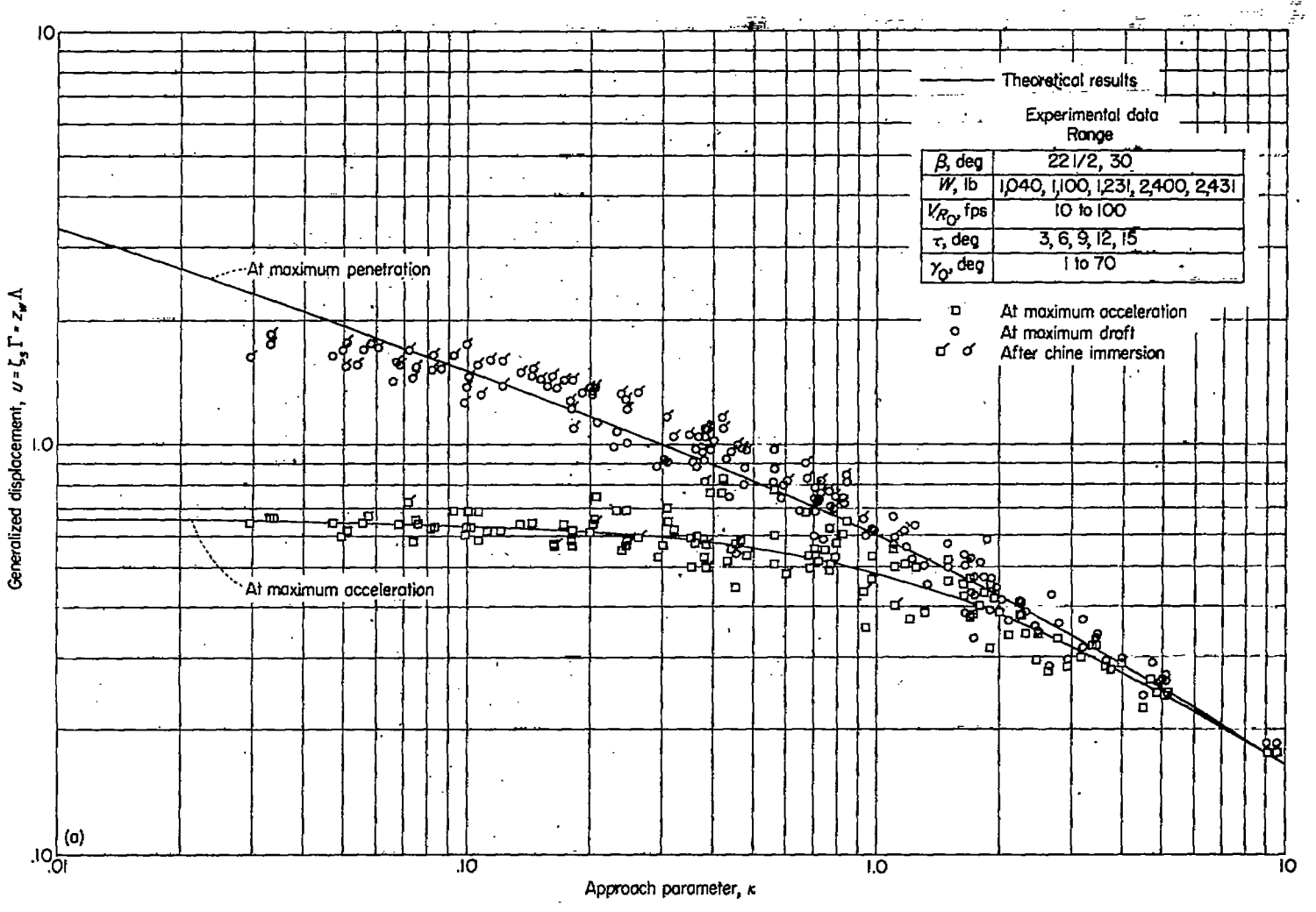

(a) Comparisons for $\beta = 22\frac{1}{2}°$ and $\beta = 30°$.

FIGURE 23.—Comparison between theoretical and experimental variations of the displacement at particular stages of the impact with the approach parameter.

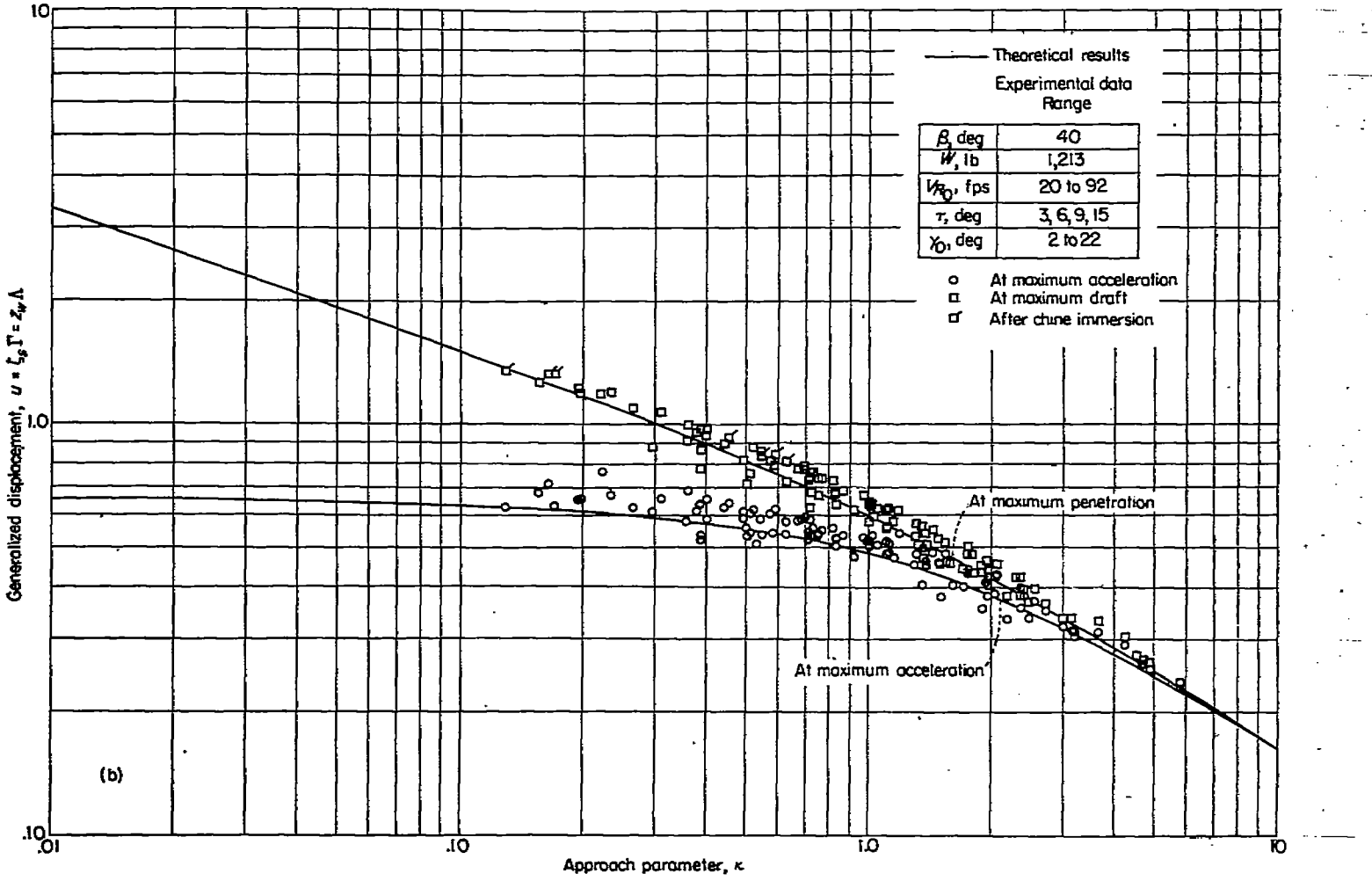

(b) Comparisons for $\beta = 40°$

FIGURE 23.—Concluded.

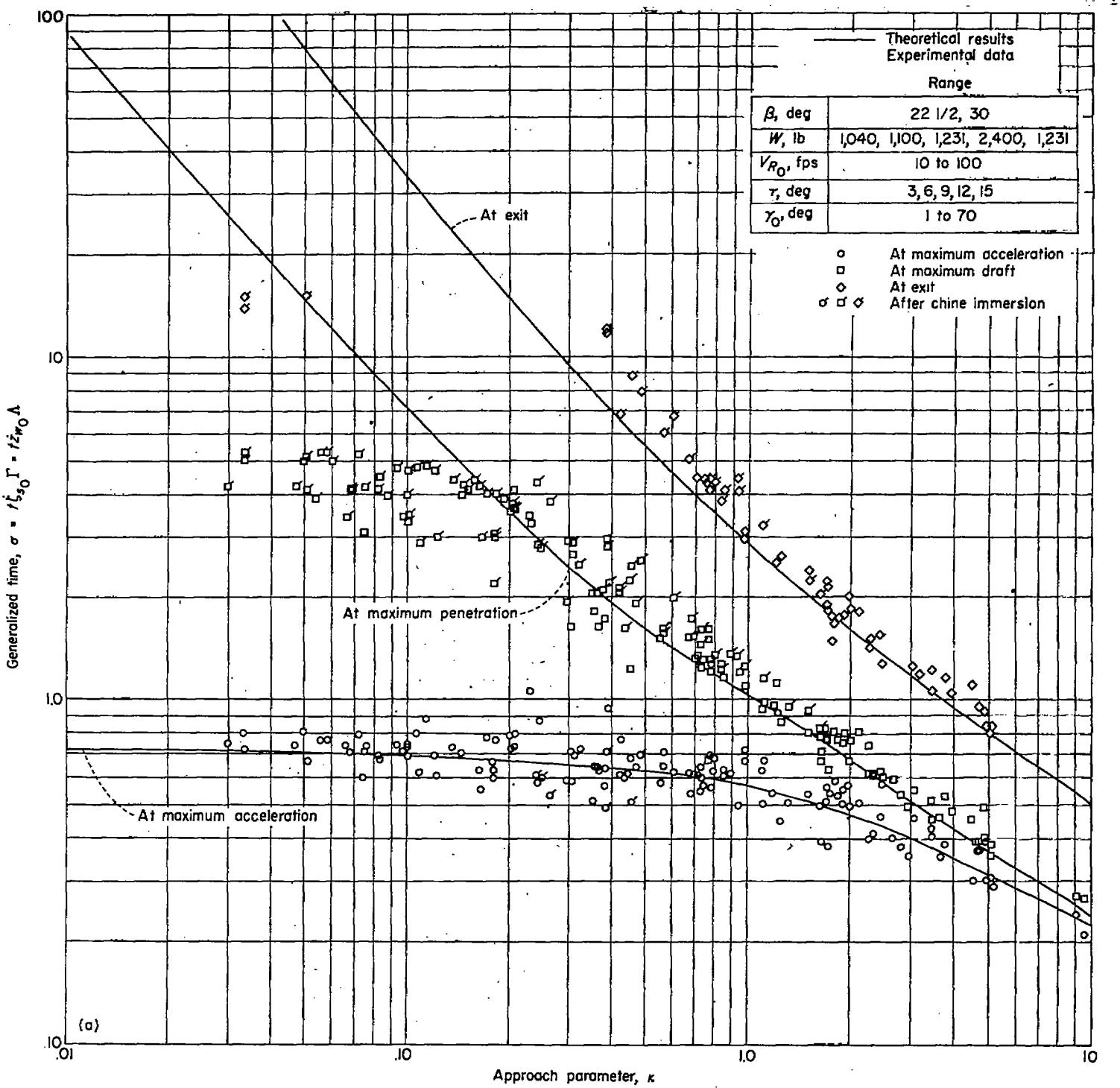

(a) Comparisons for $\beta = 22\frac{1}{2}°$ and $\beta = 30°$.

FIGURE 24.—Comparison between theoretical and experimental variations of the time at particular stages of the impact with the approach parameter.

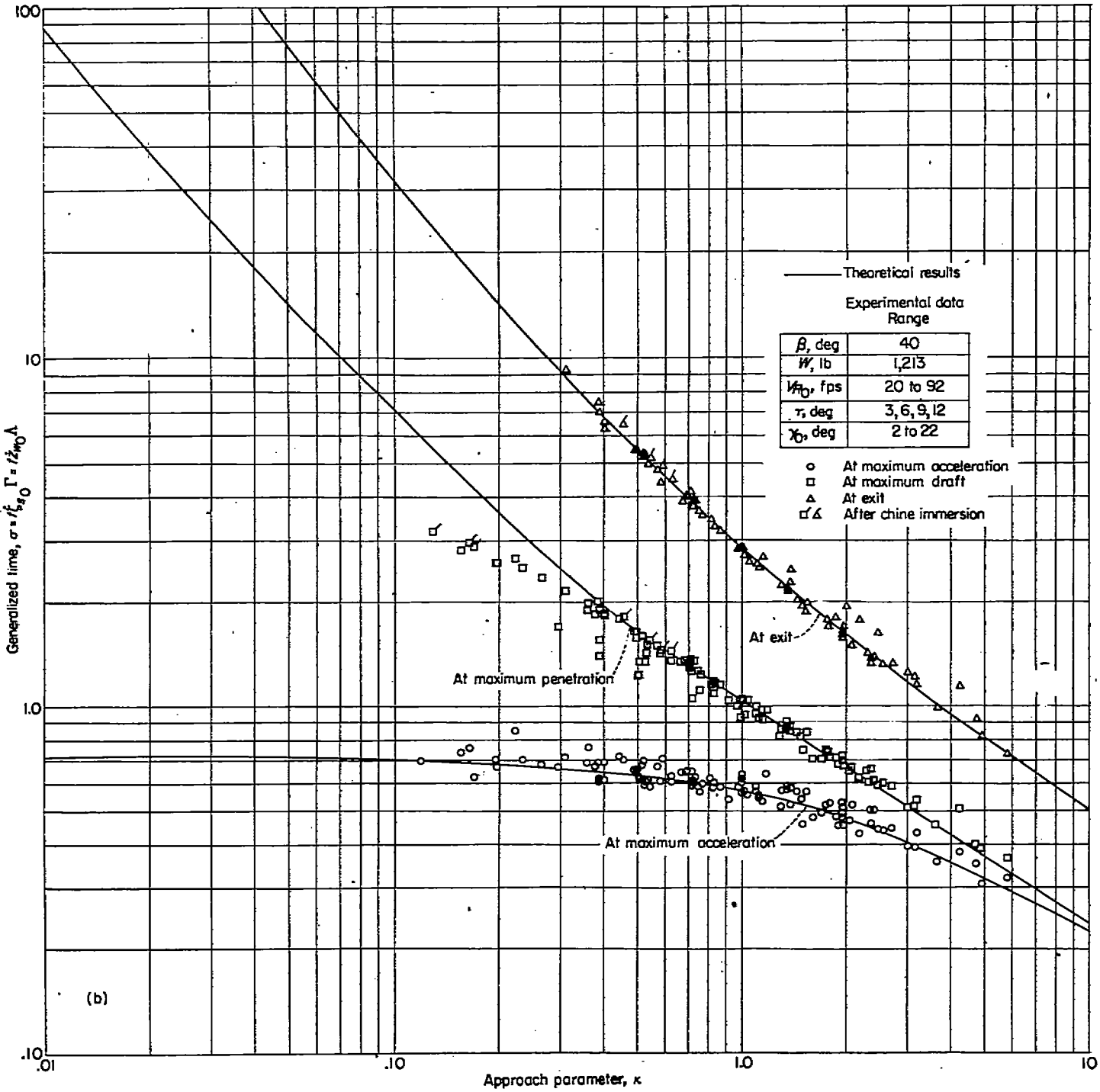

(b) Comparisons for $\beta = 40°$.

FIGURE 24.—Concluded.

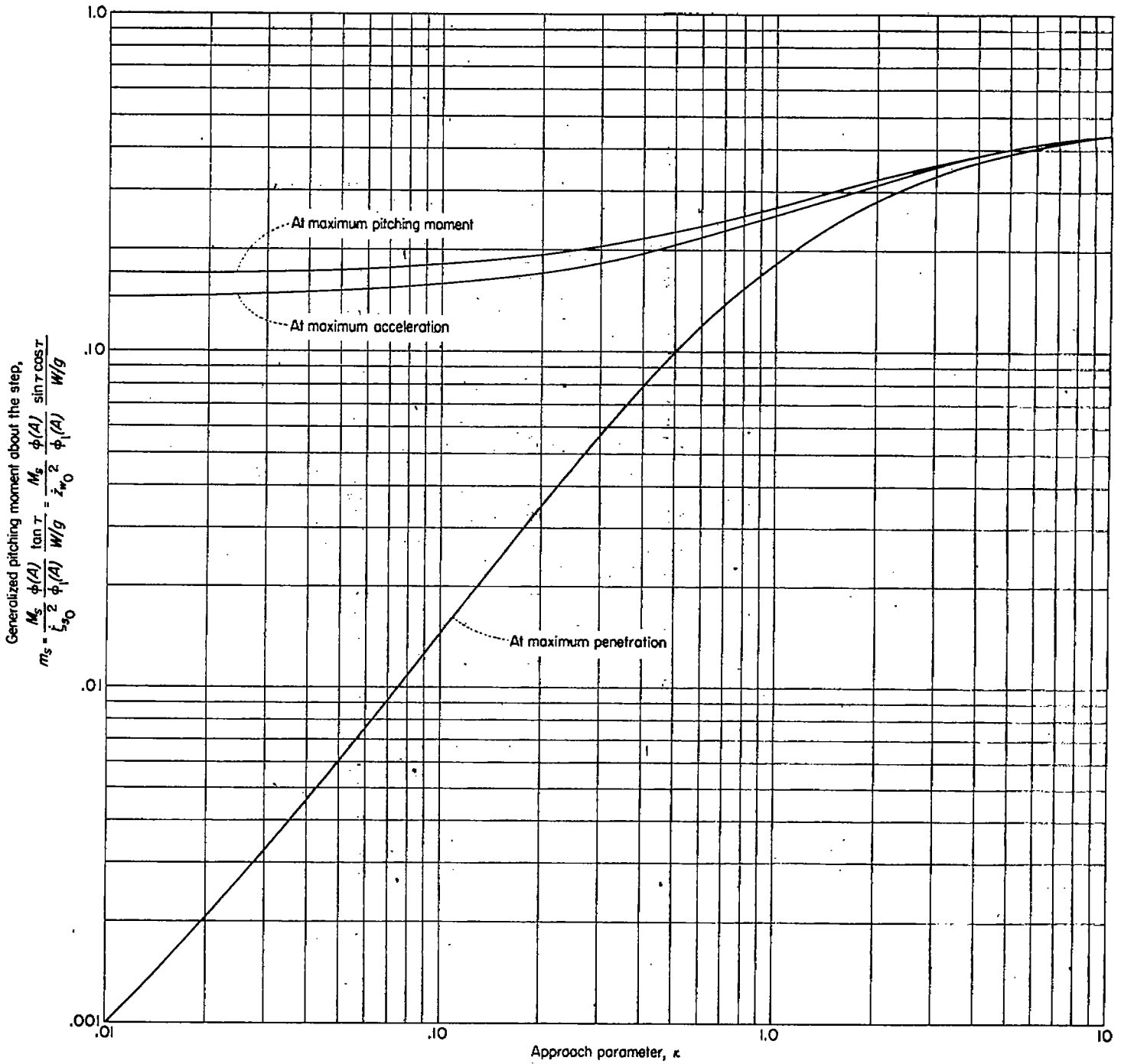

FIGURE 25.—Theoretical variation of the pitching moment at particular stages of the impact with the approach parameter.

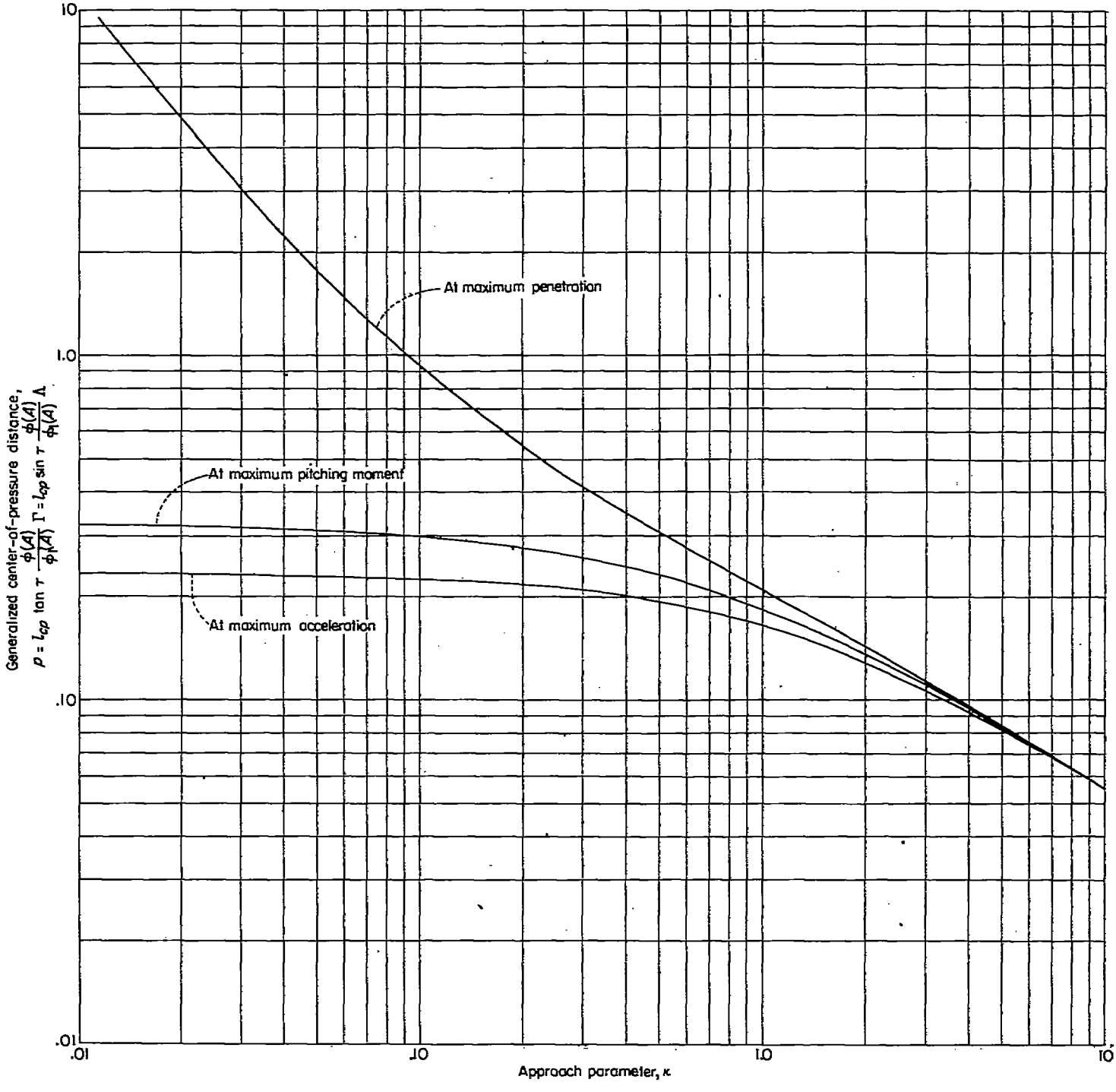

FIGURE 26.—Theoretical variation of the center-of-pressure distance at particular stages of the impact with the approach parameter.

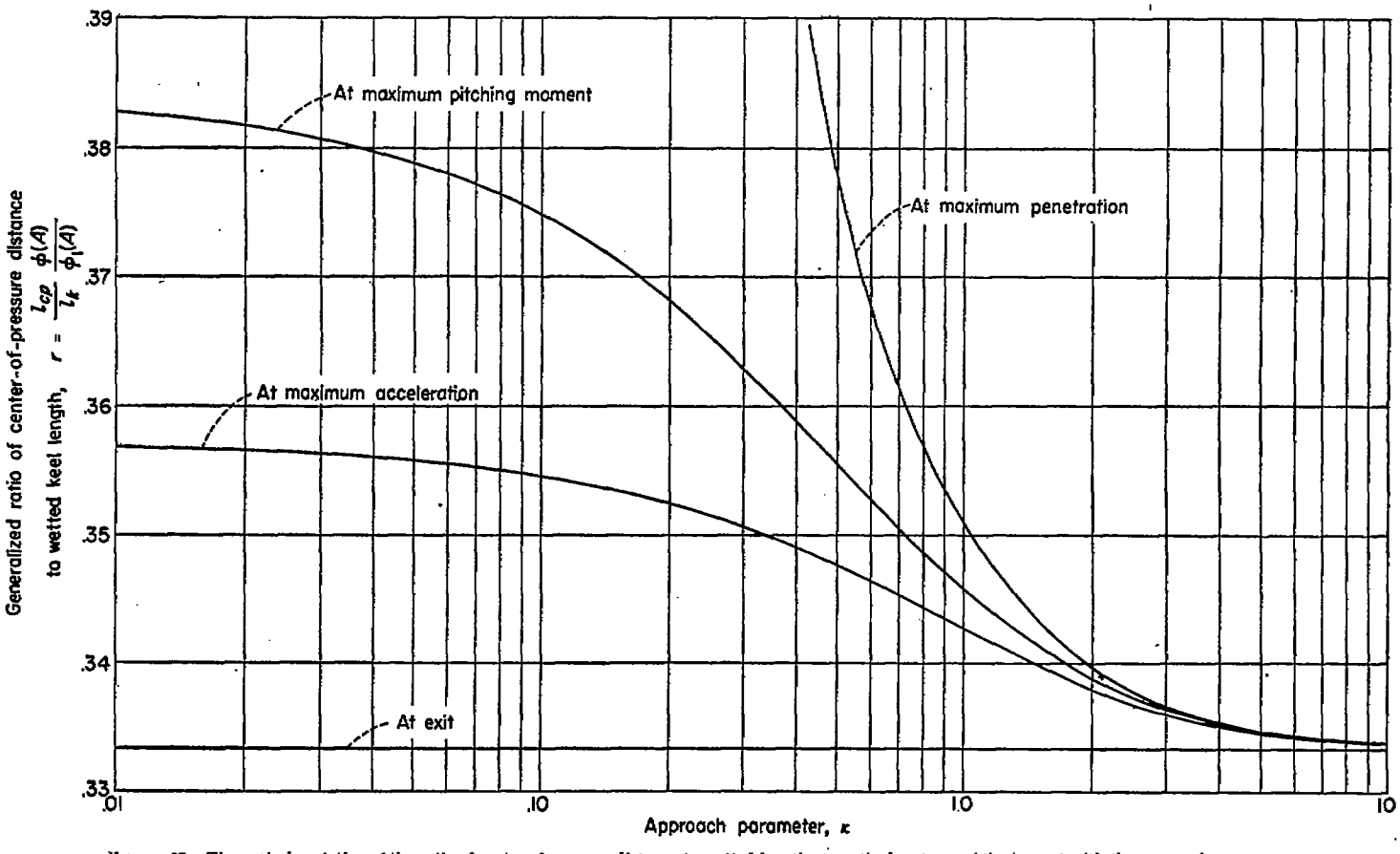

FIGURE 27.—Theoretical variation of the ratio of center-of-pressure distance to wetted length at particular stages of the impact with the approach parameter.

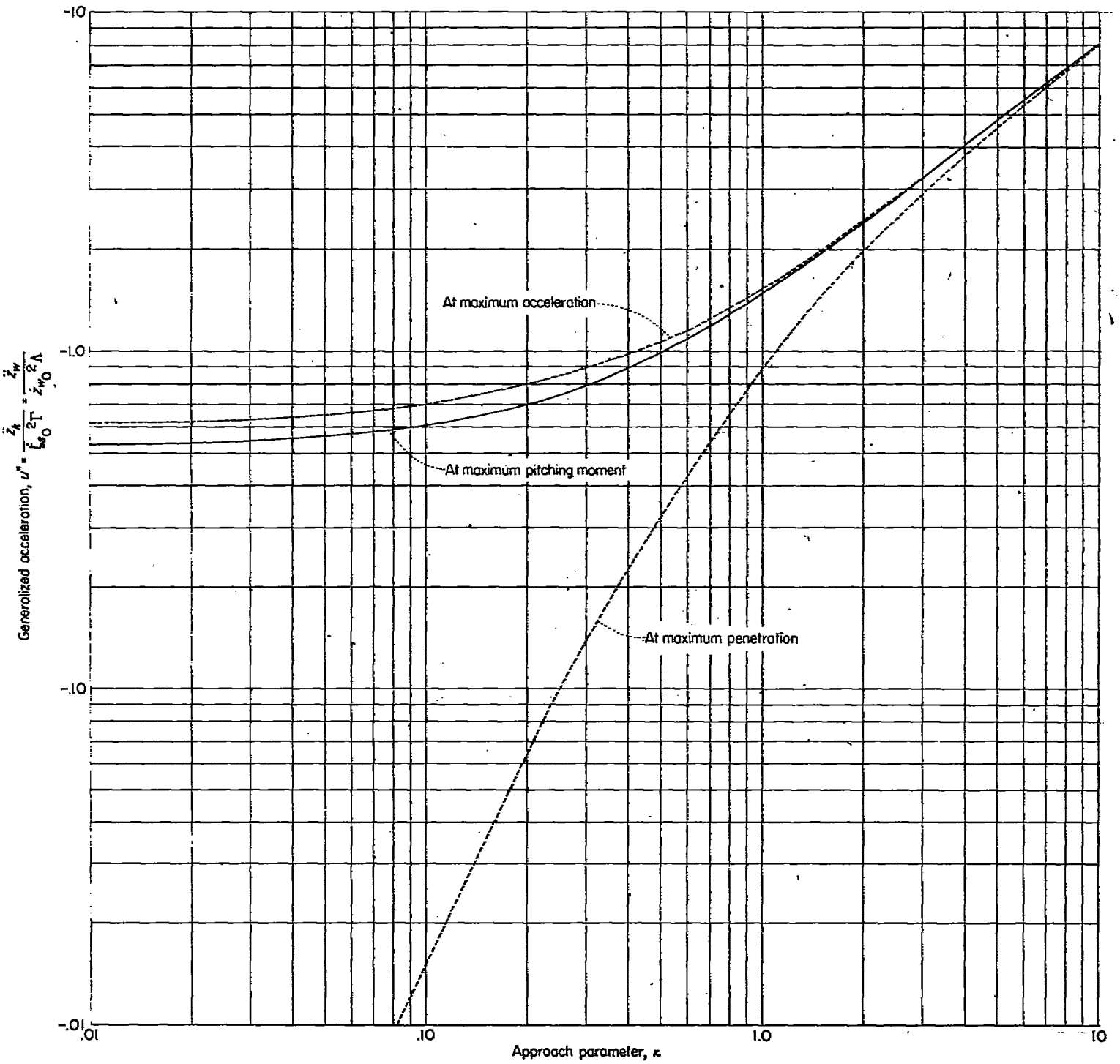

FIGURE 28.—Theoretical variation of the acceleration at the instant of maximum pitching moment about the step with the approach parameter.

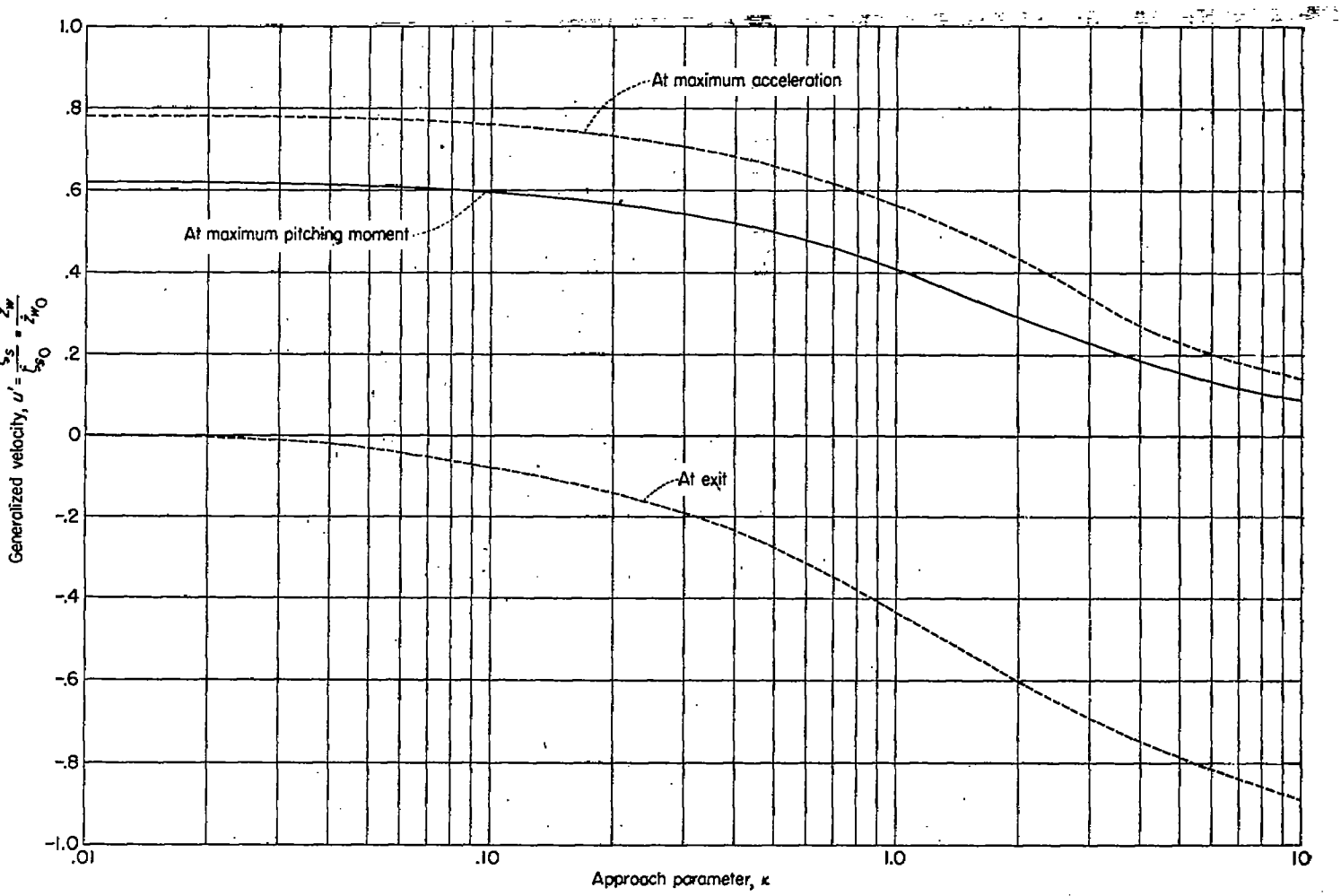

FIGURE 29.—Theoretical variation of the velocity at the instant of maximum pitching moment about the step with the approach parameter.

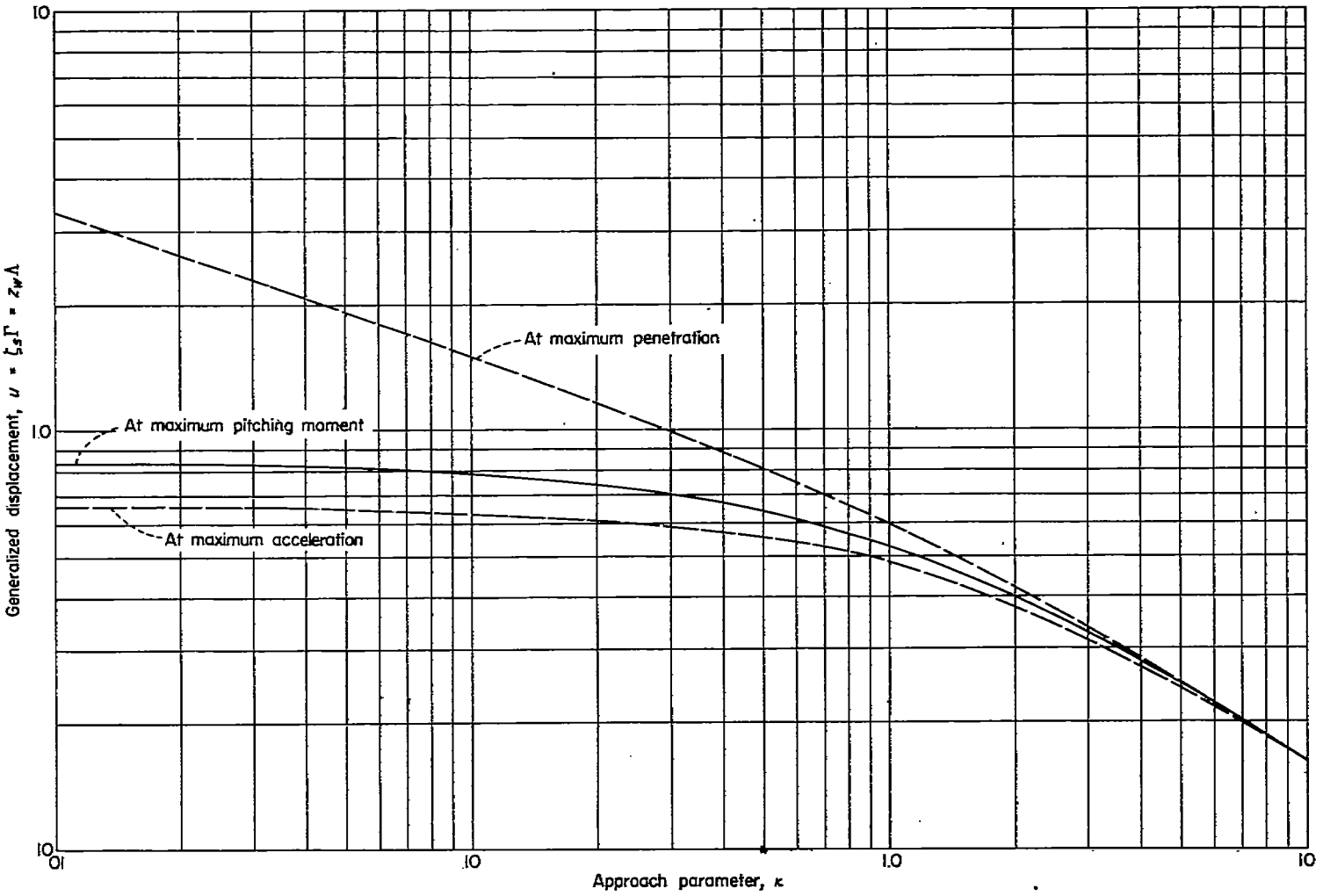

FIGURE 30.—Theoretical variation of the displacement at the instant of maximum pitching moment about the step with the approach parameter.

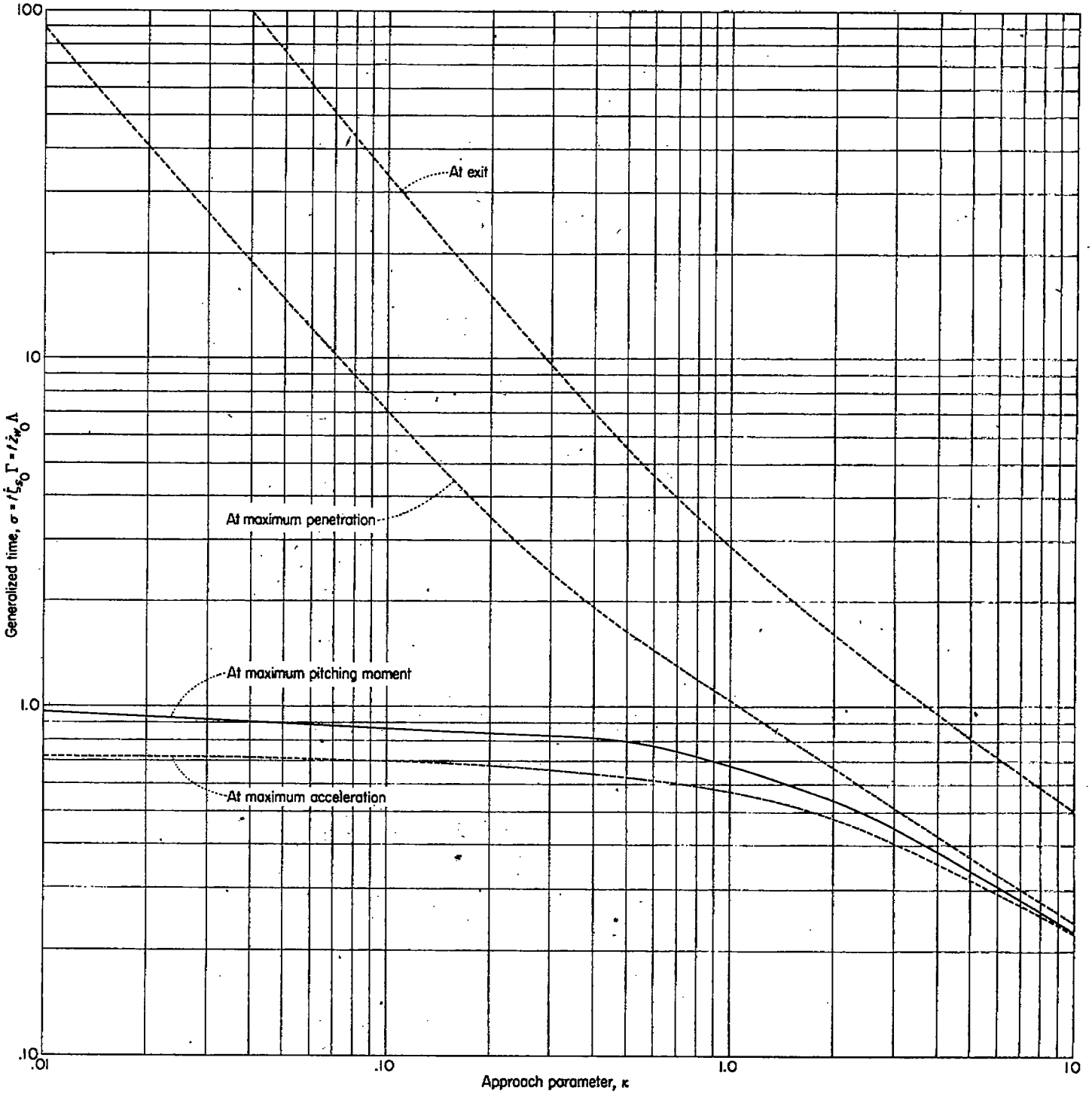

FIGURE 31.—Theoretical variation of the time at maximum pitching moment about the step with the approach parameter.

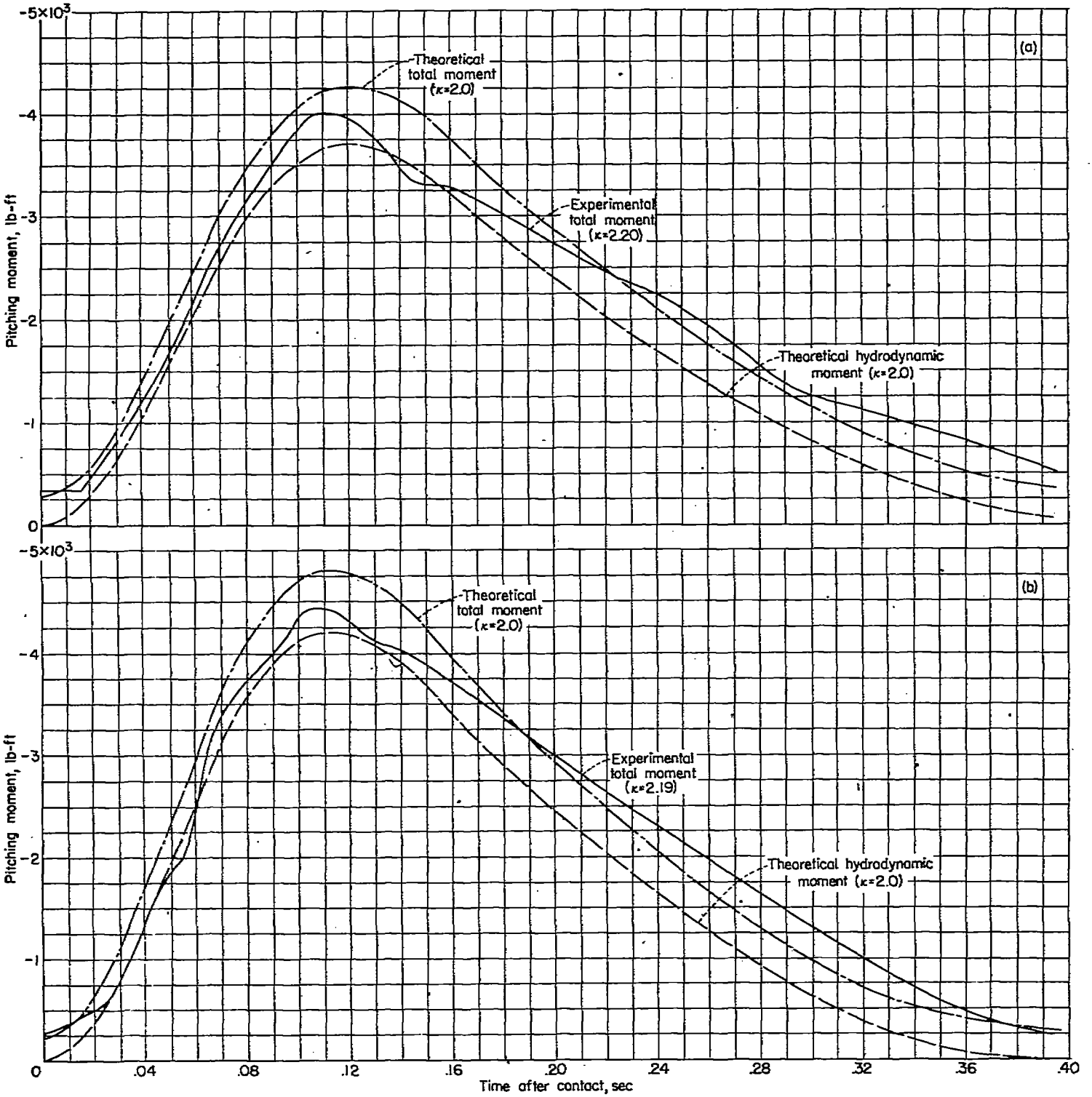

(a) Experimental data: V_{Z_0}=4.95 feet per second; V_{H_0}=54.55 feet per second; γ_0=5.18°; κ=2.20.

(b) Experimental data: V_{Z_0}=5.26 feet per second; V_{H_0}=57.89 feet per second; γ_0=5.21°; κ=2.19.

FIGURE 32.—Comparison between theoretical and experimental time histories of pitching moment for a V-bottom seaplane with an angle of dead rise of 30°. W=1,231 pounds; τ=12°.

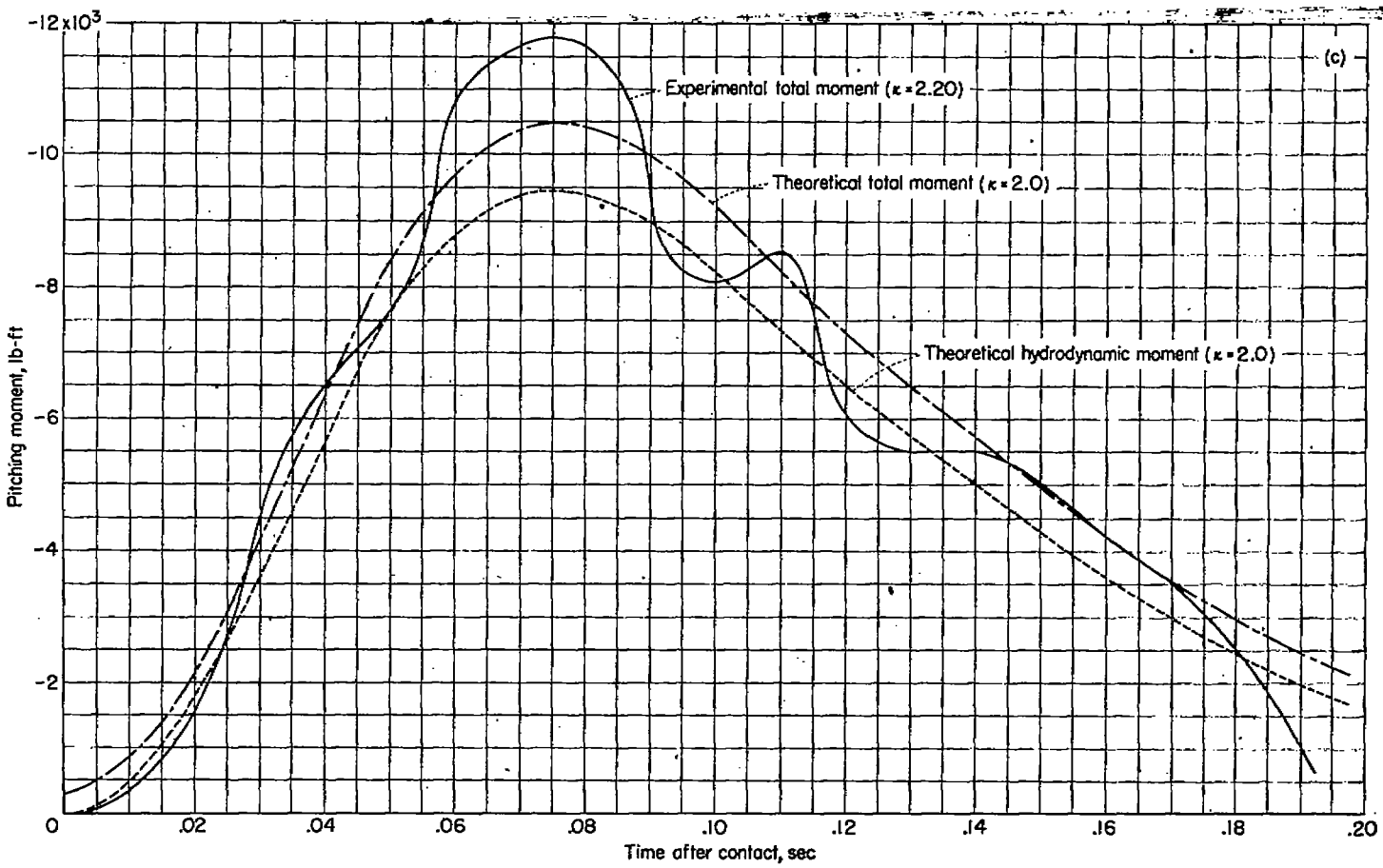

(c) Experimental data: V_{V_0}=7.92 feet per second; V_{H_0}=87.50 feet per second; γ_0=5.17°; κ=2.20.

FIGURE 32.—Concluded.

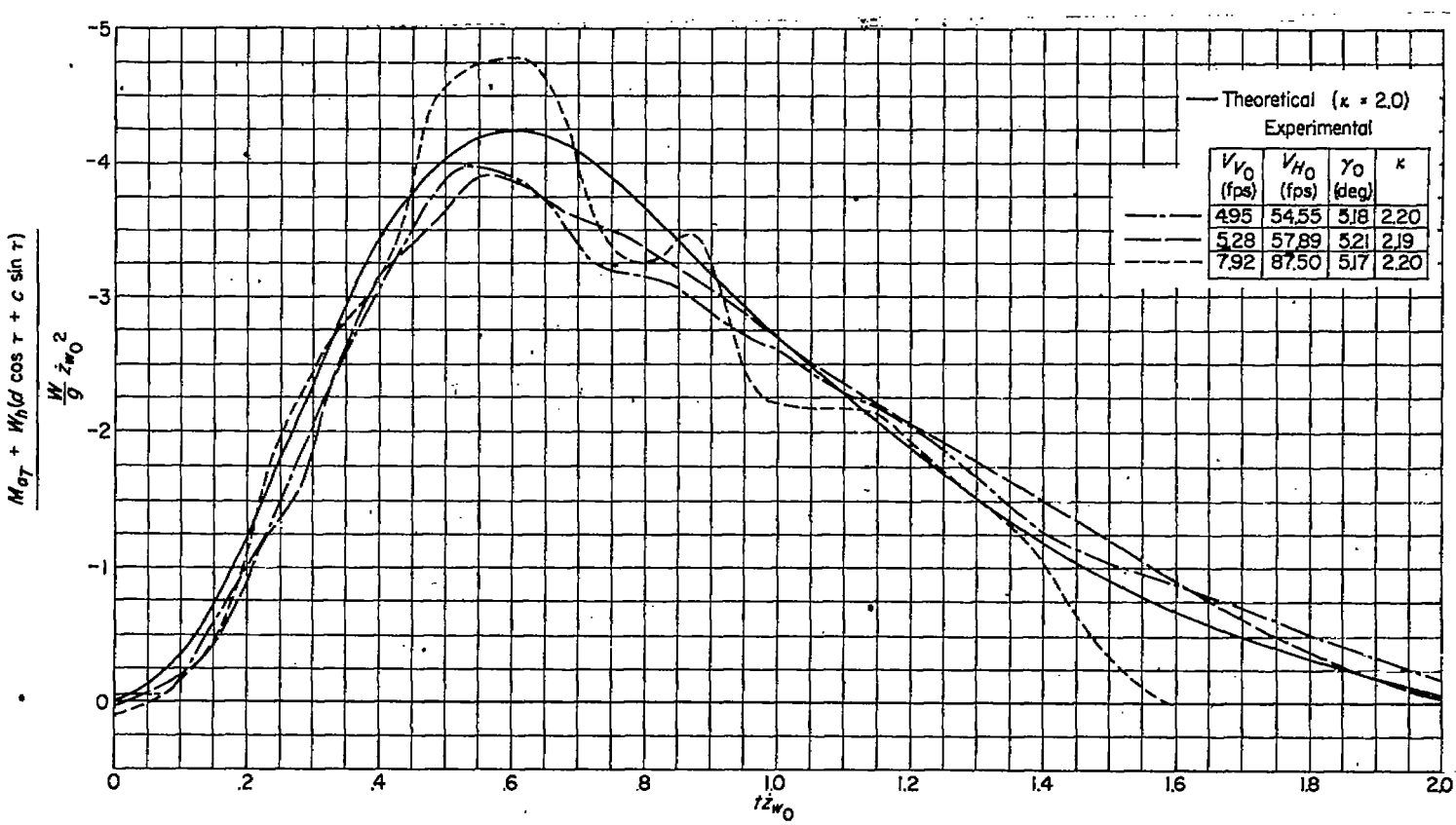

FIGURE 33.—Comparison of theoretical and experimental variation of total pitching moment for a V-bottom seaplane with an angle of dead rise of 30° and different initial conditions. W=1,231 pounds; τ=12°.

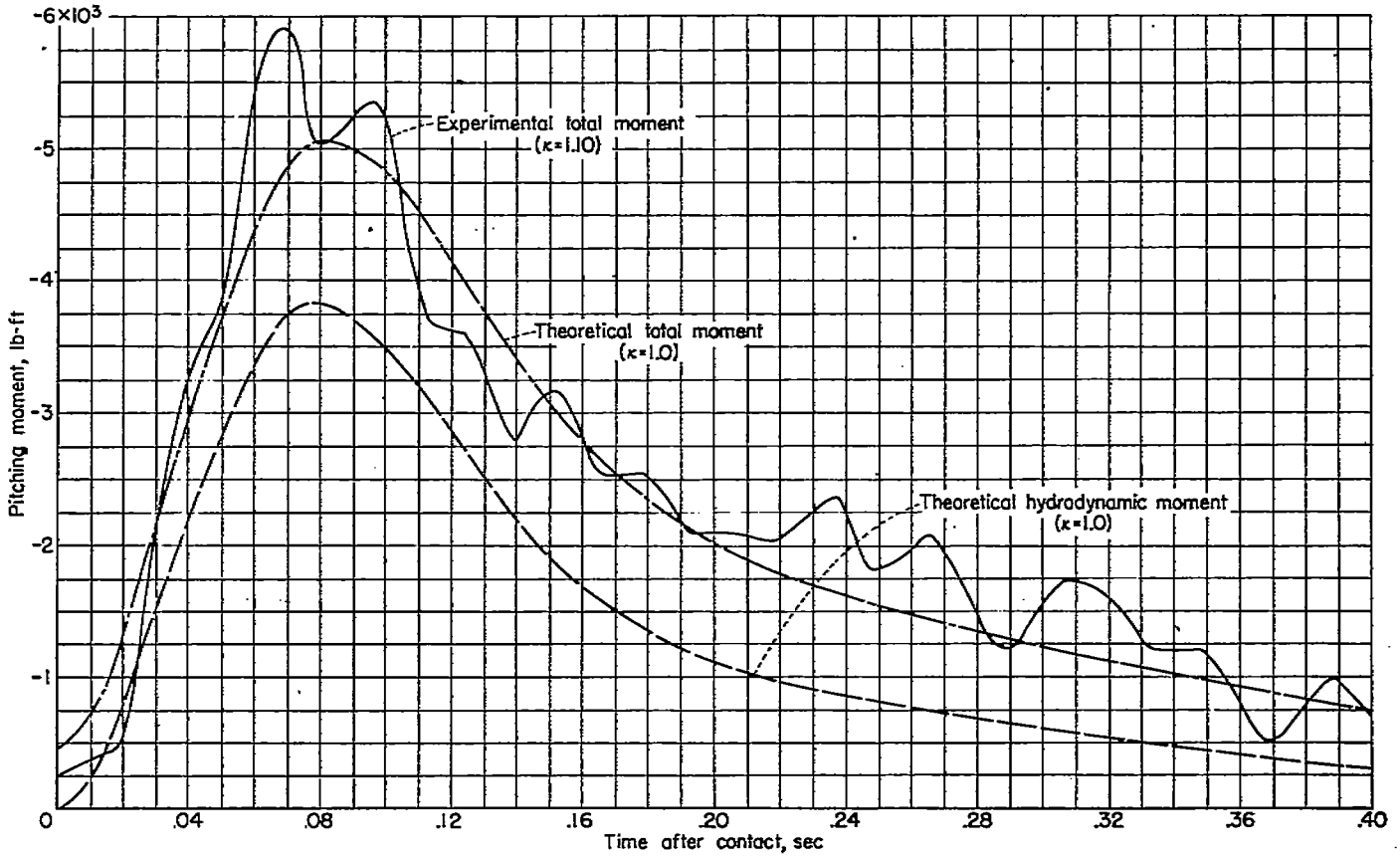

FIGURE 34.—Comparison between theoretical and experimental time histories of pitching moment for a V-bottom seaplane with an angle of dead rise of 40°. W=1,213 pounds; τ=8°; V_{Y_0}=8.75 feet per second; V_{Z_0}=63.69 feet per second; γ_0=7.82°; κ=1.10.

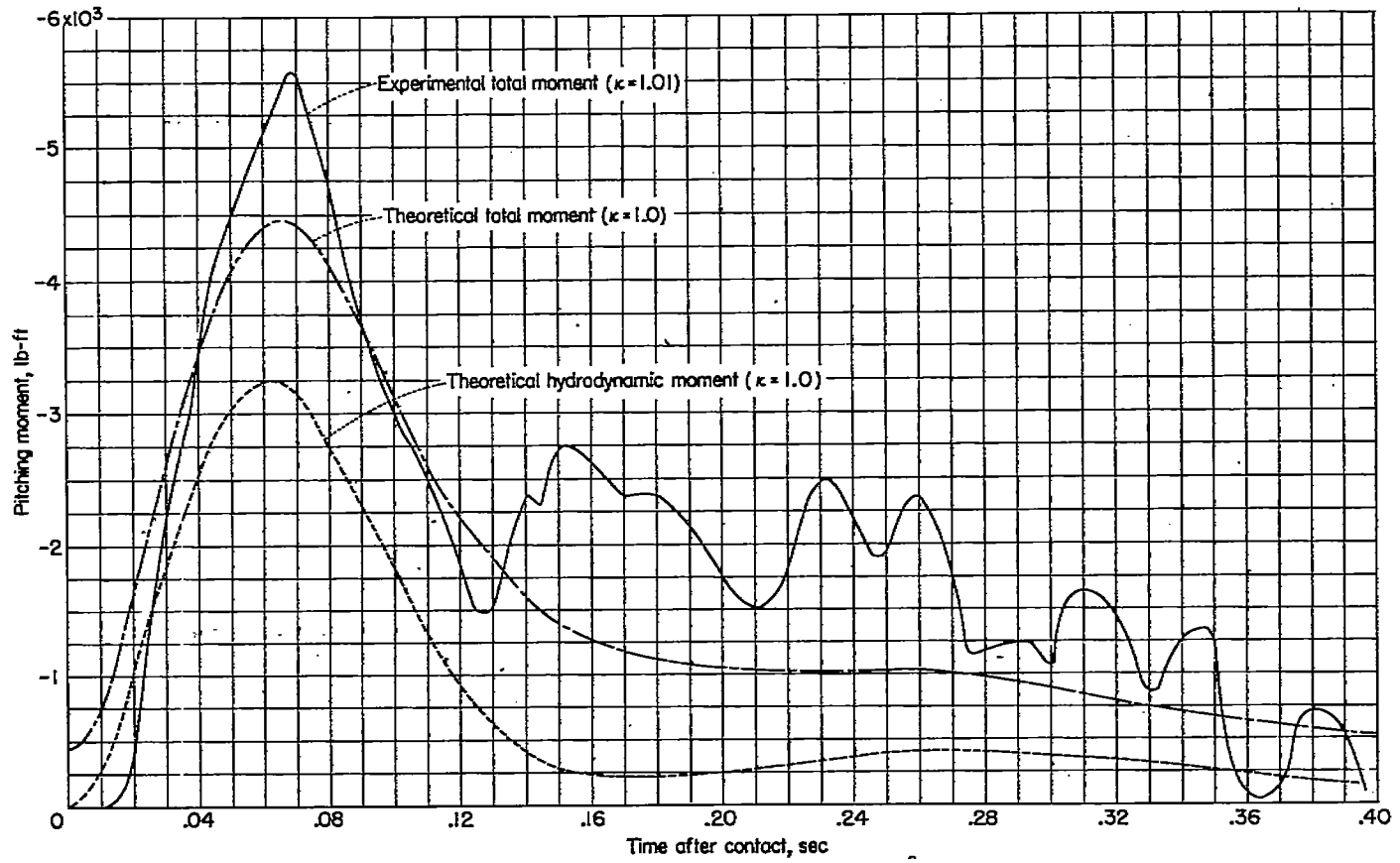

FIGURE 35.—Comparison between theoretical and experimental time histories of pitching moment for a V-bottom seaplane with an angle of dead rise of 40°. W=1,213 pounds; τ=6°; V_{Y_0}=8.67 feet per second; V_{Z_0}=85.47 feet per second; γ_0=5.79°; κ=1.0.

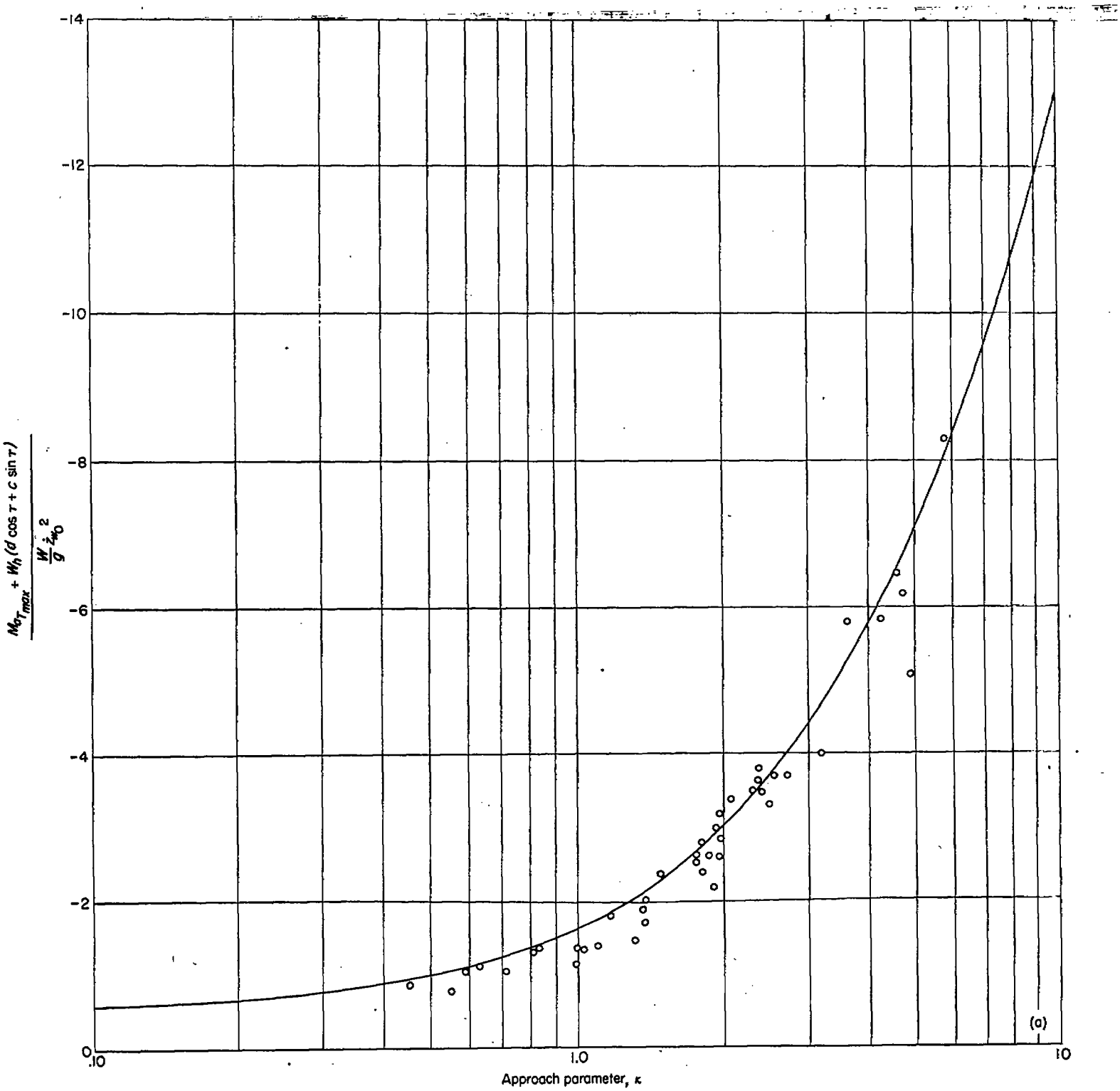

(a) $\tau=12°$.

FIGURE 36.—Comparison between theoretical and experimental variation of maximum total pitching moment with approach parameter. $\beta=40°$; $W=1{,}213$ pounds; $W_H=350$ pounds; $a=2.89$ feet; $d=1.05$ feet; $c=1.81$ feet.

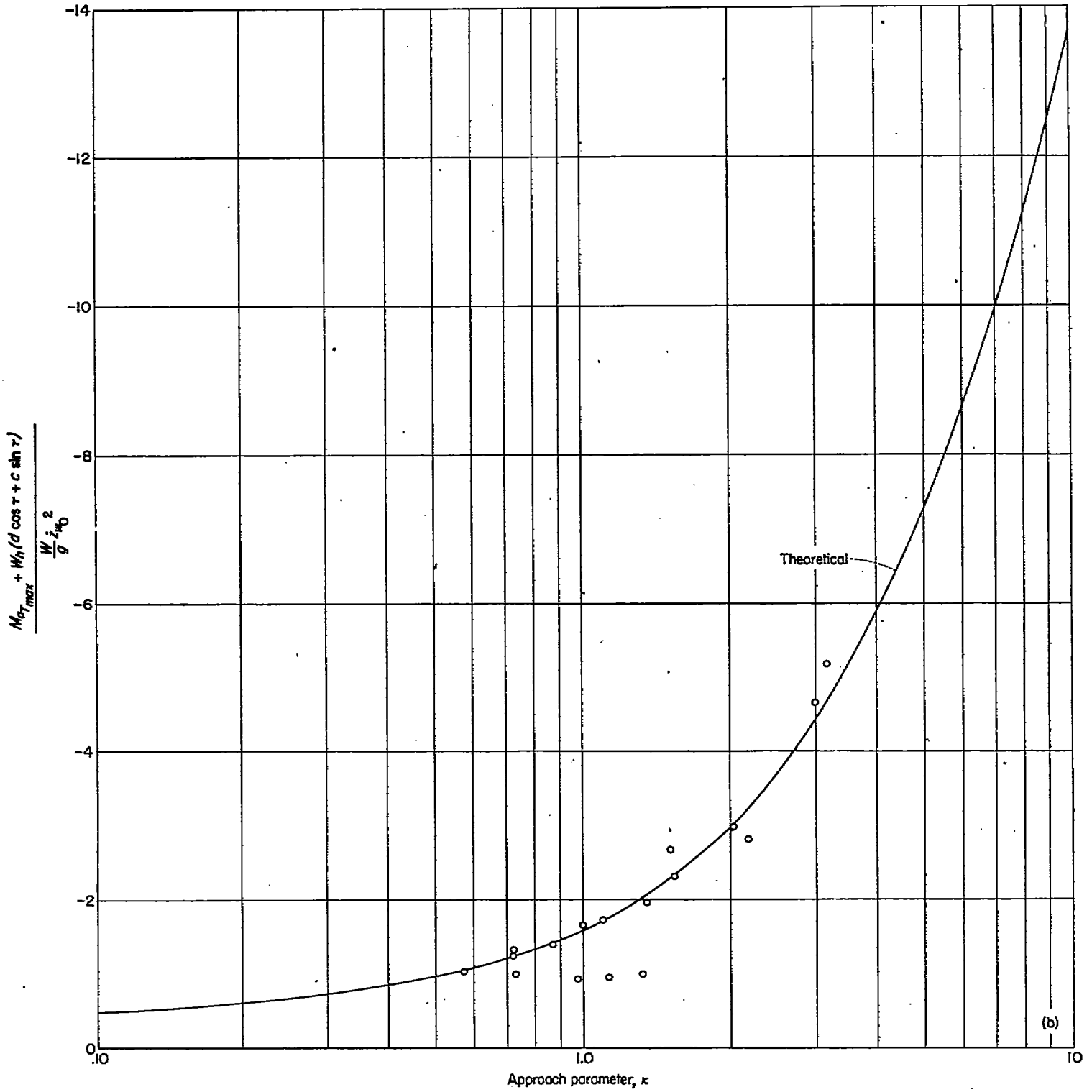

(b) $\tau=9°$.

FIGURE 36.—Continued.

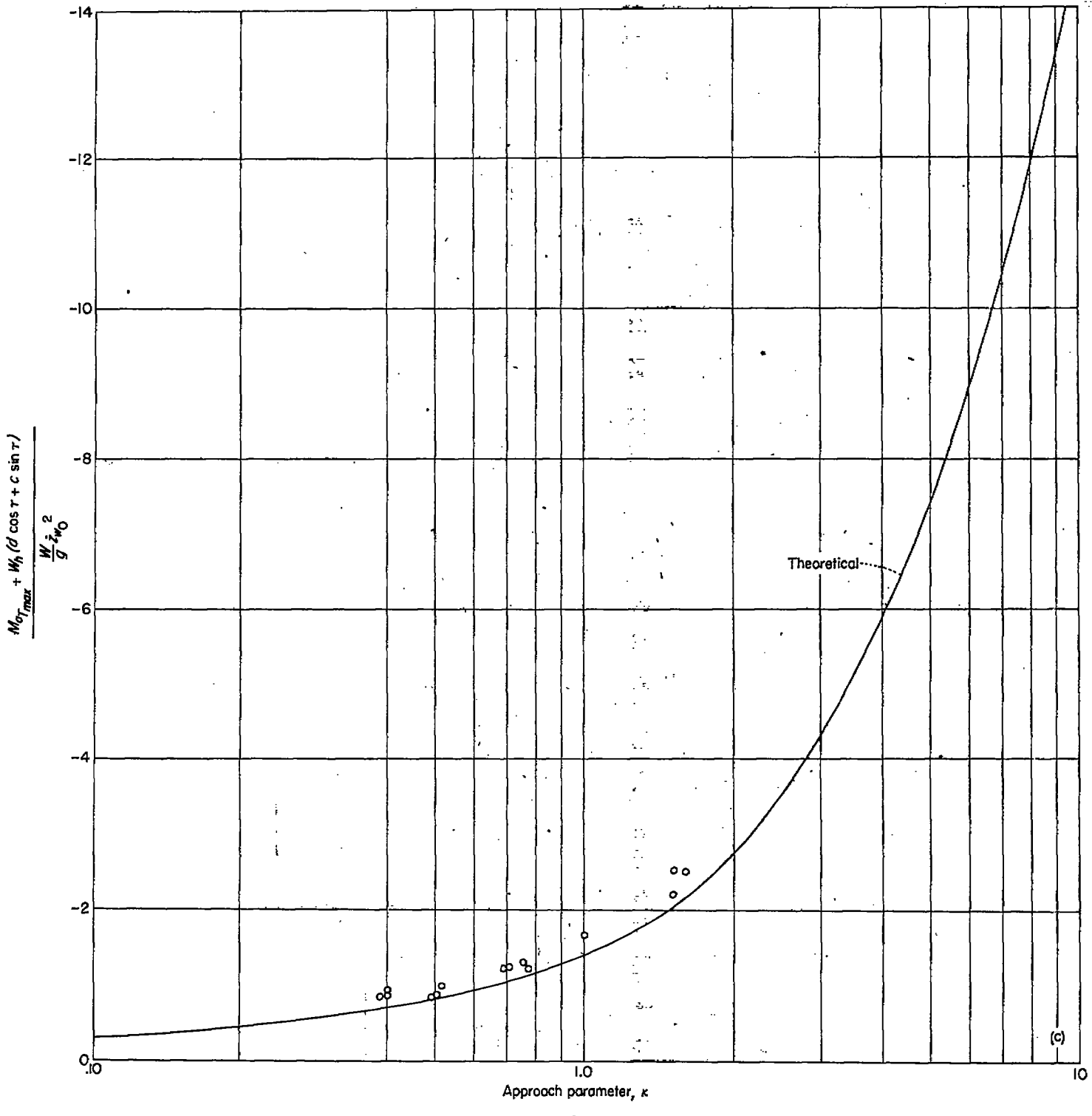

(c) $\tau=6°$.

FIGURE 36.—Concluded.

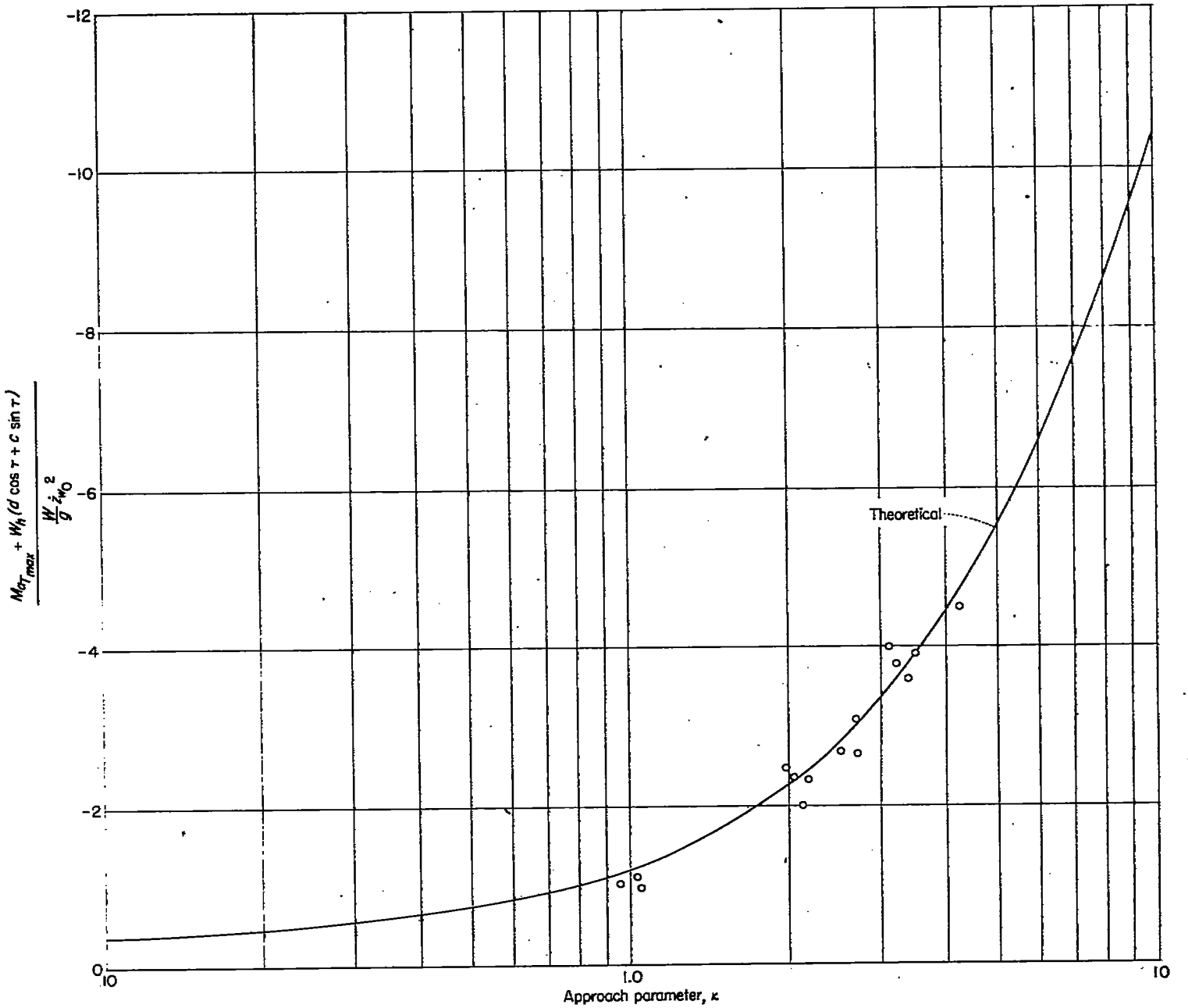

FIGURE 37.—Comparison between theoretical and experimental variation of maximum total pitching moment with approach parameter. $\beta=40°$; $\tau=12°$; $W=1{,}343$ pounds; $W_h=590$ pounds; $a=2.89$ feet; $d=-0.28$ foot; $c=1.46$ feet.

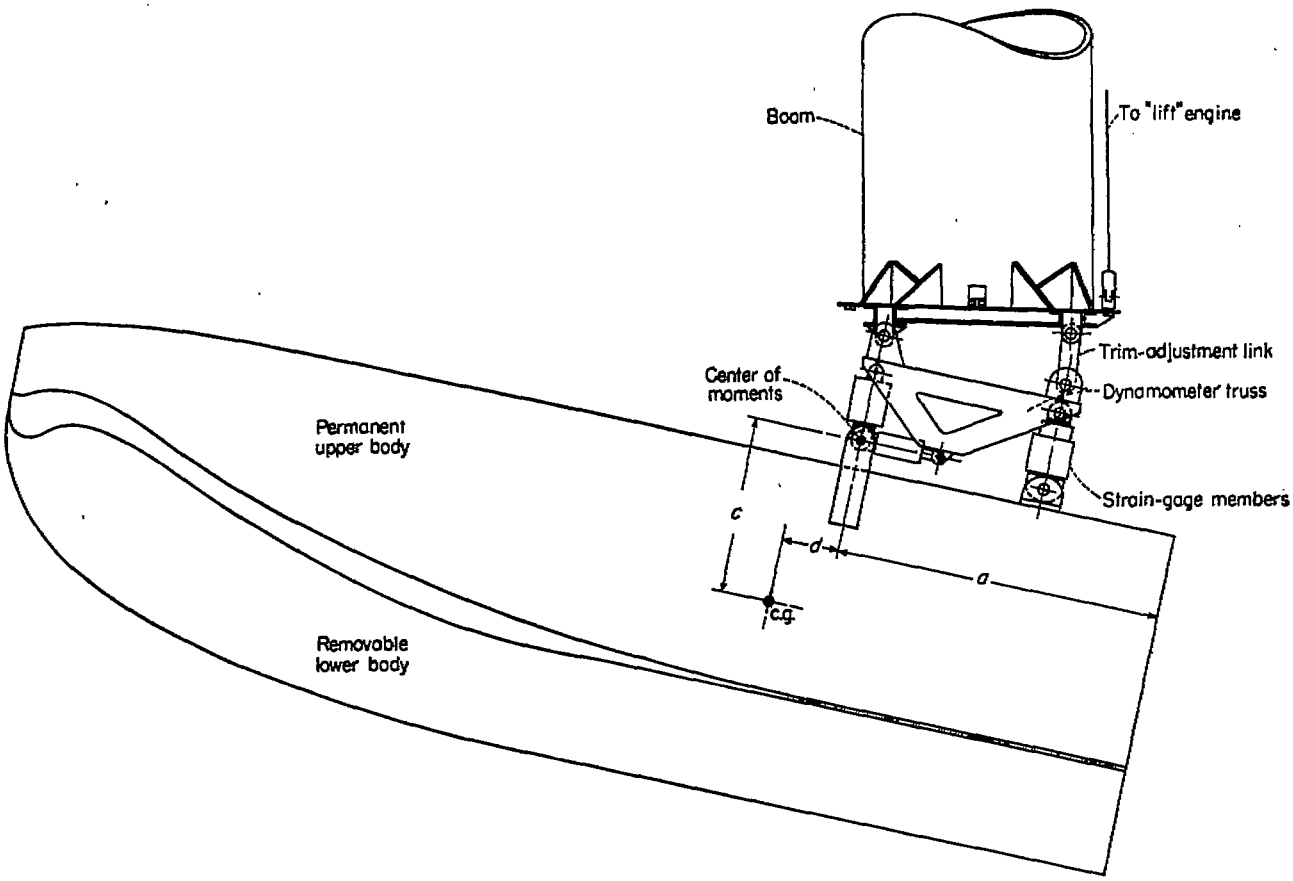

FIGURE 38.—Hull-forebody model attached to boom of impact-basin carriage by means of dynamometer truss.

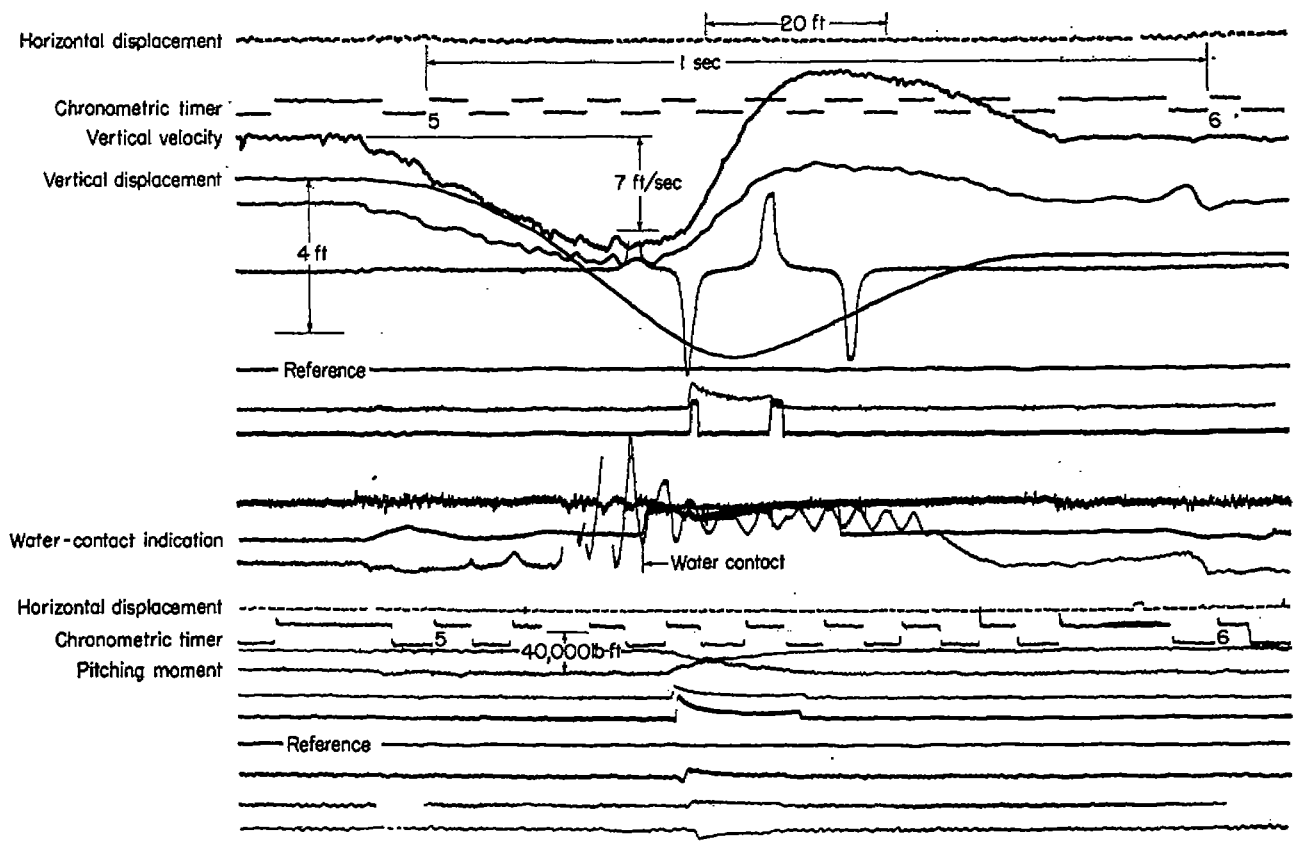

FIGURE 39.—Reproduction of typical oscillograph record obtained during tests in the Langley impact basin.

TABLE I.—CALCULATED VALUES OF THE GENERALIZED VARIABLES AT PARTICULAR STAGES OF THE IMPACT

κ	Instant of maximum acceleration							Instant of maximum pitching moment about step							Instant of maximum penetration						Instant of exit	
	u	u'	u''	σ	m_a	p	r	u	u'	u''	σ	m_a	p	r	u	u''	σ	m_a	p	r	u'	σ
0	0.659	0.778	−0.612	0.706	0.144	0.235	0.357	0.846	0.623	−0.519	0.974	0.169	0.325	0.384	∞	0	∞	0	∞	∞	------	------
.5	.560	.660	−1.065	.630	.207	.194	.348	.646	.500	−.956	.802	.227	.230	.356	0.814	−.323	1.624	.100	0.308	0.378	−0.278	5.45
1.0	.480	.562	−1.58	.570	.255	.166	.343	.532	.408	−1.466	.670	.270	.184	.346	.597	−.852	1.043	.185	.210	.351	−.432	2.35
2.0	.362	.422	−2.45	.475	.318	.130	.338	.402	.294	−2.400	.535	.327	.136	.339	.421	−1.98	.664	.284	.143	.340	−.603	1.61
3.0	.319	.334	−3.31	.404	.356	.108	.336	.329	.229	−3.272	.448	.362	.111	.336	.338	−2.96	.514	.336	.114	.337	−.693	1.19
4.0	.277	.275	−4.11	.347	.381	.093	.335	.282	.186	−4.085	.385	.385	.094	.335	.286	−3.84	.413	.368	.096	.335	−.750	.956
6.0	.220	.202	−5.56	.303	.412	.074	.334	.223	.136	−5.571	.315	.414	.075	.334	.225	−5.39	.334	.405	.075	.334	−.817	.713
8.0	.187	.160	−6.97	.252	.431	.062	.334	.188	.105	−6.905	.257	.435	.062	.334	.188	−6.73	.280	.427	.063	.334	−.862	.596
10.0	.163	.130	−8.13	.221	.442	.058	.334	.163	.088	−8.147	.223	.441	.054	.334	.164	−8.08	.240	.441	.055	.334	−.889	.504

TABLE II.—EXPERIMENTAL DATA FOR A PRISMATIC HULL MODEL WITH $\beta=22\frac{1}{2}°$

W (lb)	V_{x_0} (fps)	V_{z_0} (fps)	γ_0 (deg)	κ	At maximum acceleration				At maximum draft			At exit	
					z_w/g	$\dot{z}_w$ (fps)	z_w (ft)	t (sec)	z_w/g	z_w (ft)	t (sec)	$\dot{z}_w$ (fps)	t (sec)
							$\tau=3°$						
1100	11.90	45.16	13.93	0.208	−4.95	8.79	0.45	0.040	−0.35	0.67	0.205	No exit	No exit.
	9.96	44.09	12.73	.229	(a)	(a)	(a)	(a)	(a)	.59	.206	do	Do.
	9.96	44.54	12.60	.231	−3.45	6.78	.41	.063	−.25	.54	.202	do	Do.
	9.36	44.92	11.77	.248	−3.55	6.77	.41	.055	−.35	.50	.188	do	Do.
	7.40	44.09	9.53	.308	−2.22	5.78	.34	.038	−.37	.54	.218	do	Do.
	6.47	45.37	8.03	.367	−1.86	(a)	(a)	(a)	(a)	.62	(a)	do	Do.
	6.12	45.90	7.66	.385	−1.86	(a)	(a)	(a)	(a)	.62	(a)	do	Do.
	6.02	45.71	7.50	.394	−1.90	(a)	(a)	(a)	(a)	(a)	(a)	do	Do.
	12.33	95.55	7.35	.402	−6.99	(a)	(a)	(a)	(a)	.60	(a)	do	Do.
	12.45	100.20	7.06	.418	−6.34	(a)	(a)	(a)	(a)	(a)	(a)	do	Do.
	11.88	97.00	6.98	.424	−6.34	(a)	(a)	(a)	(a)	(a)	(a)	do	Do.
	5.38	44.60	6.88	.430	−1.65	(a)	(a)	(a)	(a)	.55	(a)	do	Do.
	10.75	97.56	6.29	.471	−6.00	(a)	(a)	(a)	(a)	.52	(a)	do	Do.
	4.91	45.06	6.22	.476	−1.33	(a)	(a)	(a)	(a)	.47	(a)	do	Do.
	10.20	100.30	5.81	.510	−6.34	(a)	(a)	(a)	(a)	(a)	(a)	do	Do.
	3.97	44.83	5.06	.587	−.97	(a)	(a)	(a)	(a)	.44	(a)	do	Do.
	8.82	100.82	5.02	.592	−4.52	(a)	(a)	(a)	(a)	.47	(a)	do	Do.
	3.68	45.29	4.56	.649	−.76	(a)	(a)	(a)	(a)	.41	(a)	do	Do.
	3.32	44.72	4.26	.701	−.78	(a)	(a)	(a)	(a)	.41	(a)	do	Do.
	6.05	96.35	3.59	.829	−3.18	(a)	(a)	(a)	(a)	.44	(a)	do	Do.
	4.29	97.83	2.52	1.188	−1.53	(a)	(a)	(a)	(a)	.33	(a)	do	Do.
	1.76	44.90	2.25	1.332	−.35	(a)	(a)	(a)	(a)	.27	(a)	do	Do.
	1.33	42.20	1.80	*1.658	−.18	(a)	(a)	(a)	(a)	(a)	(a)	do	Do.
	2.70	97.56	1.59	1.878	−.90	(a)	(a)	(a)	(a)	.35	(a)	do	Do.
	1.01	44.59	1.30	2.334	−.19	(a)	(a)	(a)	(a)	(a)	(a)	do	Do.
	1.93	99.00	1.12	2.667	−.60	(a)	(a)	(a)	(a)	(a)	(a)	do	Do.
	.80	44.75	1.02	2.929	−.14	(a)	(a)	(a)	(a)	(a)	(a)	do	Do.
	1.57	99.25	.91	3.284	−.50	(a)	(a)	(a)	(a)	(a)	(a)	do	Do.
	1.45	93.02	.89	3.358	−.35	(a)	(a)	(a)	(a)	(a)	(a)	do	Do.
							$\tau=6°$						
1040	10.00	41.67	13.49	0.422	−4.40	6.60	0.62	0.059	−0.90	0.83	0.159	−1.35	0.520
	10.60	44.30	13.46	.423	−4.65	6.84	.57	.043	−.95	.87	.150	No exit	No exit.
	7.72	42.80	10.22	.585	−3.02	4.37	.57	.070	−1.04	.72	.156	do	Do.
	5.16	41.86	6.86	.853	−1.90	2.88	.46	.090	−.62	.62	.170	do	Do.
	4.00	42.62	5.36	1.097	−1.30	1.40	.43	.118	−.82	.60	.178	do	Do.
	3.77	41.18	5.23	1.124	−.95	1.21	.38	.135	−.55	.43	.201	do	Do.
	2.60	41.67	3.57	1.654	−.62	1.00	.34	.145	−.47	.40	.209	do	Do.
	5.10	104.30	2.80	2.113	−2.56	2.60	.26	.075	−1.95	.28	.119	−2.70	.266
	1.49	42.37	2.01	2.951	−.25	.42	.21	.180	−.28	.22	.249	No exit	No exit.
	3.20	94.89	1.93	3.072	−1.52	.70	.22	.109	−.82	.23	.131	−1.80	.295
	2.30	100.00	1.32	4.498	−.75	1.10	.17	.100	−.75	.18	.149	−1.10	.360
							$\tau=9°$						
1040	9.49	42.55	12.57	0.668	−4.54	5.90	0.61	0.058	−1.23	0.79	0.143	−1.77	0.472
	7.44	42.11	10.02	.850	−3.15	3.63	.57	.075	−1.22	.72	.144	−1.26	.488
	5.21	42.86	6.93	1.247	−2.15	3.16	.44	.078	−1.02	.56	.147	−1.30	.450
	4.32	42.61	5.79	1.499	−1.52	2.09	.46	.110	−.75	.50	.165	−.74	.490
	3.81	42.45	5.13	1.697	−1.30	1.40	.41	.131	−1.05	.46	.180	−.70	.517
	3.35	43.33	4.42	1.974	−.90	.93	.38	.149	−.68	.39	.175	−.51	.533
	2.37	43.14	3.14	2.792	−.62	1.02	.29	.140	−.55	.32	.196	No exit	No exit.
	4.13	93.46	2.53	3.472	−2.01	2.39	.29	.091	−1.77	.30	.110	−2.61	.260
	3.12	95.89	1.86	4.733	−1.43	.94	.23	.104	−1.16	.25	.110	−1.67	.258

* Not available.

TABLE II.—EXPERIMENTAL DATA FOR A PRISMATIC HULL MODEL WITH β=22½°—Concluded

W (lb)	V_{F_0} (fps)	V_{H_0} (fps)	γ_0 (deg)	κ	At maximum acceleration				At maximum draft			At exit	
					z_w/g	$\dot{z}_w$ (fps)	z_w (ft)	t (sec)	z_w/g	z_w (ft)	t (sec)	$\dot{z}_w$ (fps)	t (sec)
					τ=12°								
1040	11.75	4.42	69.39	0.033	−2.52	10.20	0.66	0.061	−0.40	1.81	0.452	−1.50	1.257
	11.36	4.35	69.05	.035	−2.40	8.83	.66	.070	−.36	1.74	.440	−1.71	1.210
	11.36	5.18	65.49	.050	−2.40	9.80	.59	.070	−.24	1.68	.434	No exit	No exit.
	11.41	5.24	65.33	.050	−2.62	(*)	(*)	(*)	(*)	1.74	.445	−.92	1.315
	11.64	5.65	64.12	.056	−2.52	9.91	.64	.065	−.22	1.69	.450	No exit	No exit.
	11.64	5.78	63.59	.058	−2.52	9.68	.66	.065	−.40	1.75	.449	do	Do.
	12.04	6.81	60.51	.072	−2.44	9.39	.72	.065	−.30	1.66	.428	do	Do.
	9.10	5.62	58.32	.082	−1.59	7.55	.62	.075	−.26	1.49	.453	do	Do.
	11.23	6.97	58.17	.083	−2.52	9.28	.62	.060	−.26	1.62	.400	do	Do.
	10.25	6.57	57.33	.087	(*)	(*)	(*)	(*)	(*)	1.48	.382	do	Do.
	11.36	7.60	56.22	.098	−2.63	9.40	.58	.065	−.25	1.62	.415	do	Do.
	7.43	5.18	55.12	.099	−.95	5.82	.59	.095	−.15	1.23	.460	do	Do.
	11.36	7.97	54.95	.100	−2.58	9.41	.68	.065	−.30	1.71	.411	do	Do.
	11.36	8.33	53.75	.106	−2.63	8.83	.68	.070	−.30	1.54	.422	do	Do.
	11.36	8.82	52.17	.115	−2.63	9.54	.60	.076	−.23	1.57	.420	do	Do.
	11.06	8.85	51.33	.120	−2.63	9.16	(*)	.062	(*)	(*)	(*)	do	Do.
	11.36	9.23	50.88	.122	−2.78	(*)	(*)	(*)	(*)	1.56	.410	do	Do.
	11.12	9.77	48.70	.136	−2.63	8.75	.63	.065	−.23	1.47	.390	do	Do.
	11.36	10.50	47.25	.145	−2.77	9.67	.63	.061	−.31	1.45	.375	do	Do.
	10.66	9.93	47.03	.146	(*)	(*)	(*)	(*)	(*)	1.49	.370	do	Do.
	11.87	11.37	46.24	.152	(*)	(*)	(*)	(*)	(*)	1.40	.343	do	Do.
	11.58	11.44	45.35	.158	(*)	(*)	(*)	(*)	(*)	1.36	.350	do	Do.
	11.36	11.56	44.50	.164	−2.77	9.73	.56	.055	−.30	1.44	.365	do	Do.
	11.23	11.86	43.44	.172	−2.89	8.41	.64	.069	−.30	1.41	.351	do	Do.
	4.84	5.32	42.30	.180	−.58	3.80	.55	.123	−.10	1.07	.447	do	Do.
	11.36	12.54	42.11	.181	−2.81	9.84	.61	.058	−.23	1.40	.349	do	Do.
	11.18	12.99	40.70	.193	(*)	(*)	(*)	(*)	(*)	1.32	.343	do	Do.
	11.36	13.76	39.67	.202	−2.89	10.02	.61	.055	−.36	1.32	.319	do	Do.
	11.36	13.70	39.67	.202	−3.00	9.86	.63	.055	−.29	1.34	.334	do	Do.
	11.36	13.76	39.54	.203	−3.00	9.09	.64	.069	−.33	1.32	.324	do	Do.
	11.23	13.79	39.16	.207	−3.05	(*)	(*)	(*)	(*)	1.34	.323	do	Do.
	4.09	6.80	31.02	.295	−.50	2.88	.52	.142	−.10	.88	.469	do	Do.
	10.77	18.63	30.03	.309	−3.09	7.20	.68	.065	−.43	1.16	.269	do	Do.
	3.28	6.71	25.70	.379	(*)	(*)	(*)	(*)	(*)	.80	.514	do	Do.
	3.28	7.75	22.96	.437	−.35	2.13	.51	.180	−.10	.74	.492	do	Do.
	2.19	4.65	22.23	.454	−.12	.81	.44	.310	−.05	.53	.562	do	Do.
	10.77	27.27	21.55	.472	−3.59	8.34	.58	.080	−.77	.96	.179	do	Do.
	10.86	32.52	18.47	.566	−3.90	7.74	.59	.060	−1.37	.86	.143	−1.83	.551
	10.85	41.67	14.60	.738	(*)	(*)	(*)	(*)	(*)	.75	.145	−3.05	.404
	10.77	43.01	14.06	.769	−4.41	6.57	.62	.063	−1.36	.76	.119	−3.18	.400
	11.81	59.56	11.28	.981	−6.71	6.39	.53	.060	−2.51	.62	.091	−5.88	.252
	10.45	97.50	5.12	1.853	−6.92	3.98	.43	.050	−5.67	.47	.073	−6.56	.166
	8.60	97.50	5.04	2.263	(*)	(*)	(*)	(*)	(*)	.41	.085	−5.76	.164
	6.68	83.04	4.60	2.484	−4.00	2.94	.34	.085	−3.16	.34	.089	−4.78	.190
	4.97	98.38	2.90	3.972	−3.10	(*)	.29	(*)	(*)	.29	.095	−4.03	.202
	3.80	96.74	2.25	5.134	−2.40	1.47	.24	.075	−2.02	.27	.101	−3.17	.217
	1.90	96.44	1.13	10.27	−1.15	(*)	.16	(*)	(*)	.16	.131	−1.15	.348
1100	11.34	45.16	14.10	.767	−5.16	7.00	.51	.113	−1.60	.71	.133	−3.76	.366
	11.36	45.45	14.08	.770	−5.22	8.32	.49	.060	−1.65	.68	.142	−3.48	.376
	9.00	45.37	11.22	.982	−3.76	6.02	.47	.075	−2.47	.63	.139	−3.76	.353
	7.25	44.81	9.19	1.214	−2.76	4.14	.37	.127	−1.18	.52	.155	−3.38	.356
	5.25	44.95	6.66	1.599	−1.94	2.96	.37	.098	−1.21	.43	.148	−2.78	.367
	10.15	91.88	6.31	1.796	−3.03	4.70	.40	.058	−5.15	.51	.081	−6.96	.168
	4.66	44.76	5.96	1.900	−1.66	3.01	.32	.108	−.95	.39	.163	−2.35	.333
	3.66	45.22	4.63	2.466	−1.24	1.65	.30	.127	−1.01	.35	.173	−1.69	.426
	6.44	102.94	2.59	3.208	−4.67	(*)	(*)	(*)	(*)	.37	.194	−4.70	.187
	2.37	44.64	3.04	3.787	−.68	.85	.28	.165	−.38	.28	.223	−.80	.495
	1.02	45.83	1.28	9.060	−.25	.14	.18	.287	−.21	.19	.265	No exit	No exit.
	.94	44.44	1.21	9.587	−.30	.14	.18	.293	−.21	.19	.281	do	Do.
	.61	116.61	.30	38.80	−.37	.19	.11	.123	−.24	.11	.180	do	Do.
	.38	98.73	.22	52.93	−.17	(*)	.19	(*)	(*)	.19	(*)	do	Do.
	.33	102.38	.18	64.701	−.17	.05	.06	.149	−.06	.09	.200	do	Do.
2740	13.32	18.45	35.83	.239	−2.11	11.57	.75	.063	−.30	1.80	.444	do	Do.
	12.70	19.06	33.68	.262	−2.11	11.18	.79	.057	−.38	1.81	.410	do	Do.
	12.20	25.56	25.52	.383	−2.37	10.49	.77	.055	−.51	1.50	.333	−.40	1.345
	11.88	24.93	25.48	.384	−2.32	9.56	.68	.062	−.52	1.49	.326	−.12	1.426
	12.60	30.99	22.13	.457	−2.68	9.91	.78	.055	−.60	1.37	.270	−1.96	.966
	12.30	31.91	21.08	.484	−2.62	9.10	.72	.077	−.60	1.31	.257	−2.02	.891
	9.75	30.92	17.50	.602	−1.86	6.28	.66	.087	−.60	1.11	.279	−1.15	.950
	6.47	30.95	11.81	.930	−1.29	(*)	.59	(*)	(*)	.90	.280	−1.21	.940
	5.90	28.44	11.72	.987	−.97	4.32	.48	.114	−.61	.81	.279	−.52	.945
	6.70	38.49	9.99	1.112	−1.51	3.98	.55	.102	−.81	.80	.235	−2.13	.668
	4.63	30.72	8.57	1.307	−.81	2.88	.53	.150	−.51	.69	.281	No exit	No exit.
	11.75	89.89	7.45	1.512	−5.12	(*)	.63	(*)	(*)	.69	.109	−7.72	.261
	10.77	88.99	6.91	1.635	−5.21	6.45	.58	.050	−8.92	.69	.105	−6.80	.260
	4.63	39.93	6.62	1.709	(*)	(*)	(*)	(*)	(*)	.56	.244	−1.77	.634
	3.47	30.26	6.54	1.731	−.62	1.84	.52	.150	−.37	.46	.250	−1.15	.730
	7.75	88.57	5.00	2.282	−3.20	3.86	.52	.070	−2.81	.56	.110	−5.65	.253
	3.47	40.07	4.95	2.305	−.81	2.02	.45	.163	−.55	.53	.246	−1.33	.595
	2.30	30.30	4.34	2.637	−.37	1.15	.38	.238	−.28	.39	.355	No exit	No exit.
	2.20	29.58	4.26	2.687	(*)	(*)	(*)	(*)	(*)	.58	.370	do	Do.
	5.10	88.61	3.30	3.484	−2.51	.29	.44	.110	−2.29	.46	.122	−3.69	.289
	2.20	39.86	3.16	3.645	−.52	.69	.39	.220	−.35	.40	.284	No exit	No exit.
	3.48	87.77	2.27	5.068	−1.52	.69	.33	.120	−1.21	.36	.139	−3.23	.319
	1.68	87.55	1.10	10.350	−.71	(*)	(*)	(*)	(*)	.20	.190	−.46	.450

* Not available.

TABLE III.—EXPERIMENTAL DATA FOR A PRISMATIC HULL MODEL WITH $\beta=30°$

(a) Hydrodynamic loads and motions

W (lb)	V_{V_0} (fps)	V_{H_0} (fps)	γ_0 (deg)	κ	At maximum acceleration				At maximum draft			At exit	
					z_w/g	$\dot{z}_w$ (fps)	z_w (ft)	t (sec)	z_w/g	z_w (ft)	t (sec)	$\dot{z}_w$ (fps)	t (sec)
							$\tau=6°$						
1231	9.39	3.64	68.81	0.029	−1.63	7.69	0.66	0.082	−0.33	1.68	0.463	No exit	No exit.
	9.40	5.22	60.96	.047	−1.78	7.87	.66	.082	−.34	1.68	.460	do	Do.
	9.19	5.42	59.47	.050	−1.69	7.69	.63	.074	−.28	1.59	.460	do	Do.
	8.76	5.45	58.11	.054	(a)	(a)	(a)	(a)	(a)	1.60	.455	do	Do.
	11.62	7.94	55.66	.060	(a)	(a)	(a)	(a)	(a)	1.76	.437	do	Do.
	9.33	7.08	52.81	.068	−1.74	7.94	.66	.080	−.35	1.61	.460	do	Do.
	9.33	7.14	52.57	.069	(a)	(a)	(a)	(a)	(a)	1.60	.457	do	Do.
	9.37	7.78	50.30	.075	−1.71	7.68	.68	.079	−.28	1.58	.461	do	Do.
	9.13	9.85	42.83	.101	−1.75	7.82	.65	.077	−.20	1.49	.452	do	Do.
	6.67	12.24	28.59	.180	−1.06	5.59	.60	.104	−.16	1.26	.473	do	Do.
	3.06	9.21	18.38	.302	−.26	2.48	.53	.199	−.05	.94	.556	do	Do.
	9.14	29.10	17.44	.320	−2.27	6.73	.64	.082	−.36	1.07	.252	do	Do.
	3.27	11.56	15.79	.357	−.40	2.48	.61	.205	−.06	.93	.572	do	Do.
	3.06	11.07	15.45	.365	−.26	2.28	.61	.217	−.05	.90	.549	do	Do.
	3.33	12.50	14.92	.379	−.40	2.48	.60	.202	−.10	.93	.542	do	Do.
	9.27	36.05	14.42	.393	−2.45	4.70	.78	.106	−.50	1.00	.344	do	Do.
	5.30	29.10	10.32	.560	−.90	4.13	.51	.113	−.32	.83	.297	do	Do.
	4.35	29.75	8.32	.700	−.70	2.92	.56	.145	−.34	.74	.315	do	Do.
	8.29	57.56	8.20	.710	−2.78	5.27	.57	.076	−1.10	.75	.168	−1.40	0.557
	4.89	34.50	8.07	.722	−1.00	3.37	.58	.127	−.38	.75	.279	No exit	No exit.
	4.89	34.90	7.98	.730	−1.06	3.68	.53	.115	−.38	.76	.268	do	Do.
	4.32	31.30	7.86	.742	−.81	3.11	.59	.135	−.33	.81	.299	do	Do.
	4.22	32.10	7.49	.779	−.78	2.98	.53	.137	−.32	.73	.301	do	Do.
	2.79	31.90	5.00	1.177	−.48	1.84	.53	.200	−.28	.64	.356	do	Do.
	1.97	31.70	3.56	1.659	−.20	(a)	(a)	(a)	(a)	.39	.347	do	Do.
	1.81	33.30	3.11	1.901	−.28	.76	.46	.314	−.23	.48	.455	do	Do.
	4.60	88.90	2.96	1.998	−1.55	2.48	.40	.112	−.86	.42	.173	−1.21	.424
	1.59	35.40	2.57	2.305	−.16	(a)	(a)	(a)	(a)	.40	.404	No exit	No exit.
							$\tau=15°$						
1231	9.30	2.84	73.02	0.009	−1.10	7.89	0.90	0.108	−0.35	2.13	0.521	No exit	No exit.
	9.37	4.98	62.01	.066	−1.23	7.37	.93	.114	−.30	2.03	.528	do	Do.
	8.73	4.92	60.60	.074	−1.16	7.87	.83	.099	−.38	2.07	.523	do	Do.
	9.30	6.21	56.27	.100	−1.23	7.75	.89	.114	−.25	1.98	.521	do	Do.
	8.35	5.83	55.06	.108	−.99	7.04	.83	.108	−.30	1.88	.509	do	Do.
	8.41	6.38	52.84	.123	−1.30	7.30	.89	.105	−.38	1.99	.513	do	Do.
	9.19	9.04	45.47	.179	−1.30	7.82	.83	.099	−.12	1.82	.479	do	Do.
	6.70	11.49	30.25	.362	−.85	5.21	.83	.137	−.13	1.40	.446	do	Do.
	6.70	11.98	29.22	.380	−.91	5.52	.76	.123	−.29	1.38	.462	do	Do.
	9.43	19.40	25.92	.447	−1.78	7.75	.78	.094	−.50	1.39	.346	do	Do.
	9.30	28.72	17.94	.705	(a)	(a)	(a)	(a)	(a)	1.13	.237	do	Do.
	9.30	29.50	17.50	.726	−2.35	6.10	.79	.101	−1.00	1.17	.225	do	Do.
	9.43	32.26	16.29	.789	−2.46	6.35	.77	.096	−1.04	1.02	.210	−1.97	0.616
	9.75	33.90	16.05	.802	−2.65	5.84	.83	.102	−1.23	1.07	.197	−1.71	.535
	9.40	33.90	15.50	.835	−2.68	(a)	(a)	(a)	(a)	1.04	.195	−2.16	.595
	8.60	62.05	7.89	1.737	−2.72	4.57	.82	.092	−2.60	.68	.133	−5.14	.303
	4.70	92.49	2.91	4.851	−1.89	1.84	.35	.121	−1.55	.37	.151	−4.54	.289
2431	9.30	8.63	47.14	.165	−1.03	8.26	1.03	.109	−.33	2.50	.587	No exit	No exit.
	9.23	11.56	38.56	.247	−1.00	8.06	1.03	.115	−.35	2.34	.559	do	Do.
	9.23	11.63	38.44	.248	−1.06	7.87	1.03	.118	−.32	2.24	.549	do	Do.
	6.70	11.25	30.78	.353	−.62	5.92	.91	.139	−.29	1.88	.561	do	Do.
	9.30	27.72	18.55	.678	−1.62	7.54	.88	.106	−.53	1.49	.339	do	Do.
	4.42	88.50	2.86	4.937	−1.09	2.06	.45	.124	−1.56	.47	.165	−2.73	.310

* Not available.

(b) Pitching moments

[W=1,231 lb; W_1=400 lb; a=2.89 ft; d=0.5 ft; c=1.5 ft]

τ (deg)	V_{V_0} (fps)	V_{H_0} (fps)	γ_0 (deg)	κ	$M_{\alpha_{T_{max}}}$
12	4.95	54.55	5.18	2.20	−4,000
	5.28	57.89	5.21	2.19	−4,350
	7.92	87.50	5.17	2.20	−10,800

TABLE IV.—EXPERIMENTAL DATA FOR A PRISMATIC HULL MODEL WITH $\beta=40°$

(a) $W=1{,}213$ lb; $W_1=350$ lb; $a=2.89$ ft; $d=1.05$ ft; $c=1.81$ ft

τ (deg)	V_{T_0} (fps)	V_{H_0} (fps)	γ_1 (deg)	κ	At maximum acceleration				$M_{a_{T_{max}}}$ (lb-ft)	At maximum draft			At exit	
					$\ddot{z}_w/g$	$\dot{z}_w$ (fps)	z_w (ft)	t (sec)		$\ddot{z}_w/g$	z_w (fps)	t (sec)	$\dot{z}_w$ (fps)	t (sec)
3	9.24	23.31	21.62	0.129	−1.60	7.32	0.68	0.062	(a)	−0.32	1.49	0.377	(a)	(a)
	7.75	23.26	18.43	.154	−1.17	5.97	.74	.103	(a)	−.25	1.39	.396	(a)	(a)
	9.39	29.82	17.48	.163	−1.78	7.04	.78	.088	(a)	−.32	1.46	.344	No exit	No exit.
	8.82	29.07	16.88	.170	−1.70	7.39	.69	.077	(a)	−.25	1.45	.356	do	Do.
	7.61	28.74	14.83	.195	−1.26	5.89	.71	.100	(a)	−.15	1.33	.370	do	Do.
	7.82	29.04	14.64	.197	−1.30	5.90	.72	.093	(a)	−.32	1.30	.360	do	Do.
	9.39	40.32	13.11	.222	−1.99	6.36	.83	.098	(a)	−.28	1.29	.309	do	Do.
	8.75	39.53	12.48	.233	−1.82	6.47	.78	.087	(a)	−.25	1.30	.312	do	Do.
	7.89	40.32	11.07	.264	−1.48	6.19	.68	.094	(a)	−.32	1.20	.322	do	Do.
	4.05	22.15	9.92	.298	−.41	2.70	.66	.180	(a)	−.20	.96	.455	do	Do.
	9.46	56.50	9.51	.309	−2.17	6.90	.72	.082	(a)	−.32	1.16	.247	−0.57	1.067
	5.83	40.32	8.23	.359	−.87	4.08	.63	.128	(a)	−.25	1.00	.353	No exit	No exit.
	8.11	56.50	8.17	.361	−1.70	5.55	.75	.102	(a)	−.36	1.08	.206	do	Do.
	7.47	54.35	7.83	.377	−1.52	5.26	.67	.098	(a)	−.28	1.04	.268	do	Do.
	9.39	69.93	7.65	.386	−2.37	6.97	.69	.080	(a)	−.38	1.06	.232	−.85	.571
	3.13	23.36	7.63	.387	−.25	1.99	.57	.213	(a)	−.08	.85	.488	No exit	No exit.
	4.05	30.30	7.61	.389	−.45	2.99	.58	.162	(a)	−.19	.94	.420	do	Do.
	8.03	63.49	6.69	.443	−1.76	5.33	.69	.097	(a)	−.38	.97	.242	do	Do.
	5.97	56.50	6.03	.492	−1.05	4.12	.64	.117	(a)	−.32	.89	.256	do	Do.
	2.84	27.32	5.93	.501	−.27	1.49	.62	.252	(a)	−.08	.77	.478	do	Do.
	3.13	30.30	5.90	.503	−.27	1.99	.58	.213	(a)	−.15	.77	.428	do	Do.
	4.05	39.37	5.87	.506	−.50	2.70	.59	.165	(a)	−.28	.81	.360	do	Do.
	9.02	89.88	5.73	.520	−2.59	5.90	.67	.083	(a)	−.72	.95	.192	−1.70	.756
	3.98	40.16	5.66	.525	−.50	2.70	.58	.161	(a)	−.15	.83	.366	No exit	No exit.
	3.84	39.21	5.59	.531	−.45	2.49	.56	.170	(a)	−.10	.79	.401	do	Do.
	7.82	91.50	5.11	.582	−2.03	5.69	.59	.084	(a)	−.63	.86	.197	−1.71	.612
	5.69	68.49	4.75	.626	−1.14	3.77	.59	.120	(a)	−.32	.79	.260	No exit	No exit.
	2.84	39.06	4.16	.716	−.30	1.28	.58	.248	(a)	−.08	.68	.408	do	Do.
	3.77	54.64	3.95	.754	−.57	2.20	.59	.163	(a)	−.15	.78	.321	do	Do.
	5.69	90.10	3.61	.826	−1.26	3.56	.58	.111	(a)	−.50	.78	.228	do	Do.
	4.27	68.03	3.59	.830	−.72	2.70	.55	.148	(a)	−.31	.69	.278	do	Do.
	3.20	56.18	3.26	.915	−.41	1.85	.52	.163	(a)	−.20	.66	.350	do	Do.
	3.56	68.03	3.00	.995	−.57	1.78	.56	.184	(a)	−.40	.63	.284	do	Do.
	3.20	68.49	2.68	1.114	−.50	1.78	.53	.185	(a)	−.15	.61	.314	do	Do.
	4.12	90.10	2.62	1.140	−.84	2.42	.51	.141	(a)	−.45	.63	.241	−.57	.710
	3.63	90.09	2.31	1.293	−.75	1.85	.50	.154	(a)	−.35	.58	.247	No exit	No exit.
	2.77	90.91	1.75	1.708	−.49	1.14	.44	.193	(a)	−.15	.48	.277	do	Do.
6	8.89	34.13	14.60	.388	−1.72	6.26	.89	.107	−3032	−.32	1.35	.296	−1.07	1.085
	8.75	34.60	14.19	.400	−1.85	5.90	.91	.108	−3199	−.32	1.33	.293	−1.28	1.044
	8.89	35.21	14.17	.401	−1.76	6.33	.81	.094	−3190	−.36	1.30	.284	−1.35	.975
	9.03	43.47	11.74	.489	−1.98	6.33	.85	.100	−3281	−.50	1.22	.253	−2.28	.838
	8.89	43.29	11.61	.495	−1.99	6.04	.85	.102	−3114	−.45	1.22	.253	−1.71	.849
	8.75	44.25	11.19	.515	−1.98	6.11	.85	.107	−3421	−.50	1.18	.252	−1.71	.839
	8.89	46.73	10.77	.535	−2.03	6.47	.81	.094	(a)	−.58	1.18	.234	−1.99	.772
	8.89	56.14	8.69	.689	−2.29	5.90	.81	.100	(a)	−.75	1.08	.209	−2.56	.602
	8.98	58.47	8.46	.658	−2.33	5.76	.81	.100	−4403	−.80	1.07	.209	−2.42	.612
	8.96	60.97	8.36	.697	−2.29	5.83	.82	.101	−4281	−.89	1.10	.206	−2.35	.615
	9.03	66.22	7.77	.751	−2.45	5.76	.74	.090	−4552	−1.00	1.01	.195	−2.70	.557
	8.75	65.36	7.63	.765	−2.37	5.83	.76	.094	−4140	−.83	1.02	.194	−2.77	.557
	8.67	85.47	5.79	1.014	−2.75	5.12	.74	.091	−5354	−1.13	.89	.116	−3.34	.432
	8.53	86.21	5.65	1.040	−2.80	5.26	.70	.090	(a)	−1.32	.86	.170	−3.34	.421
	2.99	43.48	3.93	1.502	−.40	1.35	(a)	(a)	−1266	(a)	(a)	(a)	(a)	(a)
	2.99	43.67	3.92	1.506	−.40	1.35	.42	.210	−1194	−.25	.63	.349	(a)	(a)
	2.77	43.10	3.68	1.605	−.36	1.21	.56	.238	−1169	−.20	.63	.362	No exit	No exit.
9	9.24	35.89	14.55	.571	−1.85	5.76	.96	.115	−3756	−.58	1.29	.258	−2.13	.825
	9.24	44.44	11.75	.718	−2.16	6.33	.87	.103	−4620	−.75	1.18	.230	−2.63	.648
	9.46	45.45	11.78	.718	−2.25	6.75	.87	.100	−5052	−.88	1.19	.230	−2.63	.655
	9.53	45.87	11.74	.719	−2.29	8.03	.93	.102	(a)	−.92	1.22	.212	−2.77	.642
	9.46	46.08	11.60	.728	−2.25	6.61	.88	.104	−3952	−.80	1.21	.226	−2.77	.654
	8.96	51.55	9.86	.864	−2.28	5.76	.85	.104	−4718	−1.08	1.09	.207	−3.06	.585
	9.10	58.82	8.79	.975	−2.55	5.47	.84	.102	−3372	−1.25	1.04	.176	−3.56	.494
	8.60	57.14	8.56	1.002	−2.37	5.33	.81	.104	−5143	−1.18	1.03	.194	−3.13	.522
	8.75	63.69	7.82	1.101	−2.55	5.05	.82	.106	−5464	−1.30	.98	.181	−3.70	.466
	8.89	65.79	7.70	1.118	−2.71	5.40	.82	.099	−3648	−1.52	.99	.175	−3.84	.450
	9.03	77.51	6.65	1.301	−2.97	5.12	.77	.101	−3564	−1.52	.91	.151	−4.05	.391
	8.60	76.34	6.43	1.347	−2.67	4.19	.80	.109	−5907	−1.57	.90	.157	−3.98	.405
	8.67	86.20	5.74	1.513	−2.27	3.98	(a)	(a)	−8197	−2.00	(a)	(a)	−4.46	.343
	8.60	86.96	5.65	1.537	−2.97	4.12	.76	.105	−6990	−1.57	.84	.155	−4.34	.385
	3.27	43.48	4.30	2.030	−.50	1.35	.62	.227	−1672	−.28	.68	.317	−.50	.938
	3.12	44.64	4.00	2.185	−.45	1.49	.54	.218	−1503	−.25	.61	.318	−.54	.902
	2.98	58.48	2.92	3.005	−.55	1.14	.51	.210	−2023	−.35	.54	.272	−1.35	.563
	2.92	60.34	2.78	3.157	−.55	1.07	.50	.212	−2134	−.32	.54	.280	−1.28	.562

(a) Not available.

TABLE IV.—EXPERIMENTAL DATA FOR A PRISMATIC HULL MODEL WITH $\beta=40°$—Concluded

(a) Concluded

τ (deg)	V_{V_0} (fps)	V_{H_0} (fps)	γ_0 (deg)	κ	At maximum acceleration				$M_{a_{T_{max}}}$ (lb-ft)	At maximum draft			At exit	
					$\ddot{z}_w/g$	$\dot{z}_w$ (fps)	z_w (ft)	t (sec)		$\ddot{z}_w/g$	z_w (fps)	t (sec)	$\dot{z}_w$ (fps)	t (sec)
12	9.46	22.15	22.22	0.454	−1.65	6.25	1.14	0.130	−3448	−0.41	1.63	0.339	−0.92	1.202
	7.26	23.04	19.06	.545	−1.23	5.83	.95	.129	−2479	−.35	1.47	.344	−1.42	1.145
	9.53	29.67	17.81	.590	−1.86	5.83	1.09	.130	−4295	−.63	1.47	.270	−1.85	.905
	9.10	30.03	16.86	.628	−1.73	6.19	1.02	.117	−3865	−.50	1.43	.278	−2.13	.870
	8.11	30.12	15.07	.712	−1.47	5.62	.92	.130	−3198	−.50	1.29	.280	−1.78	.807
	9.46	39.84	13.36	.813	−2.17	6.04	.99	.115	−5001	−.85	1.28	.217	−2.92	.642
	9.24	39.84	13.06	.834	−2.16	5.76	.93	.115	−5039	−.96	1.20	.225	−3.06	.628
	7.75	39.53	11.09	.994	−1.65	4.34	.94	.140	−3137	−.80	1.12	.240	−2.77	.650
	7.96	40.98	10.99	1.004	−1.73	4.48	.94	.139	−3665	−.87	1.12	.229	−2.99	.632
	4.34	22.87	10.88	1.015	(a)	(a)	(a)	(a)	−1455	(a)	(a)	(a)	(a)	(a)
	4.05	22.83	10.06	1.103	−.45	2.06	.85	.247	−1379	−.15	.98	.413	(a)	(a)
	9.39	56.18	9.49	1.173	−2.64	4.19	.95	.120	−6572	(a)	1.08	.183	No exit	No exit.
	3.48	23.26	8.51	1.316	(a)	(a)	(a)	(a)	−1157	(a)	(a)	(a)	(a)	(a)
	8.11	56.18	8.21	1.365	−2.17	3.96	.71	.126	−6193	−1.52	.83	.189	−3.91	.467
	5.83	40.55	8.16	1.376	−1.14	3.34	.80	.157	−3025	−.60	.95	.256	−2.28	.664
	4.34	30.40	8.12	1.382	−.66	1.85	.81	.235	−1716	−.36	.90	.350	−.71	1.001
	9.53	69.44	7.81	1.439	−3.24	4.76	.86	.105	(a)	−2.05	.97	.155	−4.96	.372
	9.03	68.03	7.56	1.459	−2.97	4.91	.81	.105	−7722	−1.25	.93	.160	−4.62	.378
	7.82	68.49	6.51	1.739	(a)	(a)	(a)	(a)	−6824	(a)	(a)	(a)	(a)	(a)
	7.75	68.49	6.46	1.753	−2.33	3.91	.78	.118	−6271	−1.43	.85	.170	−4.12	.402
	7.61	68.49	6.34	1.787	−2.32	3.41	.78	.121	−6541	−1.48	.85	.171	−4.12	.391
	3.34	30.40	6.27	1.808	(a)	(a)	(a)	(a)	−1485	(a)	(a)	(a)	(a)	(a)
	4.34	40.98	6.05	1.876	−.75	2.06	.70	.194	−2351	−.56	.79	.288	−1.56	.730
	3.06	29.33	5.96	1.905	−.40	1.49	.71	.260	−1272	−.20	.77	.392	No exit	No exit.
	9.24	90.09	5.85	1.938	−3.68	4.27	.76	.104	−10141	−2.96	.81	.137	−5.40	.304
	5.75	56.50	5.82	1.952	−1.38	2.77	.72	.150	−10372	−.96	.81	.210	−2.99	.504
	9.10	89.29	5.82	1.952	−3.57	4.41	.73	.099	−3756	−3.10	.81	.139	−5.33	.304
	3.96	39.37	5.77	1.969	−.65	1.85	.67	.200	−2197	−.40	.78	.299	−1.64	.750
	8.75	91.00	5.49	2.073	−3.57	3.56	.76	.104	−10333	−2.37	.80	.134	−5.19	.299
	7.89	90.91	4.96	2.300	(a)	(a)	(a)	(a)	−8761	(a)	(a)	(a)	(a)	(a)
	7.68	90.91	4.83	2.364	−2.97	2.99	.70	.115	−8421	−2.25	.75	.151	−4.55	.315
	7.54	89.29	4.83	2.364	−2.92	2.27	.63	.107	−8857	−2.15	.68	.141	−4.62	.310
	5.69	68.49	4.75	2.404	−1.56	2.20	.67	.155	−4751	−1.35	.69	.189	−3.06	.426
	3.27	40.49	4.62	2.473	−.80	1.35	.59	.238	−1818	−.32	.65	.319	−.57	.871
	5.33	68.03	4.45	2.552	−1.52	2.13	.65	.144	−3351	−1.00	.70	.198	−3.13	.433
	4.12	55.87	4.22	2.713	−.87	1.35	.62	.190	−2858	−.53	.64	.250	−2.13	.565
	4.27	68.03	3.69	3.198	−1.05	1.21	.54	.178	−3230	−.70	.55	.220	−2.42	.477
	4.98	90.09	3.16	3.640	−1.76	2.28	.55	.125	−5906	−1.48	.58	.160	−3.48	.350
	3.20	67.57	2.71	4.253	−.66	1.14	.51	.208	−2357	−.50	.53	.278	−1.35	.628
	3.98	90.09	2.53	4.559	(a)	(a)	(a)	(a)	−4353	(a)	(a)	(a)	(a)	(a)
	2.92	68.49	2.44	4.729	−.66	.57	.45	.212	−2479	−.56	.47	.242	−1.49	.552
	3.70	90.09	2.35	4.913	−1.13	1.35	.45	.146	−3145	−.96	.48	.186	−2.49	.389
	3.13	90.09	1.99	5.810	−.92	.43	.42	.180	−3551	−.80	.42	.205	−1.99	.410

(a) Not available.

(b) $W=1{,}343$ lb; $W_1=590$ lb; $a=2.99$ ft; $d=-0.283$ ft; $c=1.456$ ft

τ (deg)	V_{V_0} (ft/sec)	V_{H_0} (ft/sec)	γ_0 (deg)	κ	$M_{a_{T_{max}}}$ (lb-ft)
12	8.11	39.53	11.59	0.948	−2905
	8.19	43.29	10.71	1.032	−3174
	6.32	34.01	10.53	1.051	−1593
	9.26	91.74	5.76	1.972	−8785
	7.04	72.45	5.55	2.050	−4891
	4.16	44.44	5.35	2.126	−1460
	7.90	86.21	5.24	2.174	−6091
	3.59	44.64	4.60	2.484	−1463
	3.30	44.05	4.28	2.674	−1418
	3.30	44.44	4.25	2.694	−1225
	6.17	95.24	3.71	3.093	−6328
	5.96	95.24	3.58	3.208	−5642
	4.24	70.92	3.42	3.360	−2728
	4.16	71.94	3.31	3.473	−2843
	3.37	70.42	2.74	4.206	−2144